

Biblioteka Główna i OINT
Politechniki Wrocławskiej



100100095231

Instytutu Podstaw Elektrotechniki
i Politechniki Wrocławskiej

45

15

Zbigniew Leonowicz

**Parametric methods for
time-frequency analysis of electric signals**

Wrocław 2006



Zbigniew LEONOWICZ

Parametric methods for
time-frequency analysis of electric signals



This work has been supported by the Ministry of Education and Science (Grant No. 3 T10A 040 30) and by the Faculty of Electrical Engineering, Wrocław University of Technology

Reviewers

Janusz WALCZAK
Waldemar REBIZANT

Proof-reader

Halina MARCINIAK



326571L/1

© Copyright by Oficyna Wydawnicza Politechniki Wrocławskiej, Wrocław 2006

OFICyna WYDAWNICZA POLITECHNIKI WROCLAWSKIEJ
Wybrzeże Wyspiańskiego 27, 50-370 Wrocław

ISSN 0324-945x

Drukarnia Oficyny Wydawniczej Politechniki Wrocławskiej. Zam. nr 756/2006.

Prace Naukowe Instytutu Podstaw Elektrotechniki
i Elektrotechnologii Politechniki Wrocławskiej

45

Seria:
Monografie

15

Zbigniew Leonowicz

**Parametric methods for
time-frequency analysis of
electric signals**



Oficyna Wydawnicza Politechniki Wrocławskiej · Wrocław 2006

*parametric methods, power systems, spectral analysis,
time-frequency analysis, energy quality, fault classification,
MUSIC, ESPRIT, space-phasor, band-pass filters*

Zbigniew LEONOWICZ¹

PARAMETRIC METHODS FOR TIME-FREQUENCY ANALYSIS OF ELECTRIC SIGNALS

The author presents a new approach to spectral analysis of electric signals and related problems encountered in power systems. This approach includes the use of high-resolution subspace spectrum estimation methods (such as MUSIC and ESPRIT) as replacement of widely used Fourier Transform-based techniques. The author proves that such an approach can offer substantial advantages in parameter estimation accuracy, classification accuracy and many other aspects of power system analysis, especially when analyzing non-stationary waveforms.

The problems treated in this work include theoretical analysis of the limitations of FFT-based analysis, problems in applications of Short Time Fourier Transform, description and characteristic properties of subspace frequency estimation methods – MUSIC and ESPRIT; estimation of the model order, theoretical development of time-varying spectrum, application of filter banks and advantages when applying to line spectra analysis, space-phasor for analysis of three-phase signals, power quality assessment using indices with practical application to waveforms from an arc furnace power supply, numerical analysis of performance of investigated methods and a novel approach to classification of power system events based on time-frequency representation and selection of "areas of interest" in time-frequency plane.

The author concludes that the use of high-resolution methods significantly improves the accuracy of many parameter estimation techniques applied to power system analysis.

¹ Instytut Podstaw Elektrotechniki i Elektrotechnologii Politechniki Wrocławskiej, Wybrzeże Wyspiańskiego 27, 50-370 Wrocław.

Notation

In this monograph, the symbols for discrete signals: voltages, currents and others are always mentioned; subscripts are used to distinguish between electrical phases: e.g., a, b and c. The symbols for continuous signals are explicitly mentioned. Vectors are written in boldface lowercase letters and matrices are written in boldface uppercase letters. Complex signals would have a tilde and vectors and matrices with complex signals would have tilde, as well. The meaning of the following symbols are, if nothing else is stated: X^T transpose operator, X^* complex conjugate, X^H hermitian transpose, i.e., complex conjugate transpose, $Re\{X\}$ real part of a complex quantity, $Im\{X\}$ imaginary part of a complex quantity, \mathbf{X}^+ inverse (pseudoinverse) of a matrix \mathbf{X} .

| | |
|-------------------------|--|
| $\mathring{\mathbf{A}}$ | complex amplitude |
| C | autocovariance function |
| \mathbf{C}_x | autocovariance matrix |
| $\mathbf{C}\{.\}$ | covariance matrix operator |
| $C_{n..}$ | amplitude of a harmonic/interharmonic group/subgroup |
| \mathbf{e} | eigenvector of the correlation matrix |
| $\mathcal{E}\{.\}$ | expected value |
| \mathbf{E} | matrix of eigenvectors |
| \mathbf{f} | space-phasor |
| f_1 | fundamental frequency |
| f_R, f_S, f_T | symmetric three-phase components |
| H | transmittance |
| $\downarrow M$ | M-times decimation |

| | |
|----------------------------|--|
| \mathbf{P}_X | orthogonal projection matrix |
| $P(\omega)$ | power spectrum |
| $P(t, \omega)$ | time-varying power spectrum |
| $r_x[n]$ | autocorrelation sequence |
| \mathbf{R}_x | correlation matrix of the random process x |
| $R_x(t)$ | correlation function of the random process x |
| $R(t, \omega)$ | time-varying autocorrelation function |
| \mathbf{s}, \mathbf{s}_i | vector of signal samples |
| $S_s(\omega)$ | spectrogram, energy density spectrum |
| $S_x(e^{j\omega})$ | power density spectrum x |
| \mathbf{w} | vector of components $e^{j\omega n}$ |
| $W(t, \omega)$ | Wigner-Ville distribution |
| $\delta(n)$ | discrete impulse |
| $\sigma_0^2(n)$ | noise variance |
| \mathbf{U} | matrix of eigenvectors |
| $\hat{\theta}$ | estimator of the parameter θ |
| $\{\cdot\}_{ML}$ | in the maximum-likelihood sense |
| η | vector of noise samples |
| λ | eigenvalue of the correlation matrix |
| Λ | matrix of eigenvalues |
| μ | Lagrange coefficient |
| Γ | selector matrix |
| ∇_{a^*} | complex gradient of a |

Abbreviations

| | |
|------------|---|
| AC | alternate current |
| AIC | Akaike Information Criterion |
| ESPRIT | Estimation of Signal Parameters via Rotational Invariance Technique |
| FFT | Fast Fourier transform |
| LP | Linear Prediction |
| LMS | Least Mean Squares |
| LNI | Load Nonlinearity Indicator |
| LS | Least Squares |
| LSE | Least Squares Estimator |
| MDL | Minimum Description Length |
| MIBS | Minka's Bayesian model order Selection Criterion |
| MLE | Maximum Likelihood Estimator |
| MSE | Mean Square Error |
| MUSIC | Multiple Signal Classification method |
| PHD | Pisarenko Harmonic Decomposition |
| RMS | Root-Mean Square |
| SNR | Signal-to-Noise Ratio |
| STFT | Short-Time Fourier Transform |
| STHD | Short-Time Harmonic Distortion Index |
| SVD | Singular Value Decomposition |
| TF, TF {.} | time–frequency, TF transformation, TF transform of {.} |
| THD | Total Harmonic Distortion |
| WFT | Windowed Fourier Transform |

Preface

The problem of spectral analysis can be described as the idea of finding the spectral contents of a given signal.

The meaning of the signal decomposition into its spectral components originates from the very early works of the Pythagoreans, in their analysis of the motion of the planets, in the discovery of the law of musical harmony, in the works of Newton on the spectrum of the light (1677), in the analysis of vibrating membranes by Bernoulli (1738) and Euler (1755), and in Prony approximation of vibrating mechanisms (1793).

The contemporary Fourier analysis, commonly used, takes its origins in the works of Fourier (1807), although some elements of the Fast Fourier Transform can be found in Gauss's works on orbital mechanics (1805).

One of the main tools of signal analysis is the power spectrum. Various algorithms of the power spectrum estimation found a wide application in numerous areas of science, also in power system analysis.

Accurate and fast determination of the parameters of the spectral components of the investigated signal is important for different reasons.

Real-world signals contain usually many spectral components which differ in frequency, often with additional noise, moreover, their parameters can change with time. The accuracy of the estimation is limited by the resolution, bias, variance of the estimator, length of the data sequence, interactions between individual components, phase-dependence and many other factors.

In many areas of technical sciences, like telecommunications, electronics, automatic control, power system protection and control, there is a need for identification of the working state, signal separation and estimation of the signal parameters, identification of the harmonic components and their parameters.

Between 1940 and 1960 signal processing was analog and primarily a part of physics. Then, the analog signal processing lost its importance with the onset of digital signal processors. Fast computational algorithms, such as Fourier transform, allowed the signal filtering to be performed in a very short time. Then, signal processing acquired great

support from statistics. The next revolution occurred in 1979–1980 with the advent of new methods from mathematics and quantum physics, like Wigner transform.

The signal is a physical carrier of useful information. The motivation for leaving the immediate representational space (mostly time representation in which plain data are given) and pass to a transformed space is to obtain a clearer picture of specific characteristics of the signal. It is like "looking" at the signal from a particular angle, to obtain better "view" of its properties.

Non-parametric methods require little or no *a priori* knowledge of the signal. These methods usually employ larger representational space than used for the plain data. The redundancy is compensated by better structuring of the information contained in the analyzed signal.

On the other hand the non-parametric (conventional) spectral estimators such as the FFT or autocorrelation methods are limited in their resolving power, requiring long observation intervals in order to achieve acceptable accuracy and reduce leakage. For data sets of short duration, these conventional techniques are untenable, and an alternative approach is required. This has led to parametric (model based) spectral estimation, which has proven usefulness in extracting high resolution frequency spectra from relatively short data sets, providing the structure of the signal is known. The components of a known order related structure can be accurately tracked and extracted from the background of noise and components of an unknown structure.

Research objective

This work extends and summarizes some previous publications of the author(see [29], [32]–[53], [55]–[62]). The goal is to present a new approach to many problems encountered in power systems. This approach includes the use of high-resolution subspace spectrum estimation methods (such as MUSIC and ESPRIT) as replacement of classical FFT-based techniques. The author argues that such an approach can offer substantial advantages in parameter estimation accuracy, classification accuracy and many other aspects of power system analysis, especially when analyzing non-stationary waveforms. Based on theoretical considerations and numerous practical applications, the following thesis will be proven:

High-resolution subspace methods, together with time-frequency representation and analysis of electrical signals provides substantial improvements to solutions of numerous problems of power system analysis in the frequency domain.

The problems treated in this work include:

- detailed theoretical analysis of the limitations of Fourier Transform-based analysis, problems in applications of Short Time Fourier Transform,
- description and characteristic properties of subspace frequency estimation methods – MUSIC and ESPRIT; estimation of the model order,
- theoretical development of time-varying spectrum,
- application of filter banks, advantages when applying to line spectra,
- space-phasor for analysis of three-phase signals,
- power quality assessment using indices with practical application to waveforms from an arc furnace power supply,
- numerical analysis of performance of investigated methods,
- novel approach to classification of power system events based on time-frequency representation and selection of "areas of interest".

The author argues that for the analysis of narrow-band (line-spectra) it is sufficient to analyze narrow band-limited and time-limited areas of their time-frequency representations (see Chapter 4). Such an approach not only provides sufficient information for subsequent analysis (see Section 4.2); it also improves its performance by enhancing the signal-to-noise ratio, improving the resolution (see Chapter 5) and improving the classification rate of correlation-based classification approach (see Theorem 13). The use of high-resolution methods significantly improves the accuracy of many parameter estimation techniques. Both approaches combined allow further improvements (see chapter 10 where numerous examples are shown).

Contributions

Scientific contributions of this work can be summarized as follows:

- coherent theoretical formulation and development of the basis of time-frequency analysis of electrical non-stationary signals, which include:
 - detailed description, characterization and performance analysis of two selected parametric spectrum estimation methods: MUSIC and ESPRIT,
 - formulation of conditions for time-varying spectrum estimation,
- analysis and justification of space–phasor transformation of three–phase electric signals,
- analysis of advantages of application of band-pass filters and filter banks for line spectra,
- numerical analysis of selected methods of model order selection,
- introduction, analysis and comparison of new methods of calculation of power quality indices using parametric spectrum estimation methods,
- development of a new method of classification based on selection of areas in the plane of time-frequency parametric representation of signals,
- extensive numerical simulations for comparison of various performance aspects of parametric spectrum estimation methods.

Chapter 1

Introduction

1.1. Time-domain analysis

Prior to the introduction of the Fast Fourier Transform and the implementation of the first real-time spectral analyzers, the spectral analysis was mainly performed by looking at the time waveform of the signal. Although this allowed detection and diagnosis of faults by examining the major repetitive components of a signal, complex signals with a multitude of components could not be accurately assessed¹.

Several techniques can be used to enhance the characteristics that are otherwise not easily observable from the time waveform. These include time-synchronous averaging, and auto-correlation of the signal. Time synchronous averaging uses the average of the signal over a large number of cycles, synchronous to the running speed of the machine. This attenuates any contributions due to noise or non-synchronous vibrations. The auto-correlation function is the average of the product and allows us to indirectly obtain information about the frequencies present in the signal. However, these techniques provide only a limited amount of additional information. The need to distinguish between components of a similar nature or hidden within a multi-component signal led to the mathematical representation of these signals in terms of their orthogonal basis functions, a field of mathematics whose origins date back to Joseph Fourier's investigations into the properties of heat transfer.

1.2. Frequency-domain analysis

The advent of the Fourier Series in the early 1800's by Joseph Fourier (1768–1830) provided the foundations for modern signal analysis, as well as the basis for a significant proportion of the mathematical research undertaken in the 19th and 20th centuries.

Fourier's most important work was his mathematical theory of heat conduction exposed in *Analytic Theory of Heat (Théorie Analytique de la Chaleur)* (1822). As one of

¹ This introduction is partially based on the review "Surfing the Wavelets" in [1].



Figure 1.1. Jean-Baptiste Joseph Fourier

the most important books published in the 19th century, it marked an epoch both in the history of pure and applied mathematics. In it, Fourier developed the theory of the series known by his name and applied it to the solution of boundary-value problems in partial differential equations. This work brought to a close a long controversy, and henceforth it was generally agreed that almost any function of a real variable can be represented by a series involving the sines and cosines of integral multiples of the variable. After a long and distinguished career, Fourier died in Paris on May 16, 1830 at the age of 62.

A major development which revolutionized the computational implementation of the Fourier transform was the introduction of the Fast Fourier Transform (FFT) by Cooley and Tukey in 1965, which enabled the implementation of the first real-time spectral analyzers. The FFT improved the computational efficiency of the Fourier transform of a signal represented by discrete data points. Despite the functionality of the Fourier transform, especially in regard to obtaining the spectral analysis of a signal, there are several shortcomings of this technique. The first of these is the inability of the Fourier transform to accurately represent functions that have non-periodic components, that are localized in time or space, such as transient impulses. This is due to the Fourier transform being based on the assumption that the signal to be transformed is periodic in nature and of infinite length. Another deficiency is its inability to provide any information about the time structure of a signal, as results are averaged over the entire duration of the signal. This is a problem when analyzing signals of a non-stationary nature, where it is often beneficial to be able to acquire a correlation between the time and frequency domains of a signal. Another problem of Fourier analysis is spectral smearing. It substantially affects the results obtained by conventional spectral analysis.

A variety of alternative schemes have been developed to improve the description of non-stationary signals. These range from developing mathematical models of the signal,

to converting the signal into a pseudo-stationary signal through angular sampling, and time-frequency analysis of the signal.

1.3. Time-Frequency signal analysis

As noted by Jean Ville in 1947, there are two basic approaches to time-frequency analysis. The first approach is to initially cut the signal into slices in time, and then to analyze each of these slices separately to examine their frequency content. Another approach is first to filter different frequency bands, and then cut these bands into slices in time and analyze their energy contents.

The first of these approaches is used for the construction of the Short Time Fourier Transform and the Wigner–Ville transform, while the second leads to filter-bank methods and to the Wavelet Transform.

In 1946, the first time-frequency wavelets (Gabor wavelets) were introduced by Dennis Gabor, an electrical engineer researching into communication theory. Jean Ville (1947) proposed another approach for obtaining a mixed signal representation. Ville's work was tied into the research of Hermann Wigner (1932), a physicist working in the field of quantum mechanics, and led to the development of the Wigner–Ville transform. Unfortunately the Wigner–Ville transform renders imperfect information about the energy distribution of the signal in the time-frequency domain, and an atomic decomposition of a signal based on the Wigner–Ville transform does not exist.

After the first time-frequency wavelets introduced by Dennis Gabor, there has been a proliferation of activity with comprehensive studies on the time-frequency analysis and its implementation into many fields of science.

Non-parametric (conventional, Fourier Transform based) spectral estimators such as the FFT or auto-correlation methods are limited in their resolving power, requiring long observation intervals in order to achieve acceptable accuracy and reduce leakage. For data sets of short duration, these conventional techniques are useless, and an alternative approach has been developed. The parametric (model based) spectral estimation, which has proven useful in extracting high resolution frequency spectra from relatively short data sets, providing the structure of the signal is known (*a priori* knowledge) was introduced. The components of a known order related structure can be accurately tracked and extracted from a background of noise and components of an unknown structure.

1.4. Analysis of non-stationary signals

A variety of alternative schemes to analyze the properties of non-stationary signals have been developed to improve the description of their frequency domain content. Each of these techniques has its own particular domain of application and addresses certain problems, but *not all*, encountered in the analysis of non-stationary signals. Investigations are to include angle domain analysis, parametric spectral estimation and time-frequency analysis. A comparison of these techniques is presented below, including some practical examples illustrating how they can be used to assist in the analysis of non-stationary data.

1.4.1. Classes of non-stationary signals

Two major classes have been identified, evolutionary harmonic signals and transient signals. A third class, evolutionary broad band signals also exists, however this form of non-stationary signal is rare in the domain of power systems.

Evolutionary narrow-band (harmonic) signals

Evolutionary harmonic signals consist of several non-stationary narrow band tones, superimposed on a background of random noise. These signals are usually a result of the waveforms being related to some underlying periodic time-varying phenomenon, such as the rotational speed of a generator. Further complications arise when a signal consists of a combination of stationary and non-stationary harmonic signal components, and/or involves varying signal amplitude with time.

Evolutionary broad-band signals

An evolutionary broad band signal is one whose spectral density covers a broad band of frequencies, which are of a time varying nature. The approach usually adopted when analyzing signals of an evolutionary broad band nature is to minimize the observation period while maintaining a reasonable spectral resolution, thus enabling analysis over an essentially stationary segment of the signal. A method that has proven useful in analyzing signals of this form is auto-regressive modelling, which accentuates the most prominent features, while attenuating the less prominent components.

Transient signals

Transient signals are short time events, whose time behaviour cannot be predicted and are totally varying in nature, both in time, frequency and other parameters. Transient

signals (impulsive noise) are usually a result of load or supply voltage or current steep changes.

1.4.2. Parametric spectral estimation

As previously explained, non-parametric spectral estimators are limited in their resolving power. The development of parametric (model-based) spectral estimation methods allowed extraction of high resolution spectra from relatively short data sets, providing adequate knowledge of the structure of the signal. The components of a known order related structure can be therefore accurately tracked and extracted from a background of noise and components of an unknown structure.

The basic idea is that if the signal $y(t)$ depends on a finite set of parameters, then all of its statistical properties can be expressed in terms of these parameters, including its power spectrum $P_{xx}(f)$ [84]. The most common and simplest of the parametric estimation techniques is auto-regressive (AR) modelling of the signal [85]. Auto-regressive modelling consists in estimating the order of the coefficients of the model, which when applied to the input signal will minimize the prediction-error of the signal. Normally, the minimization criterion of the model will be entropy based, which essentially maximizes the random nature of the error signal.

Non-Gaussian processes or processes that include coloured noise cannot be adequately modelled by its second order statistics, motivating higher order parametric estimation techniques, such as auto-regressive moving average (ARMA) estimation. Although AR and ARMA estimation have proven successful in analyzing signals of an evolutionary harmonic or broad band nature, the problem of transient signal analysis cannot be still adequately addressed [85]. Another mathematical model approach that has been highly successful in analyzing signals of an evolutionary harmonic nature is adaptive Kalman filtering. However, as with AR and ARMA models, an accurate knowledge of the structure of signals is required before a reasonable model can be obtained [85].

The area of parametric spectral estimation was developed in the direction of eigen-analysis-based methods, among others. These methods of spectrum estimation are based on the linear algebraic concepts of subspaces and so have been called "subspace methods" [85]. Their resolution is theoretically independent of the signal-to-noise ratio (SNR). The model of the signal in this case is a sum of sinusoids in the background of noise of a known covariance function. Pisarenko [68] first observed that the zeros of the z-transform of the eigenvector, corresponding to the minimum eigenvalue of the covariance matrix, lie on the unit circle, and their angular positions correspond to the frequencies of the sinusoids. In a later development it was shown that the eigenvectors

might be divided into two groups, namely, the eigenvectors spanning the signal space and eigenvectors spanning the orthogonal noise space. The eigenvectors spanning the noise space are the ones whose eigenvalues are the smallest and equal to the noise power. One of the most important techniques, based on the Pisarenko's approach of separating the data into signal and noise subspaces is the MUSIC method [76] and ESPRIT method [74], investigated in this work.

Extension to analysis of non-stationary signals leads to sliding time-window approaches, when the time-varying signal is assumed to be locally stationary (inside the current analysis window).

Chapter 2

Fourier Analysis

Fourier analysis is one of the major accomplishments of physics and mathematics [15]. It is rooted in the central concept of *frequency*. The frequential description of the signal gives the basis for better understanding of the phenomena analyzed. It often supplies an essential complement to the *temporal* description. There are several reasons for using Fourier analysis:

- 1) the temporal and frequential description of the signal are complementary;
- 2) mathematical structure of the Fourier transform is well suited for common transform methods;
- 3) Fourier transform serves as a basis for development of a large number of algorithms, programs, processors and machines for frequency analysis.

Classical Fourier analysis employs two complementary representations to describe the signal: the signal $x(t)$ as a time function and its Fourier transform $X(\omega)$:

$$X(\omega) = \int_{-\infty}^{+\infty} x(t) e^{-j\omega t} dt. \quad (2.1)$$

2.1. Limitations

In general, it is difficult to recognize properties of $x(t)$ from properties of $X(\omega)$. Based on the uncertainty principle it follows that $x(t)$ and $X(\omega)$ cannot be both simultaneously small [18]. The computation of one value of $X(\omega)$ necessitates the knowledge of the complete history of the signal. In the inverse Fourier transform:

$$x(t) = \int_{-\infty}^{+\infty} X(\omega) e^{j\omega t} d\omega \quad (2.2)$$

any value of $x(t)$ at the time instant t can be regarded as a superposition of an infinite number of complex exponentials, that is, everlasting and completely non-local waves. This kind of representation may in certain circumstances distort the real properties of

the signal. This is the case when dealing with transient signals, which vanish after a certain time [15].

The author's interest in time-frequency representations of electric signals is due to the fact that most multi-component (distorted) waveforms in power systems are time-varying. Widely used FFT-based methods, including STFT, present many shortcomings which in some cases lead to inaccurate results. In [4]–[6], [29], [37], [57]–[60], parametric time-frequency analysis was developed and applied to the various problems of power system operation, including arc furnace supply, synchronous machines and inverter drives. In the author's works ([32], [41], [48], [55], [53]) non-parametric time-frequency methods were also considered (STFT, S-transform and Wigner–Ville transform).

Time-frequency methods explicitly consider the time dependence of the frequency contents of the signal.

In mathematics uncertainty principles involve functions f and their transforms F . Classical uncertainty principle is called Heisenberg–Pauli–Weyl inequality [18].

Theorem 1. *If $f \in L^2(\mathbb{R})$ and $a, b \in \mathbb{R}$ are arbitrary, then:*

$$\sqrt{\int_{-\infty}^{+\infty} (x - a)^2 |f(x)|^2 dx} \cdot \sqrt{\int_{-\infty}^{+\infty} (\omega - b)^2 |F(\omega)|^2 d\omega} \geq \frac{1}{4\pi} \|f\|_2^2. \quad (2.3)$$

It follows that the support of the signal cannot be arbitrarily small both in time and in frequency domains. The experience also proves that short impulse extends over a large frequency range. This type of constraint is imposed by the Fourier duality [15]. For signal $x(t)$ with limited energy, the product of the duration Δt and the bandwidth $\Delta\omega$ of the signal is bounded from below, which is expressed by:

$$\Delta t \cdot \Delta\omega \geq \frac{1}{4\pi}. \quad (2.4)$$

The duality of the Fourier transform is the direct consequence of the definition of the latter. For the proof, see [15].

2.2. Time-Frequency Approach

Time-frequency analysis is the search for representations that present the information contained in $x(t)$ and $X(\omega)$ simultaneously. The goal is a joint description of the temporal and spectral behavior of the signal. Such a representation is two-dimensional.

The ideal time-frequency representation of $x(t)$ shows the frequency spectrum at each instant t . But this ideal representation does not exist.

Short-Time Fourier Transform (STFT)

The Short-Time Fourier Transform is the most widely used method for analysis of non-stationary signals [13]. It is based on a simple and intuitive concept: the conventional Fourier transform gives no information about the time location of the spectral peaks, because its basis functions are not localized in time. In order to extract such information, one breaks the time-localized signal into smaller time fragments and apply the Fourier analysis to each of the time segments. The sum of such partial spectra shows the time variation of the spectral content of a given signal in time.

In most of the author's research, STFT played the role of a "benchmark" or a tool for comparing the accuracy of the new methods investigated. Wide application of STFT makes it an ideal choice for this task ([50], [58]). Temporal window function as in STFT was also applied by the author for different parametric methods in order to obtain time-frequency representations of signals (e.g., [32], [44]).

When trying to achieve better time resolution, it is possible to choose shorter time intervals but up to a certain limit, when the segment spectrum becomes meaningless and without any relation to the true spectral content of the signal. In the case of parametric methods, which allow exact spectral estimation based on very short data sequences, such a limitation affects less the results ([23] ,[60]).

In order to obtain information about the signal at a certain time point t it is necessary to use the temporal window function $h(\tau)$, which preserves the signal inside a certain time interval and suppresses the signal at all other times: a modified signal is obtained by multiplying the original signal by the window function:

$$s_t(\tau) = s(\tau) \cdot h(t - \tau). \quad (2.5)$$

Due to the window function, centered around the time point t , emphasizing the signal around that point, the Fourier transform of the signal s_t also reflects the spectral content of it around that time t :

$$S_t(\omega) = \frac{1}{\sqrt{2\pi}} \int_{-\infty}^{\infty} e^{-j\omega t} s(\tau) \cdot h(\tau - t) d\tau. \quad (2.6)$$

The energy density spectrum, commonly named *spectrogram* at the time t is defined as:

Definition 2. For a given window function $h(t)$, the spectrogram of a signal $s(t)$ is defined by:

$$S_s(t, \omega) = \left| \int_{-\infty}^{+\infty} s(\tau) h^*(\tau - t) e^{-j\omega\tau} d\tau \right|^2. \quad (2.7)$$

Evaluation of the spectrogram combines a linear operation (Fourier transform of the weighted signal) with quadratic operation (modulus squared). The opposite order of operations is applied in the Wigner–Ville distribution [11], which is not considered in this work.

The total energy of the signal transformed by STFT is given by [13]:

$$|S_{STFT}(t, \omega)|^2 = \left| \frac{1}{2\pi} \int_{-\infty}^{\infty} s(\tau) h(\tau - t) e^{-j\omega\tau} d\tau \right|^2. \quad (2.8)$$

The marginals can be obtained by integrating:

- time marginal – over the frequency ω :

$$P(t) = \int_{-\infty}^{\infty} |S_{STFT}(t, \omega)|^2 d\omega = \int_{-\infty}^{\infty} |s(\tau)|^2 |h(\tau - t)|^2 d\tau \neq |s(t)|^2. \quad (2.9)$$

and similarly,

- frequency marginal – over the time t :

$$P(\omega) = \int_{-\infty}^{\infty} |S(\omega')|^2 |S_h(\omega')|^2 d\omega' \neq |S(\omega)|^2. \quad (2.10)$$

From equations (2.9) and (2.10) it follows that, in general case, the marginals of the spectrogram are not correctly satisfied, because the spectrogram scrambles the energy distribution of the signal with the energy distribution of the window function [13].

As a consequence:

- the averages of time and frequency are never correctly given by the spectrogram;
- the spectrogram does not possess any finite support property;
- there exists an inherent trade-off between the time and frequency localization of the spectrogram. The uncertainty principle quantifies this dependency;
- the choice of an optimal window function is difficult and must be done for every class of signals or for the purpose of the analysis;
- if the time window function is shortened, the result of the spectrogram approaches the instantaneous frequency of the signal, but, at the same time, the standard deviation of the signal representation goes to infinity [13].

As an illustrative example [13], the spectrogram of the signal $s(t)$ composed of one sinusoidal component and one impulse with the use of Gaussian window function $h(t)$

is given by

$$s(t) = e^{j\omega_0 t} + \sqrt{2\pi}\delta(t - t_0), \quad (2.11)$$

$$h(t) = \left(\frac{a}{\pi}\right)^{\frac{1}{4}} e^{-\frac{at^2}{2}}, \quad (2.12)$$

$$\begin{aligned} |S_t(\omega)|^2 &= \frac{1}{\sqrt{a\pi}} e^{\frac{-j(\omega-\omega_0)^2}{a}} + \sqrt{\frac{a}{\pi}} e^{-a(t-t_0)^2} + \\ &+ \frac{2}{\sqrt{\pi}} e^{\frac{-(\omega-\omega_0)^2}{a-a(t-t_0)^2}} \cos[\omega(t-t_0) - \omega_0 t]. \end{aligned} \quad (2.13)$$

The first two terms in (2.13), so called self-terms, depend on the size of the window function in such a way that if one of the terms becomes larger, the other must become smaller, and vice versa. The third term represents oscillating cross-terms which fall on the self-terms of the spectrogram [13]. For detailed discussion about the properties of STFT, see [13, pp. 102–112].

Chapter 3

Parametric frequency estimation

3.1. Eigenanalysis-based methods

3.1.1. Introduction

Parametric methods are those which take advantage of known parameters of the signal, such as the number of tones (spectral components) it contains. Non-parametric methods do not make such assumptions *a priori*. Model-based methods for estimation of the *discrete* part of the spectrum only relate to the eigenvector decomposition of the correlation matrix, unlike the model-based estimators for the continuous part of the spectrum (like auto-regressive model or maximum entropy method) which relate to the triangular decomposition of the correlation matrix [85]. Consequently, since waveforms in power systems belong mostly to the group of signals with discrete spectrum, eigendecomposition-based methods are best suited for their analysis [4].

3.1.2. Preliminaries

The following signal model is assumed:

$$x[n] = \sum_{k=1}^N A_k \exp(j\omega_k n) + z[n] \quad (3.1)$$

where $A_k \in \mathbb{C}$ is a complex number representing the magnitude and phase of the k^{th} frequency component and $z[n]$ represents the noise.

The structure of signals composed of several frequency components, usually starts with examining its autocorrelation matrix.

3.1.3. Autocorrelation matrix

The autocorrelation matrix [67] serve as a basis of further developments. It is defined as follows. Let \mathbf{x} be a stochastic vector consisting of N samples of a stochastic process \mathbf{x} :

$$\mathbf{x} = \begin{bmatrix} x(0) \\ x(1) \\ \vdots \\ x(N-1) \end{bmatrix}. \quad (3.2)$$

Correlation matrix of a discrete stochastic process is defined as:

$$\begin{aligned} \mathbf{R}_x &= \mathcal{E} \{ \mathbf{x} \cdot \mathbf{x}^{*T} \} \\ &= \begin{bmatrix} \mathcal{E} \{ |x(0)|^2 \} & \mathcal{E} \{ x(0) x^* \{1\} \} & \cdots & \mathcal{E} \{ x(0) x^* (N-1) \} \\ \mathcal{E} \{ x(1) x^* (0) \} & \mathcal{E} \{ |x(1)|^2 \} & \cdots & \mathcal{E} \{ x(1) x^* (N-1) \} \\ \vdots & \vdots & \ddots & \vdots \\ \mathcal{E} \{ x(N-1) x^* (0) \} & \mathcal{E} \{ x(N-1) x^* (1) \} & \cdots & \mathcal{E} \{ |x(N-1)|^2 \} \end{bmatrix} \\ &= \begin{bmatrix} R_x(0,0) & R_x(0,1) & \cdots & R_x(0,N-1) \\ R_x(1,0) & R_x(1,1) & \cdots & R_x(1,N-1) \\ \vdots & \vdots & \ddots & \vdots \\ R_x(N-1,0) & R_x(N-1,1) & \cdots & R_x(N-1,N-1) \end{bmatrix}. \end{aligned} \quad (3.3)$$

The autocorrelation sequence of a signal $x[n]$ is defined as:

$$\mathbf{r}_x = \mathcal{E} \{ x[n] x^* [n-k] \}, \quad (3.4)$$

and the autocorrelation matrix of $x[n]$ is defined as:

$$\mathbf{R}_x = \begin{bmatrix} r_x[0] & r_x[-1] & \dots & r_x[-N+1] \\ r_x[1] & r_x[0] & \ddots & \\ \vdots & \ddots & \ddots & \vdots \\ r_x[N-1] & & r_x[0] & r_x[-1] \\ & & r_x[1] & r_x[0] \end{bmatrix}. \quad (3.5)$$

For a stationary random signal, the correlation matrix has the form of a symmetric Toeplitz matrix.

3.1.4. Autocovariance matrix

The autocovariance matrix is defined as:

$$\mathbf{C}_x = \mathcal{E} \{ (\mathbf{x} - \mathbf{m}_x) \cdot (\mathbf{x} - \mathbf{m}_x)^{*T} \} \quad (3.6)$$

where \mathbf{m}_x is the mean value of a time series.

Estimation of covariance matrix by forward–backward approach

All of the eigenanalysis-based methods (like MUSIC and ESPRIT) derive their estimates of frequency from the sample covariance matrix $\hat{\mathbf{R}}$. Numerical experiments are claimed to show that better results can be obtained by using a modified sample covariance matrix:

$$\check{\mathbf{R}} = \frac{1}{2}(\hat{\mathbf{R}} + \mathbf{J}\hat{\mathbf{R}}^T\mathbf{J}) \quad (3.7)$$

where \mathbf{J} is the so-called *reversal matrix* :

$$\mathbf{J} = \begin{bmatrix} 0 & & 1 \\ & \ddots & \\ 1 & & 0 \end{bmatrix}. \quad (3.8)$$

Since better results can be obtained only in the case of small number of samples, the theoretical explanation for the superiority is not easy. The heuristic explanation is based on the reasoning, presented in [81]: The second term in (3.7) represents a centrosymmetrical (bisymmetrical) matrix with elements symmetric (in the real-valued case) about its main diagonal and about its anti-diagonal. The true matrix \mathbf{R} is also persymmetric¹,

whereas the sample covariance matrix $\hat{\mathbf{R}}$ is not. Therefore, it can be expected that the frequency estimates are likely to be more accurate by using the forward-backward approach.

3.2. Subspace methods – Introduction

In the next sections, two parametric algorithms: MUSIC and ESPRIT will be introduced, both of which assume a known number of components in the measured signal². The idea is better illustrated by simple cases, as shown below, which lead to the Pisarenko method in section 3.2.3 and are subsequently extended to advanced parametric methods in sections 3.3 and 3.4.

3.2.1. Single frequency component in noise

The one-component signal model can be expressed as:

$$x[n] = A_1 e^{j\omega_1 n} + z[n] \quad (3.9)$$

where $z[n]$ is the white noise. It can be shown that the autocorrelation in (3.4) becomes:

$$r_x[k] = \underbrace{|A_1|^2 e^{j\omega_1 k}}_{\text{signal}} + \underbrace{\sigma_0^2 \delta[k]}_{\text{noise}}, \quad (3.10)$$

which can be represented, using the autocorrelation matrix of (3.5) as:

$$\mathbf{R}_x = \mathbf{R}_{\text{signal}} + \mathbf{R}_{\text{noise}}. \quad (3.11)$$

In the case of one-component signal, the rank of the matrix $\mathbf{R}_{\text{signal}}$ is one, i.e., it has only one non-zero eigenvalue. Additionally:

$$\mathbf{R}_{\text{signal}} = |A_1|^2 \mathbf{e}_1 \mathbf{e}_1^{*T} \quad (3.12)$$

where $\mathbf{e}_1 = [1 \ e^{j\omega_1} \ e^{j\omega_1 2} \ \dots \ e^{j\omega_1(M-1)}]$ is an eigenvector of the matrix $\mathbf{R}_{\text{signal}}$ with eigenvalue $\lambda_1 = M|A_1|^2$.

¹ Persymmetric – matrix that is symmetric about if northeast-southwest diagonal, i.e., $a_{i,j} = a_{n-j+1, n-i+1}$

² This section is partially based on [31].

3.2.2. Multiple frequency components in noise

The simple example in 3.2.1 can be extended to a multi-component case. The signal model is expressed as follows:

$$x[n] = \sum_{k=1}^K A_k e^{j\omega_k n} + z[n]. \quad (3.13)$$

After decomposition into signal and noise parts:

$$\mathbf{R}_x = \mathbf{R}_{signal} + \mathbf{R}_{noise} = \sum_{k=1}^K |A_k|^2 \mathbf{e}_k \mathbf{e}_k^{*T} + \sigma_0^2 \mathbf{I} \quad (3.14)$$

where $\mathbf{e}_k = [1 \quad e^{j\omega_k} \quad e^{j\omega_k 2} \quad \dots \quad e^{j\omega_k(M-1)}]$. Equation (3.14) can be rewritten as:

$$\mathbf{R}_x = \mathbf{E} \mathbf{\Lambda} \mathbf{E}^{*T} + \sigma_0^2 \mathbf{I} \quad (3.15)$$

where $\mathbf{E} = \underbrace{[\mathbf{e}_1 \dots \mathbf{e}_K]}_{M \times K}$ and

$$\mathbf{\Lambda} = \underbrace{\begin{bmatrix} |A_1|^2 & & & & 0 \\ & |A_2|^2 & & & \vdots \\ & & \ddots & & \vdots \\ & & & |A_K|^2 & 0 \\ \hline 0 & \dots & \dots & \dots & 0 \end{bmatrix}}_{M \times M} \quad (3.16)$$

It can therefore be seen that the autocorrelation matrix decomposes into *signal* and *noise* subspaces.

3.2.3. Pisarenko harmonic decomposition

This idea, based on Caratheodory's theorem³, was proposed in [68]. The method assumes that $M = K + 1$, i.e., the dimension of the signal subspace is K and that of the noise is one. There exists only one noise eigenvalue and one noise eigenvector,

³ Caratheodory's theorem defines the conditions which guarantee that the parameters of representation of a signal as the sum of complex harmonics and noise can be determined uniquely.

denoted, respectively, by $\lambda_n = \sigma_0^2$ and \mathbf{u}_n . The noise eigenvector is orthogonal to the signal subspace:

$$\mathbf{u}_n \perp \mathbf{u}_{\text{signal}} \iff \mathbf{u}_n \text{ annihilates the signal components.} \quad (3.17)$$

This is equivalent to (where $\mathbf{e}_k = [1 \ e^{j\omega_k} \ e^{j\omega_k^2} \ \dots \ e^{j\omega_k(M-1)}]$):

$$\mathbf{e}_i^{*T} \mathbf{u}_n[k] e^{-j\omega_i k} = 0. \quad (3.18)$$

This leads to the statement called *annihilating filter* which can be described by:

$$\mathbf{U}_n(z) = \sum_{k=0}^K \mathbf{u}_n[k] z^{-k} = \prod_{k=0}^K (1 - e^{j\omega_k} z^{-1}). \quad (3.19)$$

Proposition 3. *The annihilating filter of (3.19) has zeros lying on the unit circle and their angular positions correspond to the frequencies of the signal. Suppose that the eigenvectors are unit norm. Then:*

$$\begin{aligned} \mathbf{u}_i \mathbf{R}_x &= \lambda_i \mathbf{u}_i, \\ \mathbf{u}_i^{*T} \mathbf{R}_x \mathbf{u}_i &= \lambda_i \mathbf{u}_i^{*T} \mathbf{u}_i = \lambda_i, \\ \mathbf{u}_i \left[\sum_{k=1}^K |A_k|^2 \mathbf{e}_k \mathbf{e}_k^{*T} + \sigma_0^2 \mathbf{I} \right] &= \lambda_i, \\ \sum_{k=1}^K |A_k|^2 |\mathbf{e}_k^{*T} \mathbf{u}_i|^2 &= \lambda_i - \sigma_0^2. \end{aligned} \quad (3.20)$$

It is possible, after the calculation of the signal frequencies, to determine the powers $|A_k|^2$ using (3.20). The phase information is obviously lost as with all correlation-based methods.

Example 4. *The procedure of estimating signal frequencies is as follows:*

- 1) From the available N data samples the autocorrelation sequence $r_x[k]$ is computed for a chosen number of delays k .
- 2) The autocorrelation matrix is formed as:

$$\mathbf{R}_x = \begin{bmatrix} r_x[0] & r_x[1] & \dots & r_x[N-1] \\ r_x[1] & r_x[0] & \ddots & \\ \vdots & \ddots & \ddots & \ddots \\ r_x[N-1] & & r_x[0] & r_x[1] \\ & & r_x[1] & r_x[0] \end{bmatrix}. \quad (3.21)$$

- 3) The autocorrelation matrix is eigendecomposed as: $\mathbf{R}_x = \mathbf{U}\mathbf{\Lambda}\mathbf{U}^{*T}$, where $\mathbf{U} = [\mathbf{u}_1, \mathbf{u}_2, \dots, \mathbf{u}_k]$.
- 4) The smallest eigenvalue λ_{min} and the corresponding eigenvector \mathbf{u}_{min} are found.
- 5) The annihilating filter is formed using the minimum eigenvector \mathbf{u}_{min} as:

$$\mathbf{U}_n(z) = \sum_{k=0}^K \mathbf{u}_{min}[k]z^{-k}. \quad (3.22)$$

- 6) The roots of (3.22) are found as $z = e^{\pm j\omega_k}$.

3.2.4. Pisarenko pseudospectrum

It is possible to plot so-called pseudospectra ("pseudo-" because the amplitude of the peaks in this spectrum carries no information about the true power of each frequency component), by evaluating (3.18) at different frequencies:

$$S(e^{j\omega}) = \frac{1}{|\mathbf{e}(\omega)^{*T} \mathbf{u}_{min}|^2}. \quad (3.23)$$

3.3. MUSIC

The performance of Pisarenko method is very poor in practical applications [85]. The idea of MUSIC (Multiple Signal Classification) was developed in [76] where the *averaging* was proposed for improving the performance of Pisarenko estimator. Instead of using only one noise eigenvector, the MUSIC method uses many *noise eigenfilters*. The number of computed eigenvalues $M > K + 1$. All eigenvalues can be partitioned as follows:

$$\underbrace{\lambda_1 \geq \lambda_2 \geq \dots \lambda_K}_{K \text{ signal eigenvalues}} \geq \underbrace{\lambda_{K+1} \geq \lambda_{K+2} \geq \dots \lambda_M}_{M-K \text{ noise eigenvalues}}. \quad (3.24)$$

Instead of one annihilating filter (as in Pisarenko's estimator), MUSIC method uses $M - K$ noise eigenfilters.

$$U_i(z) = \sum_{m=0}^{M-1} u_i[m]z^{-m}; \quad i = K + 1, \dots, M. \quad (3.25)$$

Every eigenfilter has $M - 1$ roots, K roots are common for all eigenfilters. The common K roots can be found by averaging.

Spurious peaks in MUSIC

MUSIC differs from Pisarenko's method in that correlation matrix is not limited to the dimension $K + 1$, but may be of any dimension $M > K$. This larger autocorrelation matrix is decomposed into its eigenvectors and eigenvalues, and the eigenvectors associated with the largest K eigenvalues are assumed to span the signal space. This implies that the noise space had the dimension $M - K$. Therefore, for each noise eigenvector there will be K zeros which lie on the unit circle and additional $M - K - 1$ zeros which can lie anywhere (also close to the unit circle) in the Z -plane. These additional zeros can give rise to spurious peaks which make it difficult to distinguish between the noise related peaks and the true signal peaks. Pisarenko's method is not affected because it uses only one noise vector.

3.3.1. MUSIC pseudospectrum

It is possible to plot the pseudospectra by evaluating (3.26) at different frequencies:

$$S(e^{j\omega}) = \frac{1}{\sum_{k=K+1}^M |\mathbf{e}(\omega)^* \mathbf{u}_k|^2} \quad (3.26)$$

or by using the *projection matrix* $\mathbf{P}_{noise} = \mathbf{U}_{noise} \mathbf{U}_{noise}^{*T}$, where $\mathbf{U}_{noise} = [\mathbf{u}_{K+1} \dots \mathbf{u}_M]$, as:

$$S(e^{j\omega}) = \frac{1}{\mathbf{e}(\omega)^* \mathbf{P}_{noise} \mathbf{e}(\omega)}. \quad (3.27)$$

3.3.2. MUSIC and Root-MUSIC

In spectral MUSIC the frequencies of the components can be obtained from the estimated signal pseudospectrum (3.26) by finding the position of the maxima. Alternative approach, similar to (3.22) is possible by constructing the polynomials using the eigenvectors spanning the noise subspace, as in (3.25). The roots of each of such polynomials correspond to signal zeros. Now the following expression can be defined [71]:

$$D(z) = \sum_{i=K+1}^M [U_i(z)][U_i^*(1/z^*)]. \quad (3.28)$$

The MUSIC spectrum can be obtained by evaluating $D(z)$ on the unit circle ($D(z)|_{z=e^{j\omega}} = D(e^{j\omega})$).

Using the property that all signal zeros are the roots of (3.25), equation (3.28) can be transformed to:

$$\begin{aligned}
 D(z) &= c \prod_{j=1}^M (1 - z_j z^{-1})(1 - z_j^* z) & (3.29) \\
 &= \prod_{j=1}^K (1 - z_j z^{-1})(1 - z_j^* z) \\
 &\quad \cdot c \prod_{j=K+1}^M (1 - z_j z^{-1})(1 - z_j^* z) \\
 &= H_1(z) H_1^*(1/z^*) H_2(z) H_2^*(1/z^*) & (3.30)
 \end{aligned}$$

where c is a constant and $H_1(z)$ contains the signal zeros, whereas $H_2(z)$ contains the extraneous zeros which lie inside the unit circle on the complex plane. The root-MUSIC procedure uses the most straightforward way to find the roots of $D(z)$ and identify the frequencies of the signal components by using the knowledge that all those roots lie on the unit circle.

3.4. ESPRIT

The original ESPRIT (Estimation of Signal Parameter via Rotational Invariance Technique) was described by Paulraj, Roy and Kailath and later developed, for example, in [74]. It is based on a naturally existing shift invariance between the discrete time series which leads to rotational invariance between the corresponding signal subspaces. The shift invariance is illustrated below.

Proposition 5. *The vector \mathbf{x} of N data samples of the process $x[n] = Ae^{j\omega_1 n}$ (single signal case) can be partitioned as follows:*

$$\begin{aligned}
 \mathbf{x} &= [x_0, x_1, \dots, x_{N-1}], \\
 \mathbf{x} &= A[1, e^{j\omega_1}, e^{j\omega_1 2}, \dots, e^{j\omega_1(N-1)}], \\
 \mathbf{x} &= \underbrace{[x_0, x_1, \dots, x_{N-2}, x_{N-1}]}_{\mathbf{s}_1}, \\
 \mathbf{x} &= [x_0, \underbrace{x_1, \dots, x_{N-2}, x_{N-1}}_{\mathbf{s}_2}], & (3.31)
 \end{aligned}$$

and

$$\mathbf{s}_2 = e^{j\omega_1} \mathbf{s}_1.$$

This approach can be extended to the multiple signal case. After the eigendecomposition of the autocorrelation matrix as:

$$\mathbf{R}_x = \mathbf{U}^{*T} \mathbf{\Lambda} \mathbf{U} \quad (3.32)$$

it is possible to partition a matrix by using special *selector matrices* which select the first and the last $(M - 1)$ columns of a $(M \times M)$ matrix, respectively:

$$\begin{aligned} \mathbf{\Gamma}_1 &= [\mathbf{I}_{M-1} | \mathbf{0}_{(M-1) \times 1}]_{(M-1) \times M}, \\ \mathbf{\Gamma}_2 &= [\mathbf{0}_{(M-1) \times 1} | \mathbf{I}_{M-1}]_{(M-1) \times M}. \end{aligned} \quad (3.33)$$

By using matrices $\mathbf{\Gamma}$ two subspaces are defined, spanned by two subsets of eigenvectors as follows:

$$\begin{aligned} \mathbf{S}_1 &= \mathbf{\Gamma}_1 \mathbf{U}, \\ \mathbf{S}_2 &= \mathbf{\Gamma}_2 \mathbf{U}. \end{aligned} \quad (3.34)$$

Theorem 6. (*Rotational invariance*)

For the matrices defined as \mathbf{S}_1 and \mathbf{S}_2 in (3.34), for every $\omega_k; k \in \mathbb{N}$, representing different frequency components, and matrix $\mathbf{\Phi}$, defined as:

$$\mathbf{\Phi} = \begin{bmatrix} e^{j\omega_1} & 0 & \dots & 0 \\ 0 & e^{j\omega_2} & 0 & 0 \\ \vdots & \vdots & \ddots & \vdots \\ 0 & 0 & \dots & e^{j\omega_k} \end{bmatrix} \quad (3.35)$$

the following relation can be proven [28]:

$$[\mathbf{\Gamma}_1 \mathbf{U}] \mathbf{\Phi} = \mathbf{\Gamma}_2 \mathbf{U}. \quad (3.36)$$

The matrix $\mathbf{\Phi}$ contains all information about frequency components. In order to extract this information, it is necessary to solve (3.36) for $\mathbf{\Phi}$. By using a unitary matrix

(denoted by \mathbf{T})⁴, the following equations can be derived:

$$\begin{aligned}\Gamma_1(\mathbf{UT})\Phi &= \Gamma_2(\mathbf{UT}), \\ \Gamma_1\mathbf{U} \underbrace{(\mathbf{T}\Phi\mathbf{T}^*\mathbf{T})}_{\text{eig. of } \Phi} &= \Gamma_2\mathbf{U}.\end{aligned}\quad (3.37)$$

In further considerations the only interesting subspace is the *signal subspace*, spanned by signal eigenvectors \mathbf{U}_s . Usually it is assumed that these eigenvectors correspond to the largest eigenvalues of the correlation matrix and $\mathbf{U}_s = [\mathbf{u}_1, \mathbf{u}_2, \dots, \mathbf{u}_K]$. ESPRIT algorithm determines the frequencies $e^{j\omega_K}$ as the eigenvalues of the matrix Φ .

In theory, equation (3.36) is satisfied exactly [85]. In practice, matrices \mathbf{S}_1 and \mathbf{S}_2 are derived from an estimated correlation matrix, so this equation does not hold exactly, which means that (3.36) represents an overdetermined set of linear equations.

3.4.1. Total least squares ESPRIT

Total least squares (TLS) approach takes into account possible errors ($\Delta_{S_1}, \Delta_{S_2}$) for both estimated matrices \mathbf{S}_1 and \mathbf{S}_2 . The total least squares problem has the form:

$$(\mathbf{S}_1 + \Delta_{S_1})\Phi = \mathbf{S}_2 + \Delta_{S_2}.\quad (3.38)$$

The TLS solution minimizes the Frobenius⁵ norm of the error matrix

$$\|\Delta_{S_1} \Delta_{S_2}\|_F.\quad (3.39)$$

The solution can be obtained using the singular value decomposition⁶. Let \mathbf{V} be the matrix of right singular vectors of the matrix $[\mathbf{S}_1 \mathbf{S}_2]$. If the matrix \mathbf{V} is partitioned into four square parts of equal size, as follows:

$$\mathbf{V} = \begin{bmatrix} \mathbf{V}_{11} & \mathbf{V}_{12} \\ \mathbf{V}_{21} & \mathbf{V}_{22} \end{bmatrix},\quad (3.40)$$

⁴ complex orthogonal matrix, with unit length columns, for which $\mathbf{X}^*\mathbf{T}\mathbf{X} = \mathbf{I}$.

⁵ The Frobenius norm, also called the Euclidean norm of an $m \times n$ matrix \mathbf{X} , is a matrix norm defined as $\|\mathbf{X}\|_F = \sqrt{\sum_{i=1}^m \sum_{j=1}^n |x_{ij}|^2}$.

⁶ The Singular Value Decomposition (SVD) of the matrix \mathbf{X} produces a diagonal matrix \mathbf{S} , of the same dimension as \mathbf{X} and with nonnegative diagonal elements in decreasing order, and unitary matrices \mathbf{U} and \mathbf{V} , so that $\mathbf{X} = \mathbf{USV}^T$.

then the solution is given by [85]:

$$\Phi_{\text{TLS}} = -\mathbf{V}_{12} \mathbf{V}_{22}^{-1}. \quad (3.41)$$

3.5. Properties of frequency estimation methods

The performance (error of estimation) of the subspace methods has been extensively investigated in the literature, especially in the context of the Direction-of-Arrival (DOA) estimation.

Comparison of mean square error is useful for theoretical assessment of accuracy of both methods with emphasis on root-MUSIC and ESPRIT. Both methods are similar in the sense that they are both eigendecomposition-based methods which rely on decomposition of the estimated correlation matrix into two subspaces: noise and signal subspace. On the other hand, MUSIC uses the noise subspace to estimate the signal components, while ESPRIT uses the signal subspace. In addition, the approach is in many points different. Numerous publications were dedicated to the analysis of the performance of the aforementioned methods (e.g., [70],[19],[82],[83], [71],[25],[26]). Unfortunately, due to many simplifications, different assumptions and the complexity of the problem, published results are often contradictory and sometimes misleading.

Other parametric spectrum estimation methods, like min-norm [59], were investigated by the author. Additionally, excellent resolution of these methods enabled efficient use of them as a tool for detection of closely spaced sinusoidal components in the context of detection of out-of-step operation of synchronous machines [29], [37]. However, the comparison of accuracy of two different parametric methods is for the first time presented in this work.

When roughly summarizing different results from the literature, a resume of basic parameters can be established, as shown in Table 3.1.

Table 3.1. Comparison of basic performance characteristics of parametric spectral methods.

| Method | Computational cost | Accuracy | Risk of false estimates |
|-------------|--------------------|-----------|-------------------------|
| Periodogram | small | medium | medium |
| Pisarenko | small | low | none |
| MUSIC | high | high | medium |
| ESPRIT | medium | very high | none |

3.6. Performance analysis of MUSIC

The root-MUSIC algorithm (see 3.3.2) uses the estimated covariance matrix to compute the signal zeros from (3.28). From (3.29) we can obtain the relation between the error of the signal zeros and the estimated $D(z)$ [71]. When analyzing the mean squared error (MSE) of the signal zeros estimates, the relationship between the errors in signal zeros and the estimated $D(z)$ (as in (3.29)) is as follows:

$$D(z) = c \sum_{l=1}^{L-1} (1 - (z_l + \Delta z_l)z^{-1})(1 - (z_l + \Delta z_l)^* z). \quad (3.42)$$

When evaluating the errors of $D(z)$ on the unit circle ($D(z)|_{z=e^{j\omega}} = D(e^{j\omega})$):

$$\begin{aligned} D(e^{j\omega_i}) &= c|\Delta z_i|^2 \prod_{l=1, l \neq i}^{L-1} |1 - (z_l + \Delta z_l)z_i^{-1}|^2 \\ &\approx c|\Delta z_i|^2 \prod_{l=1, l \neq i}^{L-1} |1 - z_l z_i^{-1}|^2. \end{aligned} \quad (3.43)$$

Taking the expected value on both sides, we obtain:

$$\begin{aligned} \mathcal{E}\{|\Delta z_i|^2\} &= \frac{\mathcal{E}\{D(e^{j\omega_i})\}}{c \prod_{l=1, l \neq i}^{L-1} |1 - z_l z_i^{-1}|^2} \\ &= S_{\text{MUSIC}} \frac{\mathcal{E}\{D(e^{j\omega_i})\}}{L} \end{aligned} \quad (3.44)$$

where L is the number of samples and S_{MUSIC} can be seen as a sensitivity parameter of the root-MUSIC method and is equal to [71]:

$$S_{\text{MUSIC}} = \frac{L}{c \prod_{l=1, l \neq i}^{L-1} |1 - z_l z_i^{-1}|^2} = L \lim_{\omega \rightarrow \omega_i} \frac{|1 - e^{j\omega_i} e^{-j\omega}|^2}{D(e^{j\omega})}. \quad (3.45)$$

After introducing the derivative of $\mathbf{V}(\omega)$:

$$\mathbf{V}'^T(\omega) = \frac{1}{\sqrt{L}} (0, j e^{j\omega}, 2j e^{2j\omega}, \dots, j(L-1) e^{j(L-1)\omega}) \quad (3.46)$$

and taking into account that $D(j\omega) = \mathbf{V}^H(\omega)\mathbf{P}_{noise}\mathbf{V}(\omega)$, S_{MUSIC} becomes:

$$S_{MUSIC} = \frac{L}{\mathbf{V}'^H(\omega_i)\mathbf{P}_{noise}\mathbf{V}'(\omega_i)} \quad (3.47)$$

where, (see (3.14), (3.25) and (3.27)), $\mathbf{P}_{noise} = \mathbf{I} - \mathbf{P}_{signal}$.

From (3.15) and considering that:

$$\begin{aligned} D(j\omega) &= \mathbf{V}^H(\omega)(\mathbf{I} - \mathbf{P}_{signal})\mathbf{V}(\omega) \\ &= 1 - \mathbf{V}^H(\omega) \left(\sum_{l=1}^M \mathbf{e}_l \mathbf{e}_l^H \right) \mathbf{V}(\omega), \end{aligned} \quad (3.48)$$

and that estimated $\hat{\mathbf{e}}_l = \mathbf{e}_l + \eta_l$, where η is the respective estimation error, it is possible to formulate the MSE of the roots in root-MUSIC [71], as (see (3.44)):

$$\mathcal{E}\{|\Delta z_i|^2\} = \frac{S_{MUSIC}}{L} \cdot \frac{(L-M)\sigma_{noise}^2}{N} \left(\sum_{k=1}^M \frac{\lambda_k}{(\lambda_k - \sigma_{noise}^2)^2} \right) \left| \mathbf{V}^H(\omega_i)\mathbf{e}_k \right|^2 \quad (3.49)$$

where N is the dimension of the covariance matrix and M is the dimension of signal subspace.

In the case of single signal source with the following parameters: power P_1 , $\lambda_1^{signal} = L \cdot P_1$, $\lambda_1 = \lambda_1^{signal} + \sigma_{noise}^2$, and $\mathbf{e}_1 = \mathbf{V}(\omega_1)$, the sensitivity of root-MUSIC is given by [71] (see (3.47)):

$$S_{MUSIC} = \frac{L}{\mathbf{V}_1^H(\omega_1)\mathbf{P}_{noise}\mathbf{V}_1(\omega_1)} = \frac{12L}{(L-1)(L+1)}. \quad (3.50)$$

Using (3.49), the expected error of estimation will be [70]:

$$\mathcal{E}\{|\Delta z_1|^2\} = \frac{12L}{(L-1)(L+1)} \cdot \frac{\lambda_1 \sigma_{noise}^2 (L-1)}{LN(LP_1)^2} \approx \frac{12\sigma_{noise}^2}{L^2 P_1 N}. \quad (3.51)$$

The analysis of more than one source case is analytically very difficult (see [71]) and demands more arbitrary assumptions about the SNR and other signal parameters. Although reported results of numerical simulations show good correspondence to derived analytical expressions, their usefulness is quite limited.

3.7. Performance analysis of ESPRIT

In the case of ESPRIT algorithm (see 3.4), the main source of errors is the estimate of the matrix Φ . Equation (3.36) can be solved for Φ using Least Squares or Total Least Squares approach (3.41). The choice of approach has no influence on asymptotical performance of ESPRIT as shown in [71].

The error in the matrix Φ , denoted by Δ_Φ , causes errors in the eigenvalues of Φ . The error of an eigenvalue (here denoted by Δz_i), which can be regarded as a performance index of ESPRIT and can be approximated by:

$$\Delta z_i = \mathbf{p}_i \Delta_\Phi \mathbf{e}_i \quad (3.52)$$

where \mathbf{e}_i is the eigenvector of Φ corresponding to the eigenvalue z_i , whereas \mathbf{p}_i is the corresponding *left* eigenvector, so that $\Phi \mathbf{e}_i = z_i \mathbf{e}_i$ and $\mathbf{p}_i \Phi = z_i \mathbf{p}_i$.

From (3.38), the approximation of error $\Delta \Phi$ can be derived using:

$$(\mathbf{S}_1 + \Delta_{S_1})(\Phi + \Delta_\Phi) \approx (\mathbf{S}_2 + \Delta_{S_2}) \quad (3.53)$$

as:

$$\Delta_\Phi \approx \mathbf{S}_1^+ \Delta_{S_2} - \mathbf{S}_1^+ \Delta_{S_1} \Phi \quad (3.54)$$

By substituting (3.54) in (3.52) it is possible to obtain expression for MSE of Δz_i (where Γ_1, Γ_2 are defined as in (3.33), \mathbf{U} as in (3.32) and ζ is the respective eigenvalue estimation error), as [70]:

$$\begin{aligned} \mathcal{E}\{|\Delta z_i|^2\} &= \mathbf{p}_i \mathbf{S}_1^+ (\Gamma_1 - z_i^* \Gamma_2) \mathcal{E} \left\{ \Delta_U \mathbf{e}_i \mathbf{e}_i^H \Delta_U^H \right\} \\ &\quad \cdot (\Gamma_1 - z_i^* \Gamma_2)^H \mathbf{S}_1^{+H} \mathbf{p}_i^H \\ &= \mathbf{p}_i^H \mathbf{S}_1^{+H} \left[\sum_{j=1}^M |e_{ij}|^2 (\Gamma_1 - z_i^* \Gamma_2) \mathcal{E} \left\{ \zeta_j \zeta_j^H \right\} (\Gamma_1 - z_i^* \Gamma_2)^H \right] \\ &\quad \cdot \mathbf{p}_i \mathbf{S}_1^+ \\ &= \mathbf{p}_i^H \mathbf{S}_1^{+H} (\Gamma_1 - z_i^* \Gamma_2) \left[\sum_{j=1}^M |e_{ij}|^2 \frac{\lambda_j}{N} \sum_{k=1, k \neq j}^L \frac{\lambda_k}{(\lambda_j - \lambda_k)^2} U_k U_k^H \right] \\ &\quad \cdot (\Gamma_1 - z_i^* \Gamma_2)^H \mathbf{p}_i \mathbf{S}_1^+ \end{aligned} \quad (3.55)$$

where L is the number of samples, N is the dimension of the covariance matrix and M is the dimension of signal subspace.

In the case of single signal source with the following parameters: power P_1 , $\lambda_1^{signal} = L \cdot P_1$, $U_1 = \mathbf{V}(\omega_1) = \frac{1}{\sqrt{L}} [1, e^{j\omega_1}, \dots, e^{j(L-1)\omega_1}]^T$, the dominant term of MSE of ESPRIT is given by substituting for the parameters in (3.55) [70]:

$$\mathcal{E}\{|\Delta z_1|^2\} \approx \frac{2\sigma_{noise}^2}{L^2 P_1 N}. \quad (3.56)$$

It can be noted that, approximately, the mean square error of MUSIC (3.51) is six times higher than the MSE of ESPRIT (3.56) in the case of a single signal source.

Chapter 4

Time-Varying Spectrum

4.1. Quasi-stationarity

One of the main problems in stochastic signal analysis is that it is impossible to average over the infinite sample of realizations of a stochastic process. Under the assumption of *ergodicity*, it is possible to carry out the averaging over time. In the case of non-stationary processes, even such an operation is not allowed, because the averaging over time removes all time-varying characteristic parameters of the signal [64]. When analyzing non-stationary processes the term of *quasi-stationarity* is introduced. It is assumed that the autocovariance function C of the signal changes slowly enough to satisfy the condition:

$$|C(t + \tau, t - \tau) - C_s(2\tau)| < \varepsilon(T). \quad (4.1)$$

It is assumed that at every time point t there exists a stationary function C_s and a time interval T for which the inequality (4.1) holds. The *stationarity interval* T_s is such a shortest T that satisfies this equation.

Definition 7. A stochastic process is *quasi-stationary* if $T_s > 0$ for a given $\varepsilon > 0$, where ε is a measure of approximation.

4.2. Locally stationary processes

Gaussian processes can be fully characterized by their second order moments which are often sufficient to build stochastic models, even for non-Gaussian processes [63]. Many spectral estimation algorithms allow one to estimate the covariance operator from few or only one realization, by taking advantage of its diagonalization in the Fourier basis. Since one only takes into account second order moments, the process is assumed stationary in the wide sense. When the process is non-stationary, the covariance operator may have complicated time-varying properties. Its estimation is then much more

difficult. In this work, only locally stationary processes are considered whose covariance operators have time varying properties that vary smoothly and slowly in time. To estimate the covariance of a locally stationary process one searches for a local basis which estimates the necessary covariance values. The window size must be adapted to the size of the intervals where the process is approximatively stationary. The size of approximate stationarity intervals is not known in advance, so in some publications adaptive algorithms are introduced that search for the "best" interval [15].

Locally stationary processes appear in many physical systems that change slowly in time or space. Over short time intervals, such processes can be approximated by a stationary process [13]. This is the case for many problems in electrical power systems. Many recorded waveforms have a strong almost stationary component (e.g., fundamental frequency of the power supply and weaker time-varying components of stochastic or deterministic origin which can have significant non-stationary character [5]). The length of stationary time intervals can however vary greatly depending upon the type of problem.

Since the size of approximate stationarity intervals is not known in advance, it is possible to design an algorithm that searches throughout a given time interval, for a "best" time-frequency region which allows the performance index to be maximized (e.g., best classification rate, best parameter estimation accuracy). This search can be based on the information provided by few previous realizations of the process.

Approximation by a stationary process

Let $X(t)$ be a real valued zero-mean process with correlation [63]:

$$R(t, u) = \mathcal{E}\{X(t)X(u)\}. \quad (4.2)$$

We define the covariance operator $\mathbf{C}\{.\}$ for arbitrary function $f(t) \in \mathbb{L}^2$ as:

$$\mathbf{C}\{f(t)\} = \int_{-\infty}^{\infty} R(t, u)f(u)du. \quad (4.3)$$

The inner product is a random variable which is a linear combination of the process values at different times:

$$\langle f, X \rangle = \int_{-\infty}^{\infty} f(t)X(t)dt. \quad (4.4)$$

For any $f, g \in \mathbb{L}^2$, the covariance operator yields the cross-correlation:

$$\langle \mathbf{C}\{f\}, g \rangle = \mathcal{E}\{\langle f, X \rangle \langle g, X \rangle^*\}. \quad (4.5)$$

The covariance can be expressed from the distance between t and u and their mid-point position. When the process is stationary, its covariance satisfies the condition:

$$R(t, u) = \mathbf{C}_0(t - u). \quad (4.6)$$

Under assumption that the process is locally stationary, we can assume that in the neighborhood of any $x \in \mathbb{R}$, there exists a finite interval of size $l(x)$ where the process can be approximated by a stationary process.

The covariance operator can also be interpreted as a time-varying convolution:

$$\mathbf{C}\{f(t)\} = \int_{-\infty}^{\infty} \mathbf{C}_0\left(\frac{t+u}{2}, t-u\right) du. \quad (4.7)$$

Under assumption that $\mathbf{C}(v, w)$ is a smooth function of v we can introduce a time-varying spectrum by application of Fourier transform

$$S(w, \omega) = \int_{-\infty}^{\infty} R\left(v - \frac{w}{2}, v + \frac{w}{2}\right) e^{-j\omega w} dw. \quad (4.8)$$

If the process $X(t)$ is locally stationary it is possible to show (by first order approximation) that $S(x, \xi)$ for any x, ξ can be approximated by an eigenvalue of $\mathbf{C}\{f(t)\}$ [63]. Moreover, the approximate eigenvector $\varepsilon_{x,\xi}$ is built with complex exponentials $e^{-j\xi t}$ over the interval of local stationarity $\left[x - \frac{l(x)}{2}, x + \frac{l(x)}{2}\right]$, yielding:

$$\mathbf{C}\{\varepsilon_{x,\xi}\} \approx S(x, \xi)\varepsilon_{x,\xi}(t). \quad (4.9)$$

Let $h(t)$ be a smooth window function with support $\left[x - \frac{l(x)}{2}, x + \frac{l(x)}{2}\right]$ and

$$\varepsilon_{x,\xi}(t) = h(t)e^{-j\xi t}, \quad (4.10)$$

so:

$$\mathbf{C}\{\varepsilon_{x,\xi}(t)\} \approx \int_{-\infty}^{\infty} C_0(x, t-u)\varepsilon_{x,\xi}(u)du. \quad (4.11)$$

Applying the Parseval theorem yields:

$$\mathbf{C}\{\varepsilon_{x,\xi}(t)\} \approx \frac{1}{2\pi} \int_{-\infty}^{\infty} S(x, \omega)e^{j\omega t}\hat{\varepsilon}_{x,\xi}(\omega)d\omega \quad (4.12)$$

where $\hat{\varepsilon}_{x,\xi}(\omega) = \hat{h}_x(\omega - \xi)$. Since the energy of $\hat{h}_x(\omega)$ is mostly concentrated in $\left[-\frac{\pi}{l(x)}, \frac{\pi}{l(x)}\right]$, the energy of $\hat{\varepsilon}_{x,\xi}(\omega)$ is approximately localized in $\left[\xi - \frac{\pi}{l(x)}, \xi + \frac{\pi}{l(x)}\right]$.

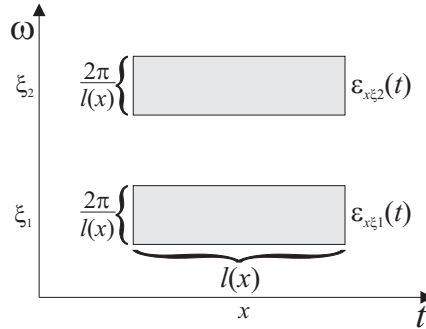


Figure 4.1. Energy concentration of two harmonic components in the time-frequency plane.

Since the Fourier transform as in (4.12) is smooth and approximately constant over $\left[\xi - \frac{\pi}{l(x)}, \xi + \frac{\pi}{l(x)}\right]$, so in the time-frequency plane (t, ω) the energy of $\varepsilon_{x, \xi}$ is mainly concentrated inside the rectangle:

$$\left[x - \frac{l(x)}{2}, x + \frac{l(x)}{2}\right] \times \left[\xi - \frac{2\pi}{l(x)}, \xi + \frac{2\pi}{l(x)}\right]. \quad (4.13)$$

An important property of locally stationary processes follows from the previous considerations, namely that $S(t, \omega)$ is approximately constant over the time-frequency support of $\varepsilon_{x, \xi}$. This property is shown in Figure 4.1.

A full covariance matrix cannot be estimated reliably from few realizations of the process. Locally stationary processes are well approximated by a covariance matrix in an appropriate local basis, which depends upon the size $l(x)$ of stationarity intervals. Usually, we do not know this interval in advance. The approximation of covariance matrix should be calculated in practice from N independent realizations of a zero mean process $X(t)$ which yields a small expected error.

In practice, such assumptions cannot be easily fulfilled. In conclusion, it can be observed that most of the processes can be analyzed inside their stationarity intervals and inside their frequency support domains (inside their time-frequency supports) where most of the energy is concentrated. Such an approximation by locally stationary processes allows straightforward analysis of most slowly time-varying signals.

The length of stationarity interval can be determined in accordance with the characteristic parameters of the signal when these parameters are known in advance. According to author's experience such a situation rarely occurs. Usually, the shortest interval is chosen which still ensures expected accuracy of spectral representation inside chosen

time interval. In the case of non-parametric methods (like STFT) the most important limitation is not the length of stationarity intervals of signal under investigation but the low resolution (spectral smearing) inherent in these methods. In the case of parametric methods, the trade-off between time and frequency-domain resolution is significantly lower [61].

Chapter 5

Filter banks for line spectra

5.1. Introduction

Traditionally, the method of spectrum estimation by using the filter banks assumes that the true spectrum of the signal $\phi(\omega)$ is constant inside a specified frequency band. This method is used when there is no information about the structure of the signal (like line spectra or rational spectra). Typical of this method is a trade-off between the resolution and statistical accuracy. If high resolution is desired, a very sharp pass-band filter is required. This is obtained only by filters that have very long impulse response. This means, according to the *Time-Bandwidth* product (TB-product), that only few samples (in frequency domain) can be used in such a case and statistical accuracy is poor. In order to improve the statistical accuracy, it is necessary to sum up many samples of filtered signals in frequency domain. According to the TB-product this means that filter impulse response has to be relatively short, i.e., filter should not be very narrow in frequency and, consequently, the resolution decreases. This approach is used by the widely known: *Thomson multitaper method* (which uses *Slepian* baseband filters) and the *Capon method*.

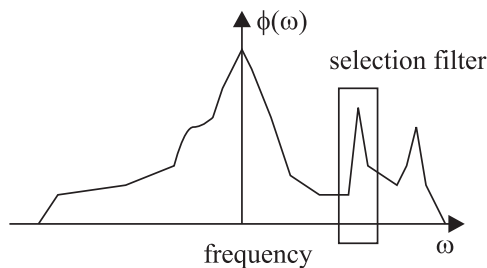


Figure 5.1. Filter bank approach for spectrum estimation

Filter banks can be effectively used as the preprocessing tool for high-resolution subspace methods [9]. First motivation which directed the author towards filterbank approach were difficulties in analyzing multi-component distorted waveforms from inverter drives [5]-[7]. Since a lower number of components inside a chosen frequency band leads to more accurate results, the subband filtering was applied. The improvement of accuracy is not only due to limitation to the number of sinusoidal components (which is important only for parametric methods [34]) but also due to SNR and resolution enhancement, as shown below.

5.2. Usefulness of filter banks

The problem of estimating the frequencies of sinusoids buried in noise has been of great interest in the signal processing since 1973 [68]. Although many methods have been proposed to solve this problem, most involve processing in the fullband. In paper [86] it was shown that with properly chosen analysis filters, the local signal-to-noise ratio (SNR) and line resolution in the subbands can be improved.

5.2.1. Subband filtering

When dealing with the problem of estimating the parameters of sinusoids buried in noise (see 3.2), the input signal model can be expressed as:

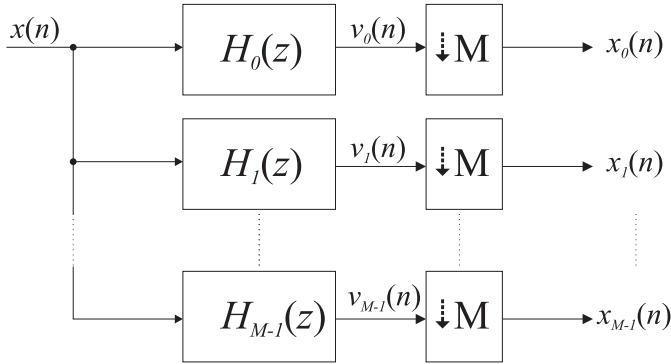
$$x(n) = \sum_{i=1}^N A_i s_i(n) + \eta(n); s_i(n) = e^{j\omega_i n}; A_i = |A_i| e^{j\phi_i} \quad (5.1)$$

where N sinusoidal signals with amplitudes A_i are buried in complex noise process η . The complex amplitudes are assumed to have constant magnitudes and phase angles ϕ which are pairwise independent. Regardless of the type of filter used in the filter bank (see Figure 5.2), the filter decomposes the input signal $x(n)$ into the subband signals $x_m(n)$ and $v_m(n)$ [86]:

$$x_m(n) = \sum_{i=1}^N A_i H_m e^{j\omega_i} e^{j\omega_n} + w_m(n) \quad (5.2)$$

$$v_m(n) = \sum_{i=1}^N A_i H_m e^{jM\omega_i} e^{j\omega_n} + \eta_m(n) \quad (5.3)$$

for $m = 0, 1, \dots, M - 1$, where $w_m(n) = h_m(n) * \eta(n)$ and $\eta_m(n) = w_m(Mn)$.

Figure 5.2. M -channel uniform analysis filter bank

Each subband signal as in (5.2) also consists of sinusoidal components with noise $\eta_m(n)$. The autocorrelation function of each subband signal has the form

$$R_{x_m}(k) = \sum_{i=1}^N P_i |H_m e^{jM\omega_i}|^2 e^{jM\omega_i k} + R_{\eta_m \eta_m}(k) \quad (5.4)$$

where P_i is the power of each sinusoidal component. Under the assumptions that the noise has the variance σ_η^2 and the magnitude of the squared response of the filter is $[|H_m e^{j\omega}|^2]_{\downarrow M} = 1$ for all $m = 0, 1, \dots, M - 1$ (see Figure 5.3), each subband noise process is white with variance σ_η^2 and each of subband signals has the same shape as the input signal. The difference is that the sinusoidal components are scaled by the frequency responses of the analysis filters and their frequencies are mapped to other locations, namely $\omega_i \rightarrow (M\omega_i \bmod 2\pi)$ [86].

In [5]–[8], the author applied non-uniform filter banks where the bandwidth and frequency are adapted to known characteristic parameters of signals under investigation.

5.2.2. Increase of the resolution of line spectra

From the previous considerations it follows that, taken as example, two line spectral components (sinusoids) are separated in the fullband by $\Delta\omega = \omega_q - \omega_p$ (see Figure 5.4), where

$$\begin{aligned} \omega_p &= \frac{2\pi m}{M} + \theta_p, \\ \omega_q &= \frac{2\pi m}{M} + \theta_q, \end{aligned} \quad (5.5)$$

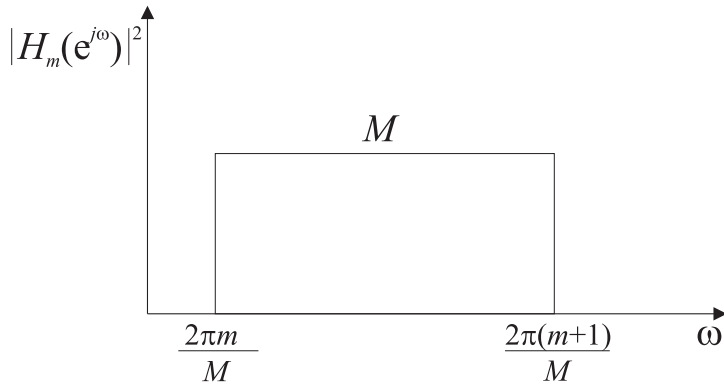


Figure 5.3. Ideal analysis filter.

for $\theta_p > 0, \theta_q < \frac{2\pi}{M}$. Additionally, $\Delta\omega_f = \theta_q - \theta_p$ and the autocorrelation function is given by:

$$R_{xms}(k) = MP_p e^{j\hat{\omega}_p k} + MP_q e^{j\hat{\omega}_q k} + \sigma_\eta^2 \delta(k) \quad (5.6)$$

where $\hat{\omega}_p = M\omega_p \bmod 2\pi$, $\hat{\omega}_q = M\omega_q \bmod 2\pi$.

Then, from (5.5) it follows that:

$$\begin{aligned} \hat{\omega}_p &= M\theta_p, \\ \hat{\omega}_q &= M\theta_q, \end{aligned} \quad (5.7)$$

and

$$\Delta\omega_s = M\Delta\omega \quad (5.8)$$

Thus, the spacing between line components increased M times. Also, the resolution of the spectrum increased. All frequency estimation methods show a certain threshold, below which two closely spaced sinusoidal components will be estimated as one. As shown in [33] and [32], such a limitation is significantly lower when comparing non-parametric and parametric methods.

5.2.3. Backward mapping of the subband frequencies into fullband

When using ideal, non-overlapping filters, the mapping is straightforward. It is not necessary to use the information from other subbands to map the frequencies correctly. The problem is much more complicated in the case of overlapping filters where one

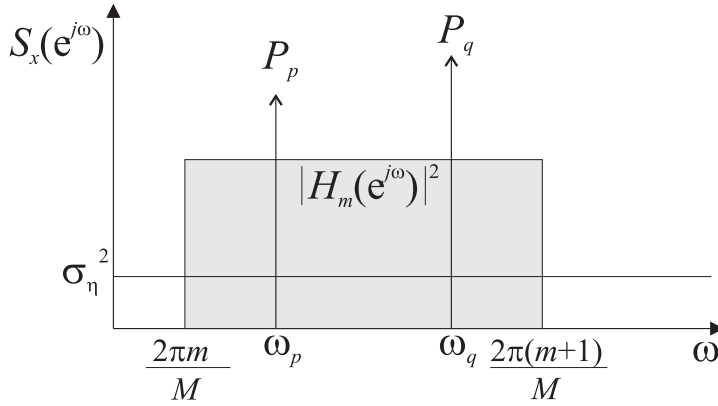


Figure 5.4. Spectrum of two sinusoidal components and filter

frequency component can be present in many subbands (for details, see [88]). The full-band components ω_f can be obtained by using the following relations from the subband components $\hat{\omega}_i$ [87].

- In the case of complex signal model:

$$\omega_{f,i} = \frac{2\pi m + \hat{\omega}_{i,m}}{M}. \quad (5.9)$$

- In the case of real signal model:

$$\omega_{f,i} = \begin{cases} \frac{\pi m + \hat{\omega}_{i,m}}{M}, & m \text{ even,} \\ \frac{\pi(m+1) - \hat{\omega}_{i,m}}{M}, & m \text{ odd.} \end{cases} \quad (5.10)$$

5.2.4. Increase of the SNR

Consider the ideal filter as in Figure 5.3 with the magnitude squared response $|H_m(e^{j\omega})|^2 = 1$ for all subbands and the subband frequency range $I_m = [\frac{2\pi m}{M}, \frac{2\pi(m+1)}{M}]$. The autocorrelation function in that case is expressed by:

$$R_{xm}(k) = \underbrace{(MP_i)}_{\hat{P}_i} e^{jM\omega_i k} + \sigma_\eta^2 \delta(k). \quad (5.11)$$

The power of each sinusoidal component in the subband is equal to $\hat{P}_i = MP_i$. From (10.1) it follows that for each $\omega_i \in I_m$

$$SNR_{subband,i} = M \cdot (SNR_{fullband,i}). \quad (5.12)$$

In the case of low SNR the increase of accuracy of the subspace methods is to be expected.

5.2.5. Limits

A simple extension of subband decomposition could lead to the conclusion that it is possible to increase indefinitely the SNR and resolution of subspace methods by using decimation factor M as large as possible. In practice, the autocorrelation is estimated from a finite number of data samples. The quality of this estimation strongly depends on the number of data samples N_s . When the length of the subband filter is N_f , then the length of each subband signal will be

$$\frac{N_s + N_f - 2}{M} + 1. \quad (5.13)$$

The large filter length which makes the subband signal longer than the original number of data samples introduces a bias to the estimate of the autocorrelation function of the subband signals, because of the small number of data samples filtered by a long filter sequence.

Chapter 6

Complex space-phasor

The method of symmetric components is widely used for analysis and visualization of the three-phase electric circuits [54]. This method has strong limitations, e.g., it allows the analysis of the stationary waveforms only.

In practice, a three-phase signal can include the main component, harmonics and noise. Additional disturbances can appear due to transient phenomena and non-linear loads. There exist many possible ways of description of three-phase quantities which aim to simplify the analysis or modelling of electric systems. One of them is the complex space-phasor¹ [30].

The time-frequency decomposition of the space phasor (computed for three-phase power system signals) using Wigner–Ville transform and min-norm method was proposed and developed by the author in [32]. It enables tracking the frequency and amplitude changes of non-stationary signals with higher resolution than FFT-based methods [45], [49], [62]. Space-phasor is also successfully applied to classification schemes in [40] and [52].

6.1. Definitions

Definition 8. *The complex space-phasor is given by [30]:*

$$\mathbf{f} = \frac{(f_\alpha + jf_\beta)}{\sqrt{2}} \quad (6.1)$$

where

$$\begin{bmatrix} f_\alpha \\ f_\beta \end{bmatrix} = \sqrt{\frac{2}{3}} \begin{bmatrix} 1 & -\frac{1}{2} & -\frac{1}{2} \\ 0 & \sqrt{\frac{3}{2}} & -\sqrt{\frac{3}{2}} \end{bmatrix} \begin{bmatrix} f_R \\ f_S \\ f_T \end{bmatrix}. \quad (6.2)$$

¹ German: Raumzeiger

It describes, in addition to the positive-sequence component, an existing negative-sequence component, harmonic and non-harmonic frequency components of the signal.

Full and unique description of the three-phase system is possible by introducing the *zero-sequence component* defined as:

$$f_0 = \frac{1}{3} (f_R + f_S + f_T). \quad (6.3)$$

6.2. The space-phasor and three-phase systems

For a three-phase system (as in symmetric components method) it is possible to formulate the space-phasor \mathbf{f} using the instantaneous quantities existing in symmetrical three-phase system as follows [75]:

$$f_R = \mathbf{A}_{(1)} \sin(\omega t + \gamma) = \frac{1}{2} (\mathbf{A}_{(1)} e^{j\omega t} + \mathbf{A}_{(1)}^* e^{-j\omega t}) e^{j\gamma}, \quad (6.4)$$

$$f_S = \mathbf{A}_{(1)} \sin\left(\omega t + \gamma - \frac{2\pi}{3}\right) = \frac{1}{2} (a^2 \mathbf{A}_{(1)} e^{j\omega t} + a \mathbf{A}_{(1)}^* e^{-j\omega t}) e^{j\gamma}, \quad (6.5)$$

$$f_T = \mathbf{A}_{(1)} \sin\left(\omega t + \gamma + \frac{2\pi}{3}\right) = \frac{1}{2} (a \mathbf{A}_{(1)} e^{j\omega t} + a^2 \mathbf{A}_{(1)}^* e^{-j\omega t}) e^{j\gamma}, \quad (6.6)$$

where $a = e^{j\frac{2\pi}{3}}$. After substituting the above equations to (6.1) we obtain:

$$\mathbf{f} = \mathbf{A}_{(1)} e^{j\omega t} e^{j\gamma}. \quad (6.7)$$

For the positive-sequence component the space-phasor rotates in the positive direction.

For the negative-sequence component it rotates in the negative direction, and is described by the formula:

$$\mathbf{f} = \mathbf{A}_{(2)} e^{-j\omega t} e^{-j\gamma}. \quad (6.8)$$

In the case of unsymmetrical sinusoidal three-phase waveforms, the space-phasor is a sum of two vectors rotating in opposite directions.

$$\mathbf{f} = \mathring{\mathbf{A}}_{(1)} e^{j\omega t} + \mathring{\mathbf{A}}_{(2)}^* e^{-j\omega t}. \quad (6.9)$$

This equation describes an ellipse whose one axis is equal to the sum of amplitudes of the positive- and negative-sequence components and the second axis is equal to their difference.

Description of the space-phasor using Fourier series

Any periodic waveform which represents the space-phasor can be transformed to Fourier series:

$$\mathbf{f}(\omega t) = \sum_{n=-\infty}^{n=\infty} \mathbf{A}_n e^{jn\omega t}. \quad (6.10)$$

Existing in the Fourier series expansion harmonics with positive indexes correspond to the positive-sequence systems which rotate in the direction of the rotor and harmonics with negative indexes correspond to the negative-sequence systems which rotate in the opposite direction to the rotor.

Two main harmonics of the space-phasor with indexes $n = 1$ and $n = -1$ correspond to the positive sequence component and negative sequence component, respectively.

Therefore, it follows that:

$$\dot{\mathbf{A}}_{(1)} = \mathbf{A}_n|_{n=1}, \quad \dot{\mathbf{A}}_{(2)} = \mathbf{A}_n^*|_{n=-1}. \quad (6.11)$$

Space-phasor and higher harmonic components

When in the three-phase system the higher harmonics (with the frequencies which are natural multiples of the main component) are present, their time waveforms can be described as [79]:

$$f_{Rk}(t) = \mathbf{A}_k \sin(k\omega t + \gamma_k), \quad (6.12)$$

$$f_{Sk}(t) = \mathbf{A}_k \sin\left[k\left(\omega t - \frac{2\pi}{3}\right) + \gamma_k\right], \quad (6.13)$$

$$f_{Tk}(t) = \mathbf{A}_k \sin\left[k\left(\omega t + \frac{2\pi}{3}\right) + \gamma_k\right]. \quad (6.14)$$

Higher harmonics in the symmetrical state of the system belong to the subsequent systems of voltages, respectively [65]:

- Harmonics with coefficients $k = 1, 4, 7, 10, \dots = 3n + 1; n \in \mathbb{N}$ build the positive-sequence voltage system,

$$\mathbf{f}_{(k)} = \dot{\mathbf{A}}_{(k)} e^{jk\omega t}. \quad (6.15)$$

- Harmonics with coefficients $k = 2, 5, 8, 11, \dots = 3n + 2; n \in \mathbb{N}$ build the negative-sequence voltage system,

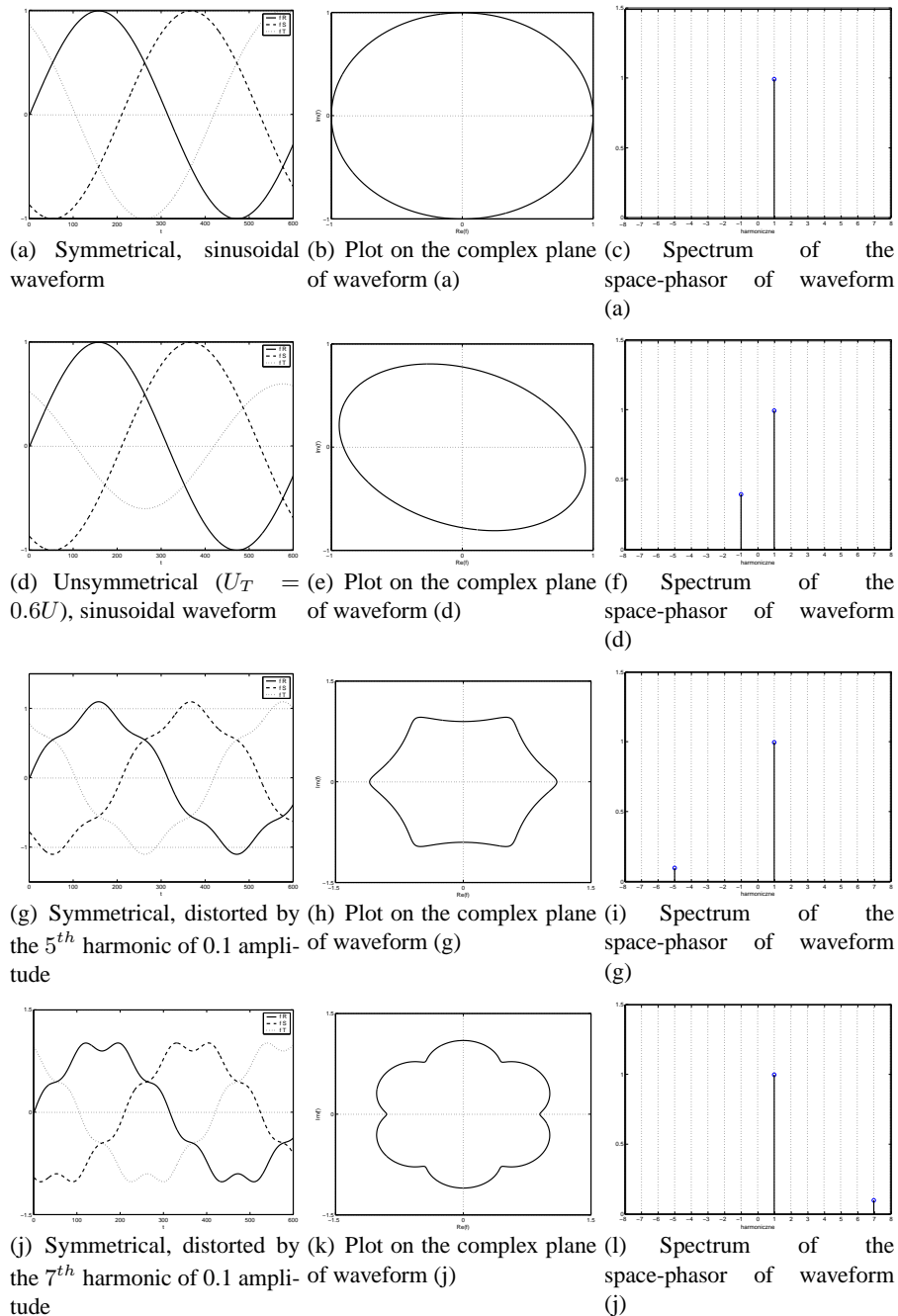


Figure 6.1. Simple cases of asymmetry and distortion of three-phase waveforms

$$\mathbf{f}_{(k)} = \mathring{\mathbf{A}}_{(k)} e^{-jk\omega t}. \quad (6.16)$$

- Harmonics with coefficients $k = 0, 3, 6, 9, \dots = 3n; n \in \mathbb{N}$ build the zero-sequence voltage system.

6.3. Visualization of the three-phase system

A plot of the space-phasor in the complex plane is the most simple and natural way of visualizing a three-phase system [75]. The interpretation of the resulting plot is straightforward only in the case of stationary waveforms with small number of harmonics.

In Figure 6.1, simple cases of asymmetry and distortion of three-phase waveforms are shown.

In the case of asymmetry of the voltages or currents in the three-phase system, a component with negative frequency appears in the spectrum of the space-phasor (see Figure 6.1(f)). In the presence of the 5th harmonic the plot on the complex plane is a hypocycloid and in the spectrum a negative frequency component appears (see Figure 6.1(h, i)), while in the presence of the 7th harmonic there appears in the spectrum an additional component with positive frequency (see Figure 6.1(l)).

Consequently, negative components appear also in the spectrum of the space-phasor, indicating the presence of asymmetry in three-phase currents and voltages in power system. The author proposed spectral representation of the space-phasor as a fast and accurate analysis tool of the three-phase system [49], [43], [58].

Chapter 7

Estimation of the order of the model

7.1. Information theoretic criteria

The necessity of determining the model order arises in many areas of signal processing. In this chapter, we will focus on approaches based on eigenvalue decomposition of the signal correlation matrix (time-delayed in vector signal case). Wax and Kailath [90] presented a new approach for estimating the number of signals in multichannel time-series, based on statistical classification criteria AIC (Akaike Information Criterion) and MDL (Minimal Description Length Criterion) [14]. Use of such statistical criteria resolves the problem of estimation of the signal and subspace dimension, which is necessary to obtain correct estimates of signal parameters, using the methods considered in this work. Recently proposed criterion [66] based on Bayesian statistics will also be investigated. In this chapter, the author presents investigations of different methods for model-order selection, compares its suitability for analysis of electric signals and summarizes research results presented in [34] and [35].

In paper [90], a new approach for estimating the number of signals in multichannel time-series, based on statistical classification criteria AIC and MDL is presented. This approach does not require any subjective threshold setting. Therefore, it resolves the problem of estimation of the signal and subspace dimension, which is necessary to obtain the correct estimates of the signal parameters using parametric methods, considered in this work.

The MDL idea, or shortest description idea, is very natural in statistical classification problems [72]. It has also been applied to order selection problems in time series, as a useful alternative to Akaike Information Criterion (AIC) and Bayesian Information Criterion (BIC) (in fact, the two-stage form of MDL model selection coincides with BIC).

It was also shown that all MDL criteria including BIC are consistent and prediction-optimal, while AIC is not prediction-optimal and inconsistent [73]. A useful observation emanating from this work is that neither MDL (or BIC) nor AIC is a superior method since all this depends on the bias-variance trade-off in the model as shown in early works on MDL in a non-parametric framework [73].

In the seminal paper, Wax and Kailath [90] presented a new approach for estimating the number of signals in multichannel time-series, based on statistical classification criteria AIC and MDL. This approach does not require any subjective threshold setting (see 3.3). This resolves the problem of estimation of the signal and subspace dimension, which is necessary to obtain correct estimates of the signal parameters, using the methods considered in this work.

7.1.1. Approach based on "observation"

The most common approach is to calculate the eigenvalues of the correlation matrix \mathbf{R} of the signal, denoted by:

$$\lambda_1 \geq \lambda_2 \geq \dots \geq \lambda_p. \quad (7.1)$$

The set of the smallest eigenvalues with values equal to the noise variance σ^2 has the dimension $p - q$ [90]. If the correlation matrix is exactly known, the number of signals q can be determined as the number of the smallest eigenvalues. However, the correlation matrix, estimated from a *finite* sample size has all different eigenvalues. In real-life problems, the method of determining the number of signals based on observation of the eigenvalues is difficult and unreliable, although often used and recommended in practice. In earlier works the author used the simple "threshold" approach, which he found to be unreliable and difficult in practical applications [48]. In most problems it is necessary to adjust individually the threshold for each investigated type of signal. Moreover, it is very difficult to build precise rules which could justify this approach.

7.1.2. Approach based on information theoretic criteria

The information theoretic criteria for model order selection address the following problem:

Problem 9. *Given a set of N observations $X = \{x_1, x_2, \dots, x_N\}$ and a parameterized family of probability densities $f(X|\Theta)$ (a family of models), select one model that fits best the set of observations N [90].*

Akaike [3] proposed the following criterion defined by:

$$\text{AIC} = -2 \log f(X|\hat{\Theta}) + 2k \quad (7.2)$$

where $\hat{\Theta}$ is the maximum likelihood estimate of the parameter vector Θ and k is the number of freely adjustable parameters in Θ . The first term represents the log-likelihood of the maximum likelihood estimator of the parameters of the model and the second term assures that AIC becomes an unbiased estimate of the mean Kullback–Leibler divergence¹ between the modelled and estimated densities of $f(X|\Theta)$.

Further work of Schwartz and Rissanen [73], inspired by Bayesian considerations and a minimum code-length model yielded the following criterion:

$$\text{MDL} = -\log f(X|\hat{\Theta}) + \frac{1}{2}k \log N. \quad (7.3)$$

In [90], both AIC and MDL criteria were adapted for detection of the number of signals. This procedure is recalled here in simplified form.

Based on the assumption that observations are statistically independent complex Gaussian random vectors, the parameter vector of the signal model is composed of the eigenvalues, eigenvectors of the covariance matrix and the noise variance.

After some calculations [90] the log-likelihood term in (7.2) or (7.3) becomes the ratio of the geometric mean to arithmetic mean of a number of the smallest eigenvalues.

The number of free parameters in $\hat{\Theta}$ is obtained as the number of the degrees of freedom of each of the parameters. Finally, both criteria are given by:

$$\text{AIC}(k) = -2 \log \left(\frac{\prod_{i=k+1}^p \lambda_i^{\frac{1}{p-k}}}{\frac{1}{p-k} \sum_{i=k+1}^p \lambda_i} \right)^{(p-k)N} + 2k(2p-k), \quad (7.4)$$

$$\text{MDL}(k) = -\log \left(\frac{\prod_{i=k+1}^p \lambda_i^{\frac{1}{p-k}}}{\frac{1}{p-k} \sum_{i=k+1}^p \lambda_i} \right)^{(p-k)N} + \frac{1}{2}k(2p-k) \log N. \quad (7.5)$$

The number of signals is determined as the value of $k \in \{0, 1, \dots, p-1\}$ which minimizes the value of (7.4) or (7.5).

¹ Kullback–Leibler divergence is a natural distance measure from a "true" probability distribution P to an arbitrary probability distribution Q and defined as $D_{KL}(P|Q) = \sum_i P_i \log \frac{P_i}{Q_i}$ for discrete variables.

The consistency of the above criteria was examined under assumption of increasing sample size. AIC under this condition yields an inconsistent estimate, by overestimating the number of signals, whereas the MDL gives always correct results [90].

7.1.3. Bayesian model selection – Minka's Bayesian model order Selection Criterion (MIBS)

This method is also based on eigenvalues of the data covariance matrix [66], but uses the Bayesian framework and Laplace method for approximation of integrals [2].

The PCA model assumes Gaussian distribution of the sources (this model works reasonably well also for non-Gaussian sources [66]) and the observation vector \mathbf{X} is generated from a smaller sources' vector \mathbf{s} by linear transformation with additive noise \mathbf{e} ,

$$\mathbf{X} = \mathbf{H}\mathbf{s} + \mathbf{m} + \mathbf{e}. \quad (7.6)$$

The probability of the model evidence q can be calculated from the eigenspectrum of the data covariance matrix,

$$p(\mathbf{X}|q) = p(U) \left(\prod_{j=1}^q \lambda_j \right)^{-N/2} \sigma_{\text{ML}}^{-N(p-q)} \cdot (2\pi)^{(m+q)/2} |A_z|^{-1/2} N^{-q/2} \quad (7.7)$$

where $p(U)$ denotes a uniform prior over all eigenvector matrices, N – number of observations, $\hat{\sigma}_{\text{ML}}$ – estimate of the noise in the maximum-likelihood sense, $m = pq - q(q+1)$, and

$$p(U) = 2^{-q} \prod_{j=1}^q \Gamma((p-j+1)/2) \pi^{\frac{-(p-i+1)}{2}}, \quad (7.8)$$

$$|A_z| = \prod_{i=1}^q \prod_{j=i+1}^p N(\hat{\lambda}_j^{-1} - \hat{\lambda}_i^{-1})(\lambda_i - \lambda_j). \quad (7.9)$$

where λ_l denotes an eigenvalue, $\hat{\lambda}_l = \lambda_l$ for $l \leq q$ and $\hat{\lambda}_l = \sigma_{\text{ML}}^2$, otherwise.

To find the signal subspace "latent dimension" such value of q is chosen which maximizes the approximation of the model evidence $p(\mathbf{X}|q)$.

Chapter 8

Power quality assessment

8.1. Introduction

The term *power quality* covers a number of electromagnetic phenomena which deal with the interaction of power-system networks and end-user equipment. End-user equipment is sensitive to certain types of voltage disturbances in the system, but the equipment on its turn may produce current disturbances, which pollute the system. As many sensitive processes in industrial systems do care about the disturbances in the supplied voltages, industries are more concerned about the operational and economic aspects of these disturbances. Running extensive power quality monitoring programs is important in order to understand, identify and solve problems regarding power quality. In many cases, such monitoring programs end up in a huge amount of measured data which makes analysis difficult [16]. Therefore, the development of automatic tools for assessment of the measured data is required to help utilities, regulators and customers to have a clear understanding of what is happening in their networks. Power quality monitoring systems are demanded nowadays to be able to identify and classify events automatically in order to solve problems in electrical networks in accurate, fast and intelligent way. The evolution of power quality monitoring in terms of technology and users is presented in Figure 8.1, as a time-line. In the 1990's, the technology applied in classification tended to merge power-system engineering knowledge with signal processing techniques. In the latest years, pattern recognition, data mining, decision-making and networking were incorporated as new technologies for automatic classification. This entire advancement aims at processing raw data and extracting information to obtain knowledge in order to solve problems with less or without human action. Moreover, users of power quality event classification schemes have spread from a few field-service engineers in the 1970's to hundreds of people in the 2000's; in power utilities, consultant companies and governmental agencies; working to assess power networks and to include power quality indexes in power-system economic performance studies [16].

| TECHNOLOGY | | | |
|------------------------|----------------------|-----------------------------|---------------------|
| 1970's | 1980's | 1990's | 2000's |
| Voltmeter | Oscilloscopes | Digital Signal Processing | Pattern recognition |
| Paper | Graphics | Computers | Data mining |
| Tape | Oscillographs | Mass storage devices | Decision-making |
| | | Communitacions | Networking-internet |
| USERS | | | |
| Field service engineer | Utility companies | | Regulatory agencies |
| | Power Quality groups | | ISO |
| | | Industrial/plant/facilities | IPP |

Figure 8.1. Evolution of power quality monitoring equipment [16]

The author's research in the field of power quality encompasses methods of harmonic distortion measurements presented in [58] and [60] dealing with industrial frequency converters operation, [8], [4] and [5] – with DC arc furnaces supply, [6] – traction systems, [7] – analyzing the influence of compensation devices (active and passive filters, STATCOM, hybrid systems) and [9] where he proposed a new power quality indices' computation approach, presented in this work (see also Section 10.4).

8.2. Power Quality Indices

A number of power system applications require an accurate knowledge of the spectral components of non-stationary current and voltage waveforms. Especially, the power quality field, due to the great and increasing interest deserves our attention [4]. The main application of spectral components in the field of Power Quality refers to the calculation of waveform distortion indices. Several indices are in common use for the characterization of waveform distortions. However, they generally refer to periodic signals which allow an "exact" definition of harmonic components and require only a numerical value to characterize them. When the spectral components are time-varying in amplitude and/or

in frequency (as in the case of non-stationary signals), a wrong use of the term harmonic can arise and several numerical values are needed to characterize the time-varying nature of each spectral component of the signal. The IEC Standard drafts [21], [22] deal with signals which are time-varying. They define, for practical purposes, the harmonic (interharmonic) frequency as an integer (non-integer) multiple of the fundamental frequency. The same IEC Standard drafts – with reference to Discrete Fourier Transform with 5 Hz resolution of frequency (200 ms of window length for 50 Hz fundamental frequency) – introduce the concept of harmonic and interharmonic groupings and characterize the waveform distortions with the amplitudes of these groupings. Figure 8.2 shows an example of two harmonic subgroups ($n = 7$ and $n = 8$) and of one interharmonic subgroup ($n = 7.5$). The amplitudes of the harmonic and interharmonic subgroups $C_{n-200ms}$ and $C_{n+0.5-200ms}$ can be evaluated, respectively, as:

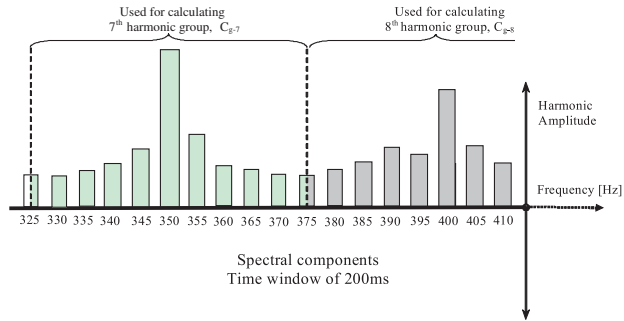
$$C_{n-200ms}^2 = \sum_{k=-1}^1 C_{10n+k}^2, \quad (8.1)$$

$$C_{n+0.5-200ms}^2 = \sum_{k=-2}^8 C_{10n+k}^2, \quad (8.2)$$

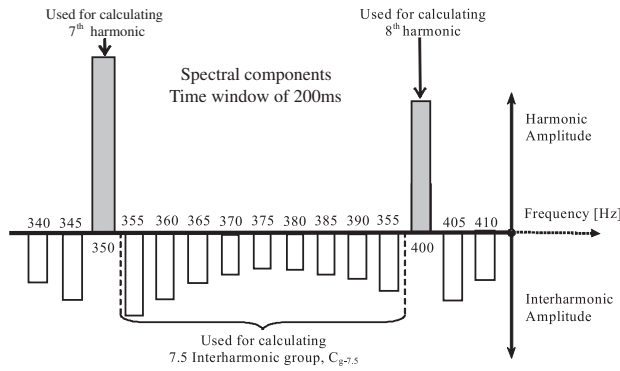
where C_{10n+k} are the spectral components (RMS value) of the spectral (DFT) output.

According to the norms cited relations (8.1) and (8.2) are computed on 15 successive 200 ms windows in order to obtain values averaged over a 3-second interval. Therefore, the obtained indices have low resolution in time. Recently, many papers deal with waveform distortion indices in the case of aperiodic signals. In practice, the main efforts are devoted to the extension of usual indices – such as Total Harmonic Distortion (THD), k -factor, communication interference factors and others – to the field of aperiodic signals, taking into account the special characteristics of the processing technique employed. In paper [20], an extension of power quality indices based on the Windowed Fourier Transform (WFT) is proposed for aperiodic power system signals. The short term harmonic distortion index (STHD) has been defined there. If the width of the window is TW , the STHD is defined as:

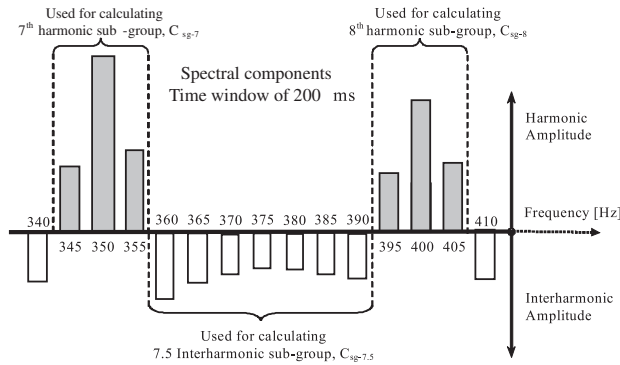
$$STHD = \frac{\sqrt{\sum_{i \neq \frac{50}{\Delta f} + 1}^{N_f} WDFT_i^2}}{WDFT_{\frac{50}{\Delta f} + 1}} \quad (8.3)$$



(a) harmonic groups



(b) interharmonic groups



(c) harmonic and interharmonic subgroups

Figure 8.2. Examples of harmonic (\uparrow) and interharmonic (\downarrow) subgroups according to IEC Standard drafts 61000-4-7 and 61000-4-30 [4]

where: N_f is the number of frequencies for which the WFT has been calculated; $WDFT_i$ is the i^{th} component from the WFT; Δf is the frequency resolution.

Similar extensions for other waveform distortion indices such as the k -factor and the crest factor have been reported.

In this work, the IEC harmonic and interharmonic subgroups introduced by the IEC Standard drafts, the Total Harmonic Distortion and the spectral component frequency time variation (time-varying amplitude and frequency of signal components, as in Figures 10.14, 10.15, 10.40, 10.41) are considered.

Chapter 9

Automatic Classification of Events

The decomposition of a band-limited one-dimensional time-domain signal into two-dimensional time-frequency domain can reveal more details of the signal and help to improve the classification performance or pattern recognition [13]. One of many automatic classification techniques, based on correlation [27], is adopted in this chapter for classification of events in electric power systems. The classifier proposed makes use of available *a priori* knowledge about the signal, in many ways; it uses the knowledge about the main characteristics, such as: the expected number of components, parameters of frequency bands which contain most useful information, time interval where the most significant changes occur. In preprocessing stage, many "regions of interest" in the time-frequency plane are defined in order to enhance the classification performance. Previous work of the author includes classification problems of fault-mode operation of inverter drives (application of neural classifiers [52], [39]), application of correlation and advanced preprocessing techniques in [10]. The approach presented in this chapter follows the same idea; in order to evaluate the performance of preprocessing approach presented, a simple time-domain correlation is chosen as a classifier, since complicated classification technique can obscure the influence of improperly chosen preprocessing and make a fair comparison impossible [10].

9.1. Preliminaries

The main goal is to design a classification scheme which, using 2-D time-frequency parametric representation of a signal, performs better than a straightforward correlation-based classifier. It is assumed that the transformation to 2-D time-frequency domain allows one to reveal more details of the signal and therefore improves the accuracy of pattern matching. Additionally, it helps to reveal the correct pattern buried in noise (disturbances) by exposing the important characteristics of analyzed signal. The transformation to time-frequency domain allows an easy use of *a priori* knowledge: only selected areas of the time-frequency plane can be used for the correlation-based classification. In [39], the moments computed from time-frequency representation of

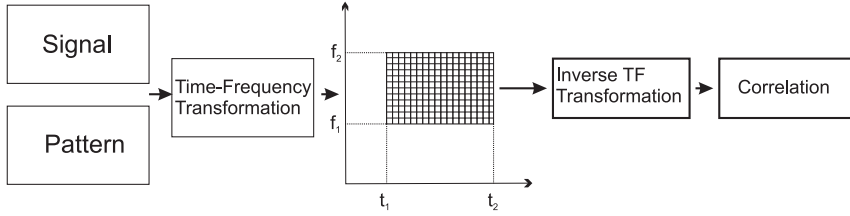


Figure 9.1. Scheme of correlation-based classification relying on TF transformation.

the signal are selected as features. This approach destroys a part of useful information, so a complicated classifier is needed to obtain acceptable performance. The correlation scheme developed here improves the performance in the case of matching pattern and decreases the false classification rate in the case of non-matching patterns when using the maximum of available information and at the same time enhancing "meaningful" parts of the signal. Waveforms encountered in power systems have usually quite well known structure, so it is straightforward to select the frequency band where the signal of interest shows most characteristic patterns. Similarly, the time point of the occurrence of a specific pattern can be either determined as the starting point of an event (e.g., beginning of a short-circuit) or using other techniques (e.g., change-point detection algorithms, wavelets) [59]. In this way, a rectangular area or multiple areas on the time-frequency plane can be determined where the correlation-based pattern recognition algorithm can show possibly best performance. A simplified scheme of this procedure is shown in Figure 9.1. After the TF transformation of signal and pattern, a specific area of the TF plane is selected. Then, the inverse transformation (or approximate reconstruction, e.g. in the sense of equal energy of the original and reconstructed signal of the time-domain signal from its calculated parameters) allows usual correlation of time-domain signals and patterns. Similar approach was presented in [78], although applied to different problems.

9.2. Correlation of signal and pattern

Let us assume a band-limited and time-limited signal $s(t)$ and pattern $p(t)$, with its time-frequency representation, as follows:

$$\text{TF}\{p(t, f)\} \equiv 0 \quad \forall \{t \in [t_1, t_2], f \in [f_1, f_2]\} \quad (9.1)$$

where $[t_1, t_2]$ and $[f_1, f_2]$ define supports in time and frequency domains, respectively.

Lemma 10. Any finite and band-limited signal $s(t) \subseteq [t_1, t_2]$ can be decomposed as follows, when using its time-frequency representation $\text{TF}\{s(t, f)\}$:

$$\text{TF}\{s(t, f)\} = \text{TF}\{s_1(t, f)\} \cup \text{TF}\{s_2(t, f)\} \quad (9.2)$$

where $\text{TF}\{s_1(t, f)\} = \text{TF}\{s(t, f)\}$ and $\text{TF}\{s_2(t, f)\} = \text{TF}\{s(t, f)\} \cap \text{TF}\{s_1(t, f)\}$.

Such a decomposition assumes that $s_1(t)$ is the part of signal $s(t)$ which has the same support in time and frequency as pattern $p(t)$ has and $s_2(t)$ represents the remaining part of the signal $s(t)$.

If we assume that both signals and the pattern have their respective inverse time-frequency transforms, then

$$s(t) = s_1(t) + s_2(t). \quad (9.3)$$

Theorem 11. For any band-limited and finite signal $s(t)$ and pattern $p(t)$, which can be decomposed into $s(t) = s_1(t) + s_2(t)$ the following condition is fulfilled:

$$\max [|\text{R}(s_1(t), p(t))|] > \max [|\text{R}(s_2(t), p(t))|] \quad (9.4)$$

where $\max [|\text{R}(u(t), v(t))|]$ (maximum of the magnitude of the normalized correlation function) is defined as:

$$\max [|\text{R}(u(t), v(t))|] = \max \left[\left| \frac{\int_{-\infty}^{\infty} u(t)v^*(t - \tau)dt}{\sqrt{\int_{-\infty}^{\infty} u^2(t)dt}\sqrt{\int_{-\infty}^{\infty} v^2(t)dt}} \right| \right]. \quad (9.5)$$

Equation (9.4) is a consequence of the assumptions that the signal $s_1(t)$ is similar to the pattern $p(t)$ and has the same localization in time-frequency plane and $s_2(t)$ lies outside the area in the time-frequency plane where the pattern $p(t)$ is localized.

Proof. From the above assumption it follows that:

$$\max [|\text{R}(s_1(t), p(t))|] > \max [|\text{R}(s_2(t), p(t))|]. \quad (9.6)$$

The normalized correlation of the signal $s(t) = s_1(t) + s_2(t)$ is:

$$\text{R}(s(t), p(t)) = \frac{\int_{-\infty}^{\infty} s_1(t)p(t + \tau)dt + \int_{-\infty}^{\infty} s_2(t)p(t + \tau)dt}{\sqrt{\int_{-\infty}^{\infty} [s_1^2(t) + 2s_1(t)s_2(t) + s_2^2(t)] dt}\sqrt{\int_{-\infty}^{\infty} p^2(t)dt}} \quad (9.7)$$

Since:

$$\sqrt{\int_{-\infty}^{\infty} [s_1^2(t) + 2s_1(t)s_2(t) + s_2^2(t)] dt} > \sqrt{\int_{-\infty}^{\infty} s_1^2(t)dt}. \quad (9.8)$$

It follows that:

$$\max [|\mathbf{R}(s_1(t), p(t))|] > \max [|\mathbf{R}(s(t), p(t))|]. \quad (9.9)$$

■

In the case of single pattern in the time-frequency plane, the above considerations show that the presence of the pattern in the signal assures the highest correlation coefficient when correlating pattern and signal.

In the case of multiple patterns, some precautions must be observed. The main condition for the classification scheme to work properly is to assure that all patterns occupy mutually exclusive areas in the time-frequency plane. This condition is usually easily fulfilled for waveforms commonly encountered in power systems [50].

Corollary 12. *In the case of patterns $p_{i,j}$ which do have non-disjoint time-frequency representations, such as:*

$$\text{TF}\{p_i(t, f)\} \cap \text{TF}\{p_j(t, f)\} \neq \emptyset \quad (9.10)$$

the problem can arise, namely a high correlation coefficient in the case where the pattern is not present in the signal. It is necessary to define a mutually exclusive pattern to any other pattern. This is quite straightforward when dealing with the representation of signal in the time-frequency plane.

Any pattern $p(t)$ can be represented as a sum of two mutually exclusive patterns, $p_k(t), p_l(t)$, where $p_l(t)$ represents part which is nullified for any disjoint set of patterns (it represents the non-disjoint part of any set of patterns),

$$p(t) = p_k(t) + p_l(t). \quad (9.11)$$

Theorem 13. *If the signal $s(t)$ is weakly correlated with the pattern $p(t)$, then the correlation of $s(t)$ with pattern $p_k(t)$ yields smaller correlation coefficient than in the case of correlation of the signal $s(t)$ with $p(t)$,*

$$\max [|\mathbf{R}(s(t), p(t))|] > \max [|\mathbf{R}(s(t), p_k(t))|]. \quad (9.12)$$

Proof. Equation (9.12) can be transformed in a similar way as (9.7):

$$\max [|\mathbf{R}(s(t), p(t))|] = \max \left[\frac{\int_{-\infty}^{\infty} s(t)p_k(t + \tau)dt + \int_{-\infty}^{\infty} s(t)p_l(t + \tau)dt}{\sqrt{\int_{-\infty}^{\infty} [p_k^2(t) + 2p_k(t)p_l(t) + p_l^2(t)] dt} \sqrt{\int_{-\infty}^{\infty} s^2(t)dt}} \right] \quad (9.13)$$

and (see (9.5))

$$\max [|\mathbf{R}(s(t), p_k(t))|] = \max \left[\left| \frac{\int_{-\infty}^{\infty} s(t)p_k(t + \tau)dt}{\sqrt{\int_{-\infty}^{\infty} p_k^2(t)dt}\sqrt{\int_{-\infty}^{\infty} s^2(t)dt}} \right| \right]. \quad (9.14)$$

From (9.12), assuming the mutual exclusivity of the patterns $p_k(t)$ and $p_l(t)$ (9.11), the following can be concluded:

$$\left| \int_{-\infty}^{\infty} s(t)p_l(t + \tau)dt \right| > \left| \int_{-\infty}^{\infty} s(t)p_k(t + \tau)dt \right| \quad (9.15)$$

and

$$\sqrt{\int_{-\infty}^{\infty} [p_k^2(t) + 2p_k(t)p_l(t) + p_l^2(t)] dt} \approx \sqrt{\int_{-\infty}^{\infty} p_k^2(t)dt}. \quad (9.16)$$

Finally, from equations (9.13)–(9.16), it follows that the proof is completed, so:

$$\max [|\mathbf{R}(s(t), p(t))|] > \max [|\mathbf{R}(s(t), p_k(t))|]. \quad (9.17)$$

■

The considerations presented above show that transformation of the signal to time-frequency domain, selection of particular areas in time-frequency plane (mutually exclusive areas), subsequent calculation of parameters of the signal and pattern inside the preselected "areas of interest" leads to an *increase* of the maximum correlation coefficient of the correlated signal and pattern (when signal and pattern are similar) and to a *decrease* of the maximum correlation coefficient when both signal and pattern are dissimilar.

Chapter 10

Experiments and simulations

10.1. Signal-to-Noise Ratio (SNR)

By using a known property of the autocorrelation function [28] it is possible to define two useful SNR measures. For a zero-mean, wide-sense stationary process composed of i sinusoidal components, where P_i is the power of each sinusoidal component and η represents the noise process (wide-sense stationary random process uncorrelated with the signal).

The local SNR is defined as:

$$\text{SNR}_{local,i} = \frac{P_i}{R_\eta(0)}. \quad (10.1)$$

It can be regarded as the measure of the correctness of estimation of the frequency of a given spectral component.

The global SNR is:

$$\text{SNR}_{global} = \frac{\sum_{i=1}^N P_i}{R_\eta(0)}. \quad (10.2)$$

This measure can give the likelihood of the estimation of the frequencies in the average.

10.2. Basic performance comparison of MUSIC and ESPRIT

Several experiments with simulated, stochastic signals were performed, in order to compare different performance aspects of both parametric methods MUSIC and ESPRIT, compared to commonly used power spectrum (FFT based method). Testing signals are designed to belong to a class of waveforms often present in power systems. Each run

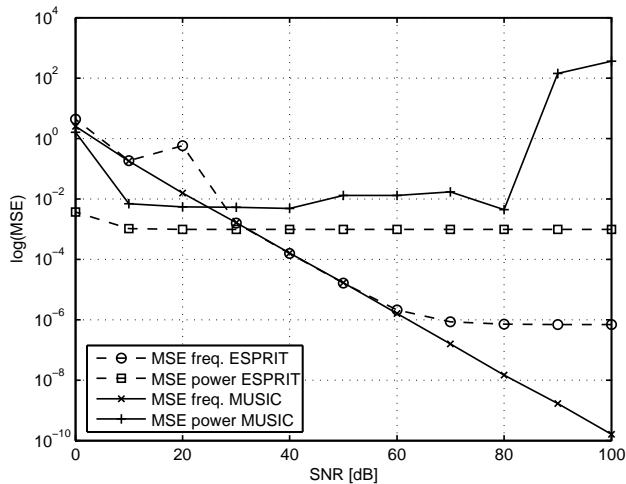


Figure 10.1. MSE of frequency and power estimation (ESPRIT, MUSIC) depending on SNR. Averaged 1000 independent runs

of spectrum and power estimation is repeated many times (Monte Carlo approach) and the mean-square error (MSE) is computed.

Parameters of test signals:

- one 50 Hz main harmonic with unit amplitude,
- random number of higher odd harmonic components with random amplitude (lower than 0.5) and random initial phase (from 0 to 8 higher harmonics) if not otherwise specified,
- sampling frequency 5000 Hz,
- each signal generation repeated 1000–100000 times with reinitialization of random number generator,
- SNR = 20 dB if not otherwise specified,
- size of the correlation matrix = 50 if not otherwise specified,
- signal length 200 samples if not otherwise specified.

Selected results are presented below:

Figure 10.1 shows a strong dependence of the accuracy of the frequency estimation on SNR and almost no dependence of amplitude estimation (with exception to MUSIC which shows higher errors for very low and very high noise levels).

The size of the correlation matrix must be chosen very carefully, as can be seen from

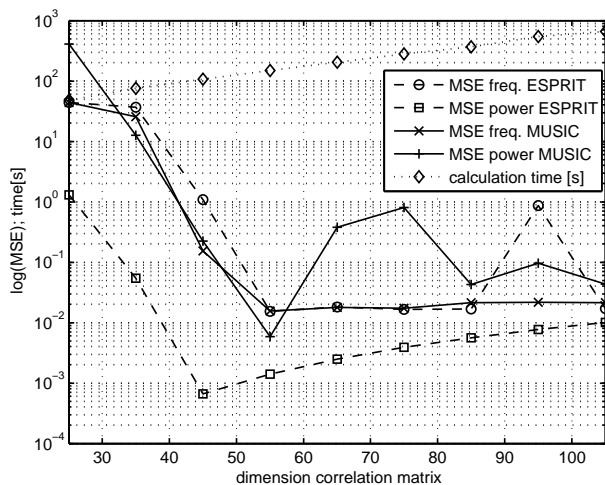


Figure 10.2. MSE of frequency and power estimation (ESPRIT, MUSIC) depending on the size of correlation matrix. Averaged 1000 independent runs

Figure 10.2. In the case of both methods, there exists an optimum of the size (relative to the data length) which assures lowest estimation error. There exists a trade-off between increasing accuracy of the estimated correlation matrix and increasing numerical errors with the matrix size.

The data sequence length has stronger influence for the accuracy of MUSIC method than ESPRIT (Figure 10.3). For shorter data lengths ESPRIT method is faster to calculate; this advantage vanishes with increasing number of data samples taken in calculation.

The investigation of the method of calculation of the correlation matrix shows surprisingly (see Subsection 3.1.4) that the forward-backward approach causes higher estimation error than simple forward approach (Figure 10.4). It is only advantageous when the size of the correlation matrix is large. In this case, the matrix is better conditioned which eases the operation of matrix inversion.

In Figures 10.5 and 10.6 the results are shown where the amplitude of higher harmonics was gradually increased from 0.1 to 0.9 of the fundamental 50 Hz component. In such a way the problem of masking the higher low-amplitude harmonic components by a strong fundamental component was investigated. The results show an extremely high masking effect in the case of power spectrum, while MUSIC and ESPRIT methods show

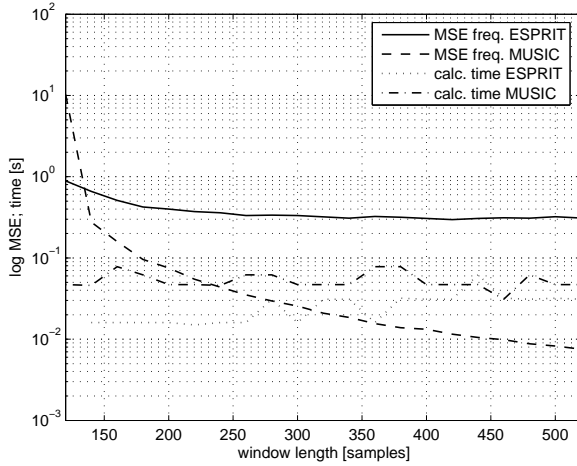


Figure 10.3. MSE of frequency and power estimation (ESPRIT, MUSIC) and average calculation time depending on the data window length. Averaged 10000 independent runs

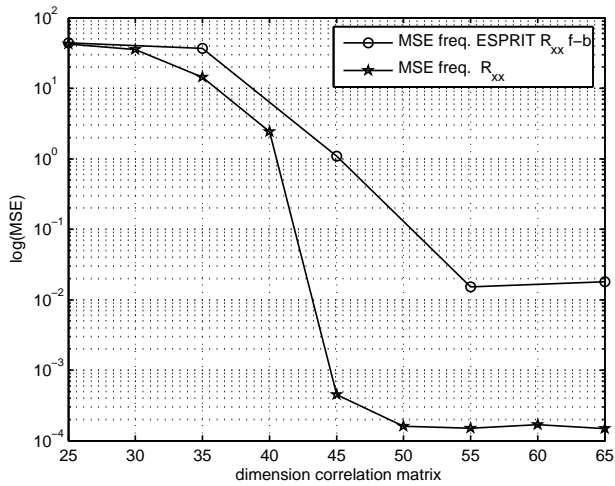


Figure 10.4. MSE of frequency and power estimation (ESPRIT, MUSIC) depending on the method of calculation of the correlation matrix (straight versus forward–backward approach). Averaged 1000 independent runs

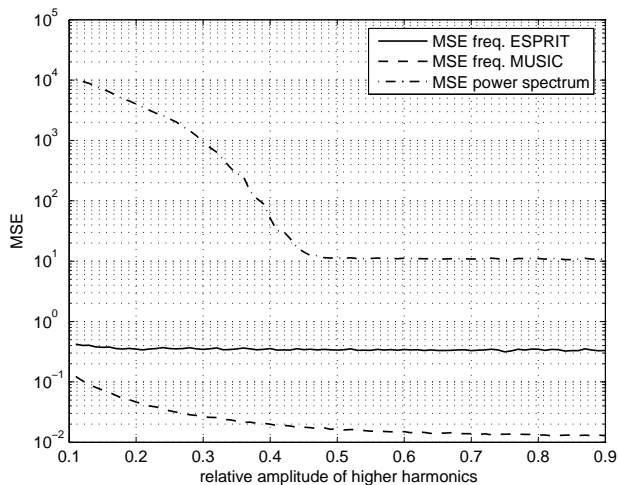


Figure 10.5. MSE of frequency estimation (ESPRIT, MUSIC, power spectrum) depending on the relative amplitude of higher harmonics amplitudes. Averaged 10000 independent runs

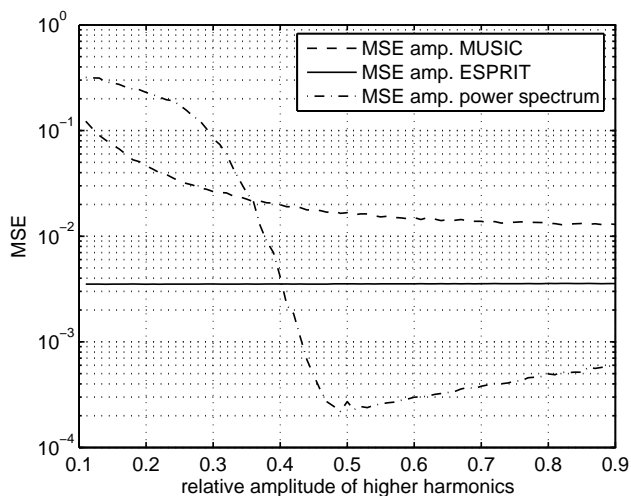


Figure 10.6. MSE of amplitude estimation (ESPRIT, MUSIC, power spectrum) depending on the relative amplitude of higher harmonics amplitudes. Averaged 10000 independent runs

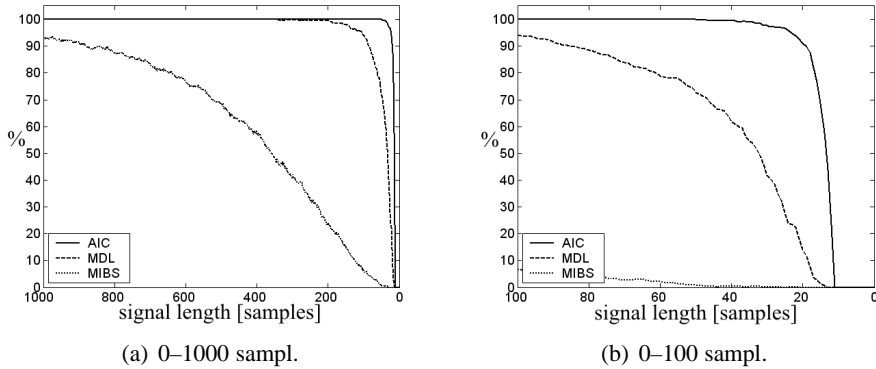


Figure 10.7. Accuracy of the dimension estimation by AIC, MDL and MIBS depending on the signal length

very little dependence (almost no dependence in the case of ESPRIT method). This is a very important feature which partially explains excellent performance of parametric methods in the task of calculation of power quality indices (see Section 10.4).

10.3. Estimation of the number of components

The performance with regard to accuracy of the estimation of the number of components is tested using simulated signals with Gaussian noise [35]. The sampling frequency was set to 1000 Hz and each calculation was repeated 1000 times for independent realizations of the signal. Firstly, the estimation accuracy is determined as a percentage of runs when a signal parameter was estimated correctly. It was investigated depending on the signal length (two sinusoids of 50 and 150 Hz with unit amplitude and SNR 20 dB¹).

Figure 10.7 shows that the accuracy of MIBS strongly depends on the number of samples and achieves only 68% accuracy for the window of 500 samples chosen for further investigations. Excellent performance of AIC should be noted as it achieves over 90% for 20 samples only.

Figure 10.8 presents the masking problem of the weaker components by the stronger one. One component with the basic frequency has the fixed amplitude and the second has it gradually decreasing. Generally MDL offers best accuracy close to 100% down to

¹ SNR [dB] = $10 \log_{10} \left(\frac{\sigma_s^2}{\sigma_n^2} \right)$

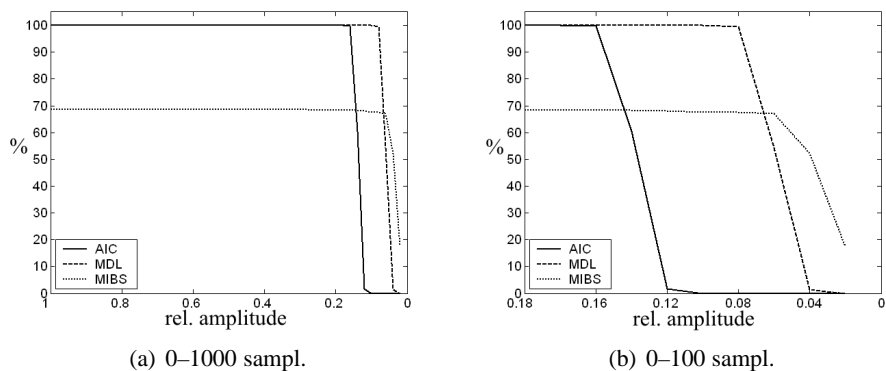


Figure 10.8. Accuracy of the dimension estimation by AIC, MDL and MIBS depending on the relative amplitude of two sinusoidal components

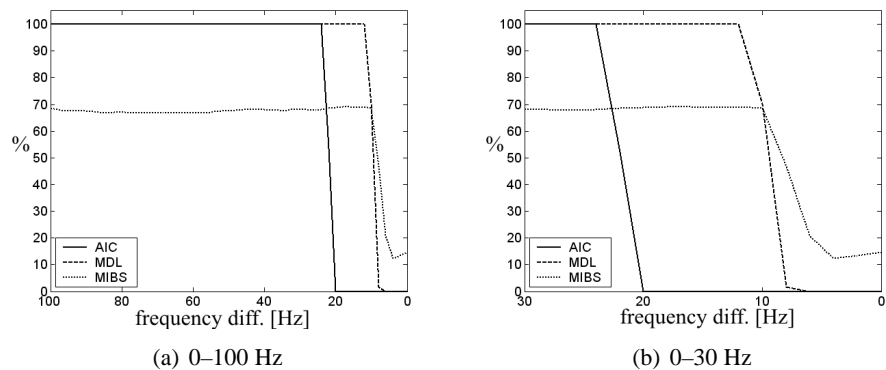


Figure 10.9. Accuracy of the dimension estimation by AIC, MDL and MIBS depending on the difference of frequencies of two sinusoids with equal amplitude

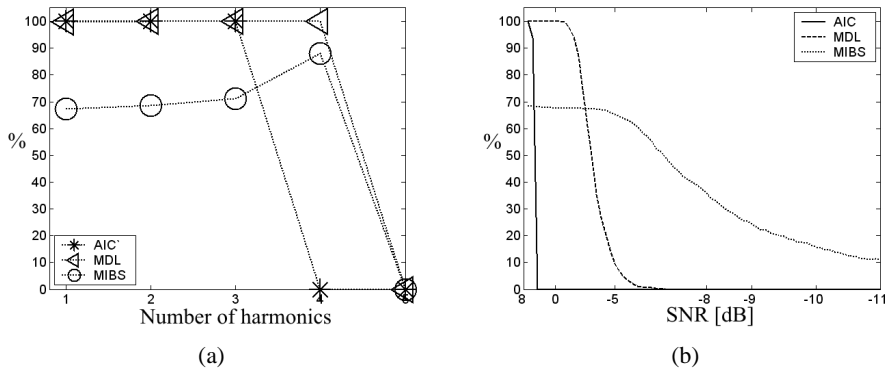


Figure 10.10. Accuracy of the dimension estimation by AIC, MDL and MIBS depending on the number of signal components (a) and on SNR (b)

0.08 with exception of the smallest relative amplitudes where MIBS achieves over 50% accuracy for values as low as 0.04.

In Figure 10.9, the results are presented which show the lowest difference in frequency that still allows two separate components of the same amplitude to be detected. AIC performs poorly and fails by the values of 50 and 74 Hz (24 Hz difference), whereas MDL needs only 12 Hz difference for correct estimation. As before, MIBS offers advantage for the lowest values of difference.

An increasing number of sinusoids with the same amplitude was also estimated, see Figure 10.10a. AIC failed when the number of components increased to four and other methods – when by five (the frequencies were 50, 100, 150, 200, 250 Hz).

The Gaussian noise has little influence on accuracy as shown in Figure 10.10b. The highest immunity shows MIBS with accuracy of almost 70% for SNR as low as -5 dB, followed by MDL (100% for -2 dB) and AIC (100% for 4 dB).

Analysis of current during the switching of the capacitor banks

The switching of the capacitor bank in the transmission line was simulated using the EMTP software [12] with the simulation parameters as shown in Figure 10.11. The sampling frequency was 10 kHz and the length of the analysis window was set to 100 samples (0.01 s). The A-phase current is shown in Figure 10.12, and its short-time Fourier transform in Figure 10.13. The first capacitor bank was switched on at the time $t = 0.03$ s and the second capacitor bank at the time $t = 0.09$ s.

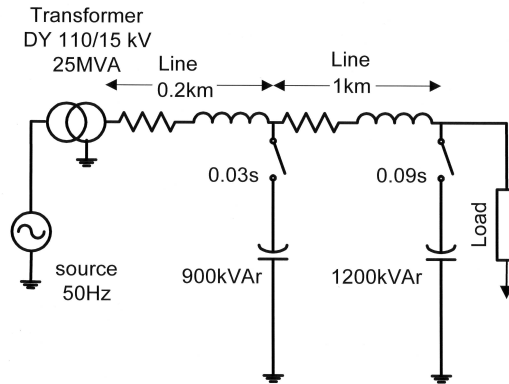


Figure 10.11. Scheme of the simulated transmission line system

The number of components was determined online using the AIC criterion (with limitation to maximum of four components) for each analyzed time interval of 100 samples. To keep the picture legible, in Figure 10.14 only the first two components are shown. Components were sorted according to their frequency.

In Figure 10.15 the corresponding amplitudes (derived from components' powers computed by the *root-MUSIC* procedure) are shown. The first component corresponds to the fundamental harmonic of 50 Hz. With exception to short intervals (around the switching points) where the stationarity assumption is not satisfied, the results of estimation of frequency are reliable and correspond precisely to the time waveform. The second component has a transient, exponentially decaying character with frequency of 476 Hz after the switching of the first capacitor bank which changes to 270 Hz after the second switching operation.

The application of statistical model order selection (in this case, estimation of the number of sinusoidal components) allow the parameters of the signal to be tracked on-line. It can also be used as one of the input values of the system of automatic detection and classification [34], [35].

In this section, the influence of the estimation accuracy of the sample correlation matrix (depending on the length of the signal), as well as the influence of the number of components and of their relative amplitudes on the accuracy of statistical estimation of the number of components has been presented. The use of information-theoretic criterion like AIC, together with high-resolution parametric estimation method, like ESPRIT or

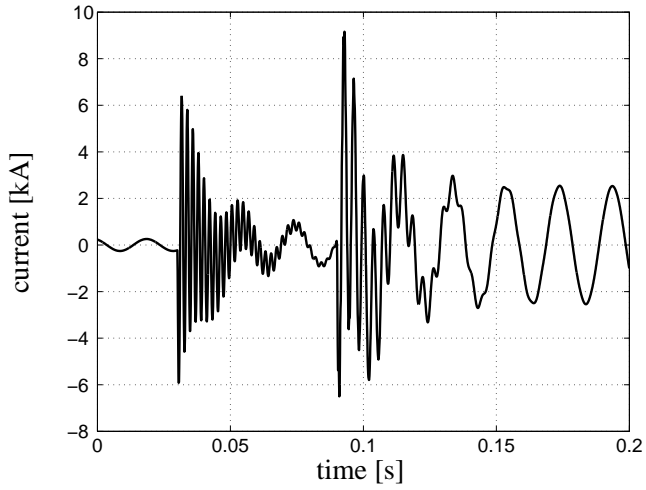


Figure 10.12. Waveform of the A-phase current during switching of the capacitor banks in the transmission line

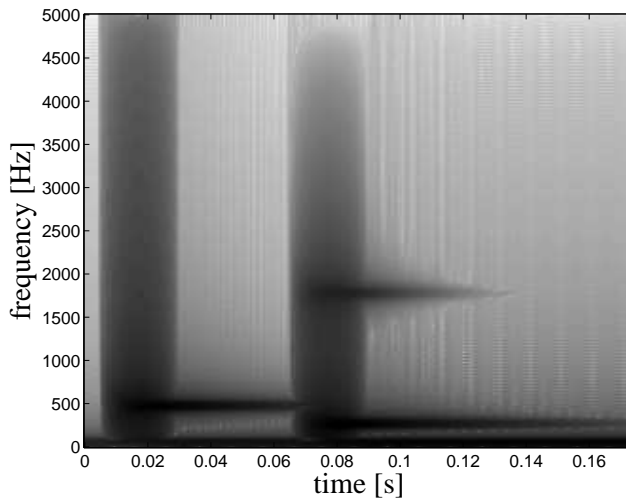


Figure 10.13. Short-Time Fourier Transform of the A-phase current during switching of the capacitor banks in the transmission line

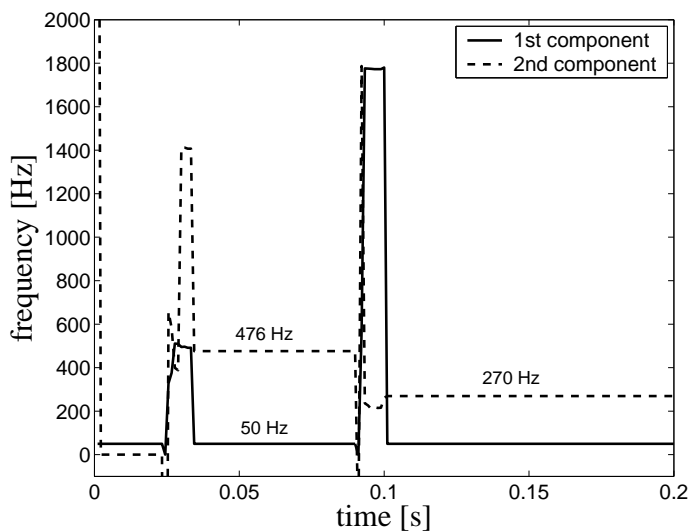


Figure 10.14. Time-varying frequency of two components of the current

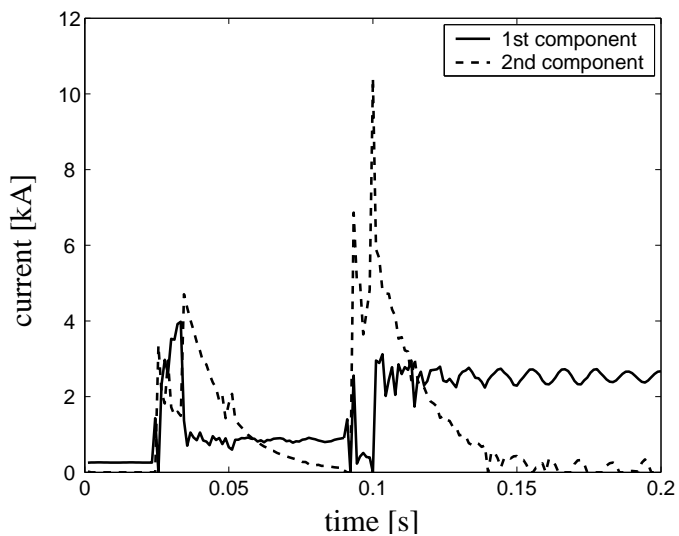


Figure 10.15. Time-varying amplitude of two components of the current

MUSIC, allows precise on-line estimation of the signal parameters by using the sliding window approach in the case where the parameters of the components are time-varying.

10.4. Power quality indices

In this section, the waveforms obtained from a power supply of a typical DC arc furnace plant are analyzed. The IEC groups and subgroups are estimated by using FFT and the results are compared with advanced methods: the ESPRIT and the root-MUSIC methods.

10.4.1. Experimental setup and preprocessing

The simulated DC arc furnace plant consists of a DC arc furnace connected to a medium voltage ac busbar with two parallel thyristor rectifiers that are fed by transformer secondary windings with Δ and Y connections, respectively, it is shown in Figure (10.16). The power supply of arc furnace is modelled using Power System Blockset in Matlab[®]. The electric arc was simulated with a Chua's circuit², which shows good similarity with real measurements [8].

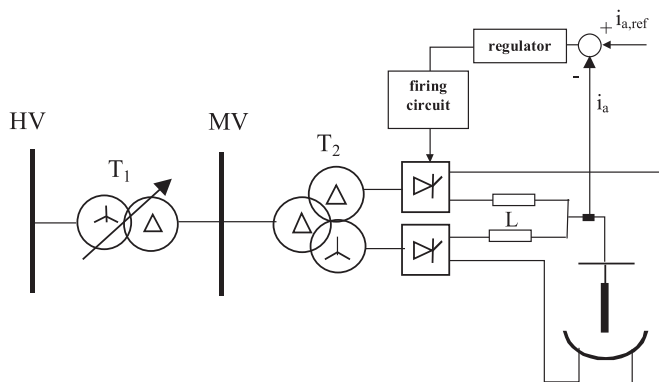


Figure 10.16. Simulated DC arc furnace plant

² Chua's circuit is a simple electronic circuit that exhibits classic chaos theory behaviour. Introduced in 1983 by Leon O. Chua.

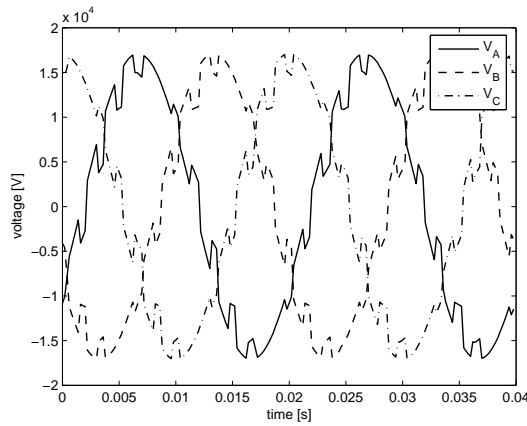


Figure 10.17. Voltage waveform of the arc furnace supply – medium voltage AC busbar

The medium voltage busbar is connected to the high voltage busbar with a HV/MV transformer whose windings are Δ -Y connected. The power of the furnace is 80 MW. The other parameters are: Transformer T_1 – 80 MVA, 220kV/21kV; Transformer T_2 – 87 MVA, 21kV/0.638kV/0.638kV. Examples of waveforms at the arc furnace supply on the MV side are shown in Figures 10.17 and 10.18.

- The evaluation of harmonic and interharmonic subgroups has been made using the following assumptions: window length – 200 ms non-overlapping. For each window, the n^{th} harmonic subgroup includes all spectral components inside the frequency interval $[n \cdot f_1 - 7.5, n \cdot f_1 + 7.5]$ Hz. The interharmonic subgroup includes all the spectral components inside the frequency interval $]n \cdot f_1 + 7.5, (n + 1) \cdot f_1 - 7.5[$ Hz [9]. When applying parametric methods filters have been applied for preprocessing of data. In particular, a bandstop Butterworth IIR filter blocking the main (50Hz) component; a lowpass (40 Hz) Butterworth IIR filter applied for analyzing interharmonics groupings for $n = 0.5$ and bandpass Butterworth IIR filters for other subgroups.
- The evaluation of Total Harmonic Distortion (THD) has been done with following assumptions: The window length is assumed to be 200 ms and the successive windows until 3 s non-overlapping. For each window, the THD includes all harmonic and interharmonic components up to 1000 Hz.

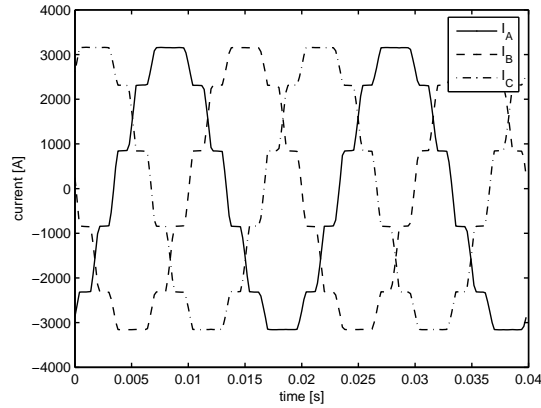


Figure 10.18. Current waveform of the arc furnace supply – medium voltage T2 input

10.4.2. Results and discussion

From the analysis of subsequent Figures 10.20–10.36, it can be noted that the results obtained by using "Ideal IEC" give a very high value of the progressive average referred to the IEC interharmonic subgroups. This difference can be explained by the problem of spectral leakage present in the DFT based algorithms (STFT) and therefore the high energy content leaking into the neighborhood of the fundamental component of the voltage waveform. As shown below, the high resolution methods give results closer to the "Ideal IEC" than the ones obtained with STFT for the evaluation of the progressive average related to the 11th in Figure 10.25 and 13th in Figure 10.26 for harmonic subgroups.

Figure 10.19 reports the THD values obtained with the different techniques. It should be noted that there is no visible advantage of using advanced spectral methods for estimation of THD.

When analyzing current as well as voltage waveforms, a poor performance of root-MUSIC (shown in Figures 10.20 and 10.29) can be observed. This can be attributed to spurious roots (see Section 3.3) which in rare cases can ruin the results. STFT and ESPRIT methods give comparable results.

In some rare cases parametric methods give less accurate results (Figure 10.23) or almost identical when comparing to non-parametric STFT (Figure 10.24).

The advantage of using parametric methods becomes evident when analyzing higher harmonic groups of the currents (Figures 10.25 and 10.26) and voltages (Figures 10.33–10.36).

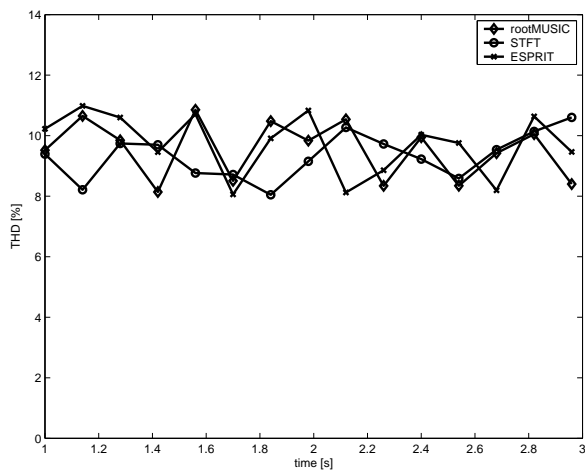


Figure 10.19. Total Harmonic Distortion of the current evaluated with parametric spectral methods

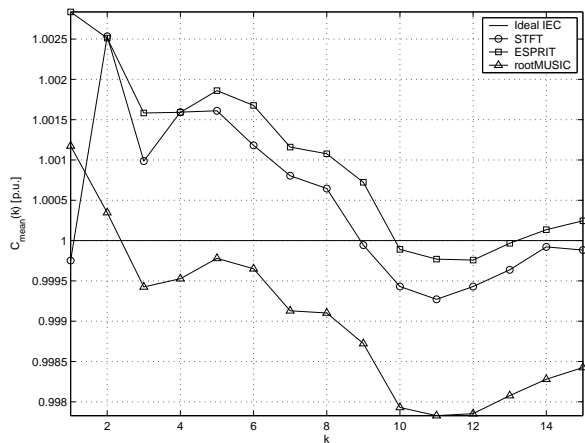


Figure 10.20. Progressive average of the first harmonic subgroup of the current

In the case of voltage harmonic subgroups estimation (Figures 10.29–10.32) the results are comparable to those obtained using STFT. Again, root-MUSIC performs poorly in first harmonic subgroup estimation (Figure 10.29).

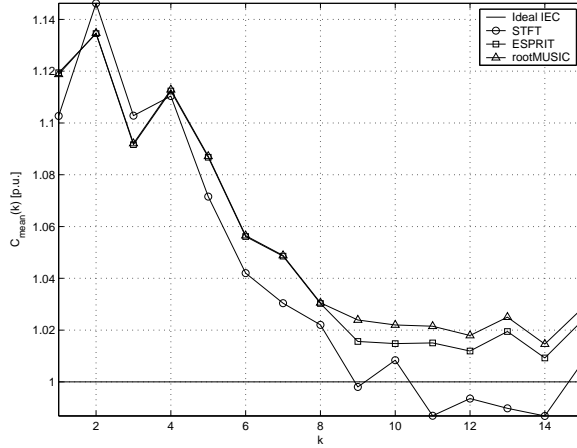


Figure 10.21. Progressive average of the third harmonic subgroup of the current

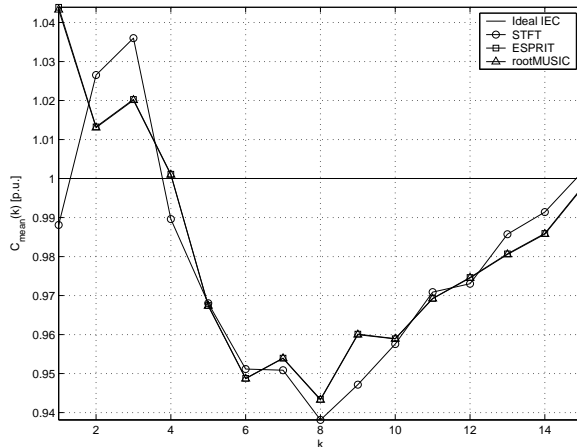


Figure 10.22. Progressive average of the fifth harmonic subgroup of the current

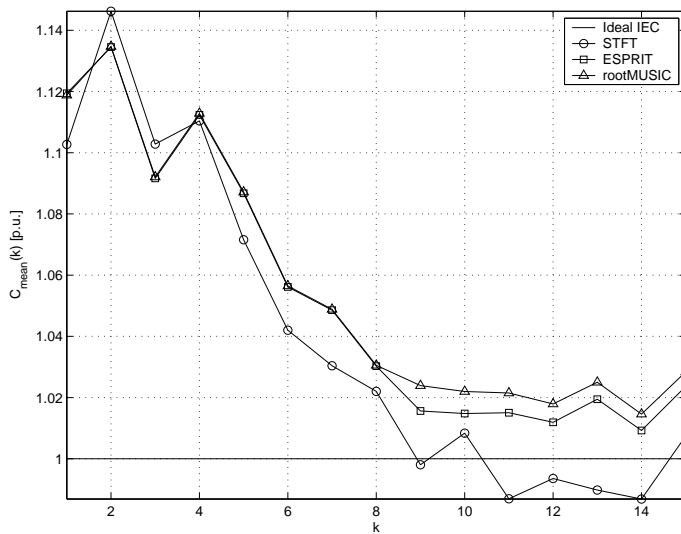


Figure 10.23. Progressive average of the third harmonic subgroup of the current

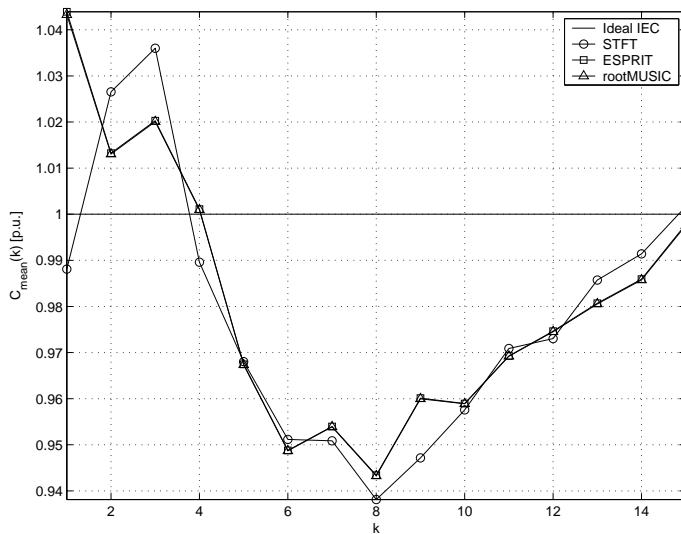


Figure 10.24. Progressive average of the fifth harmonic subgroup of the current

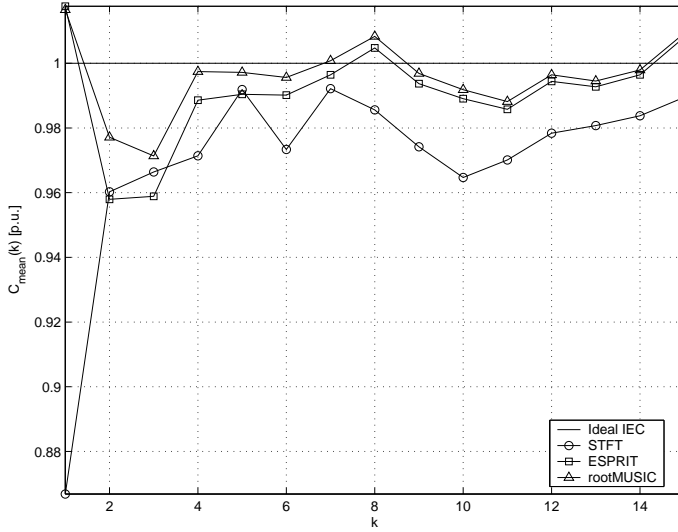


Figure 10.25. Progressive average of the eleventh harmonic subgroup of the current

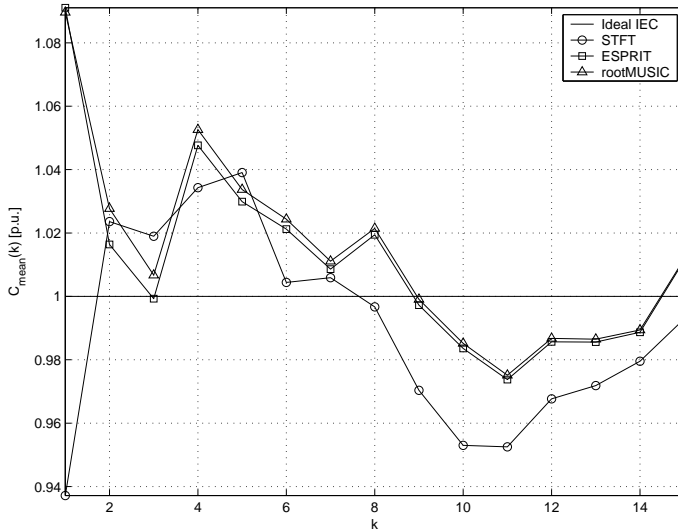


Figure 10.26. Progressive average of the thirteenth harmonic subgroup of the current

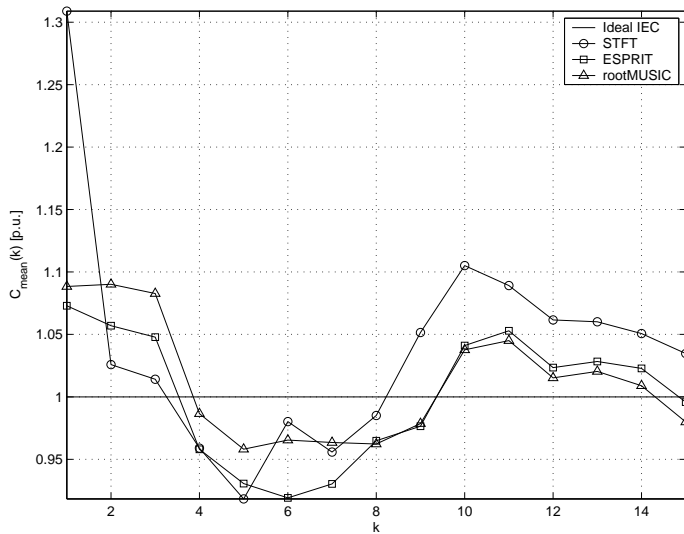


Figure 10.27. Progressive average of the first interharmonic subgroup of the current

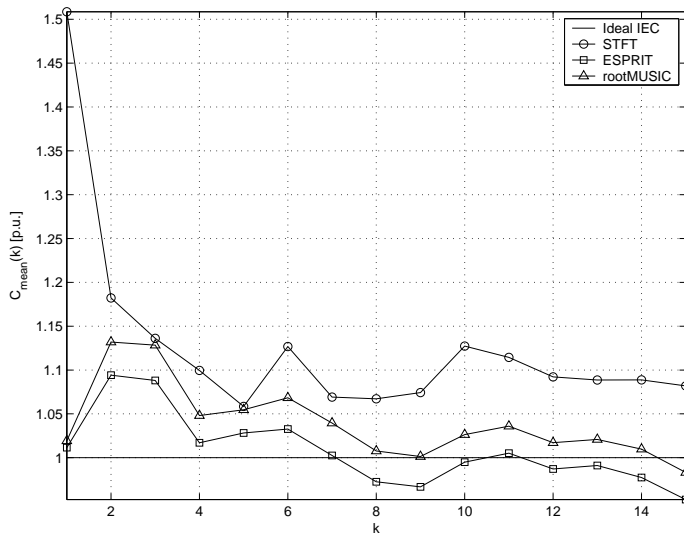


Figure 10.28. Progressive average of the second interharmonic subgroup of the current

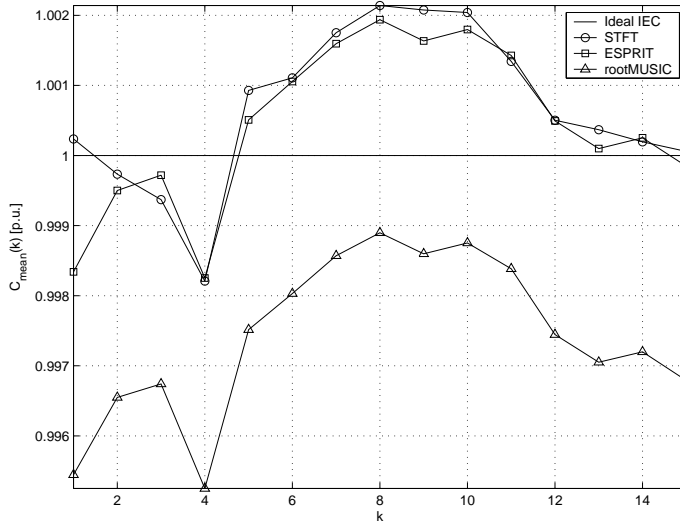


Figure 10.29. Progressive average of the first harmonic subgroup of the voltage

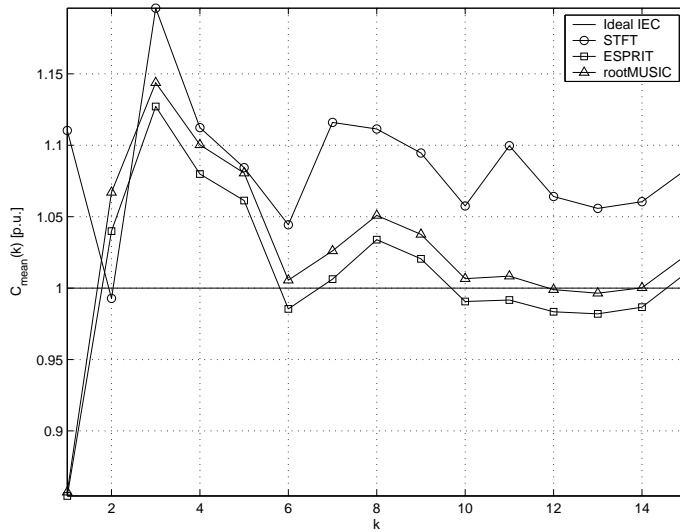


Figure 10.30. Progressive average of the fifth harmonic subgroup of the voltage

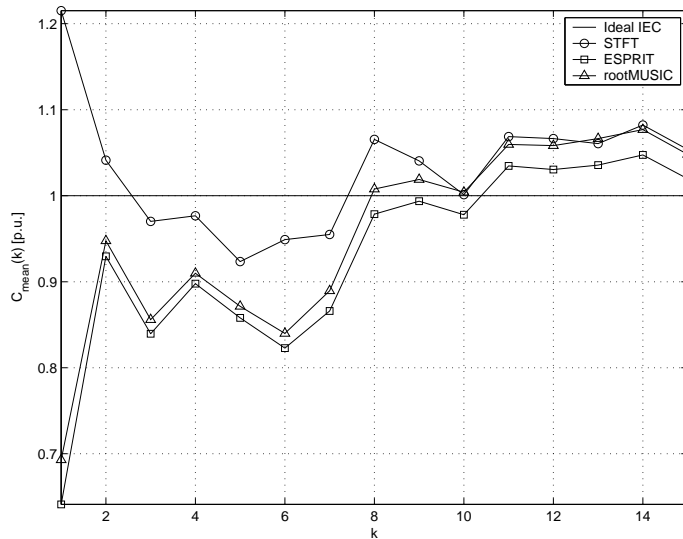


Figure 10.31. Progressive average of the seventh harmonic subgroup of the voltage

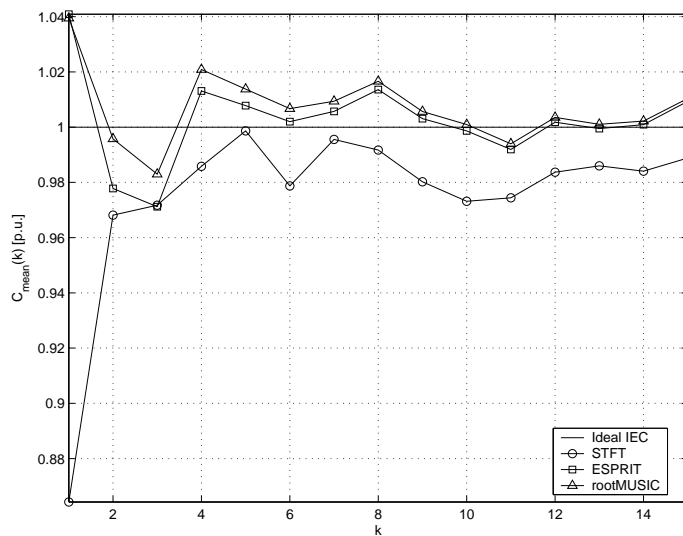


Figure 10.32. Progressive average of the eleventh harmonic subgroup of the voltage

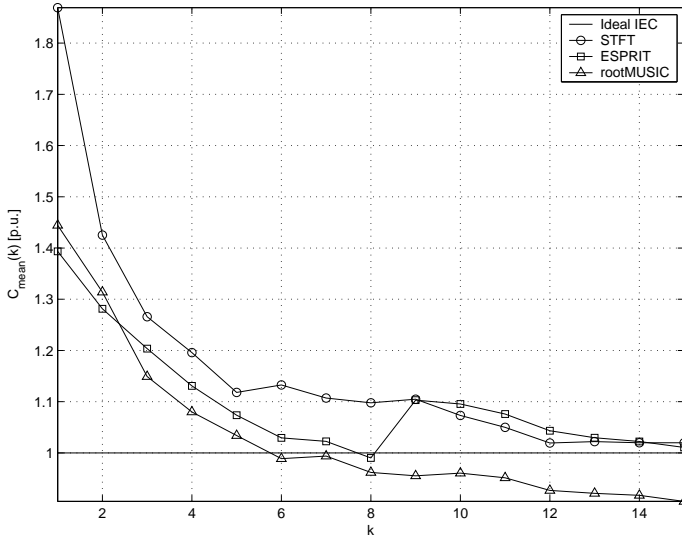


Figure 10.33. Progressive average of the first interharmonic subgroup of the voltage

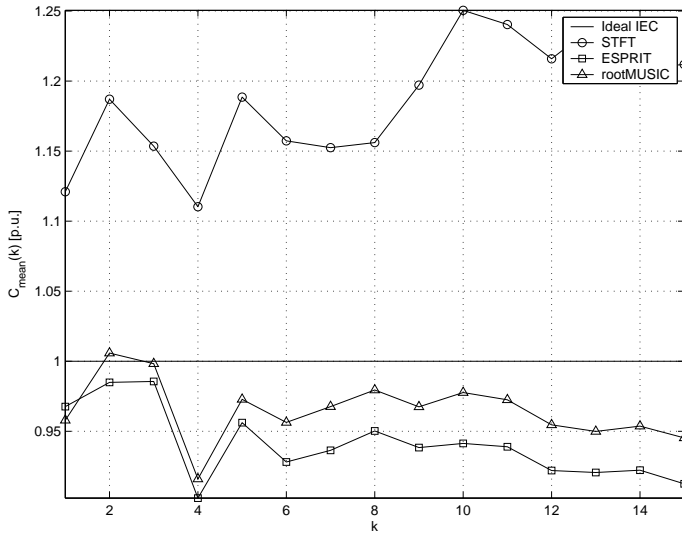


Figure 10.34. Progressive average of the second interharmonic subgroup of the voltage

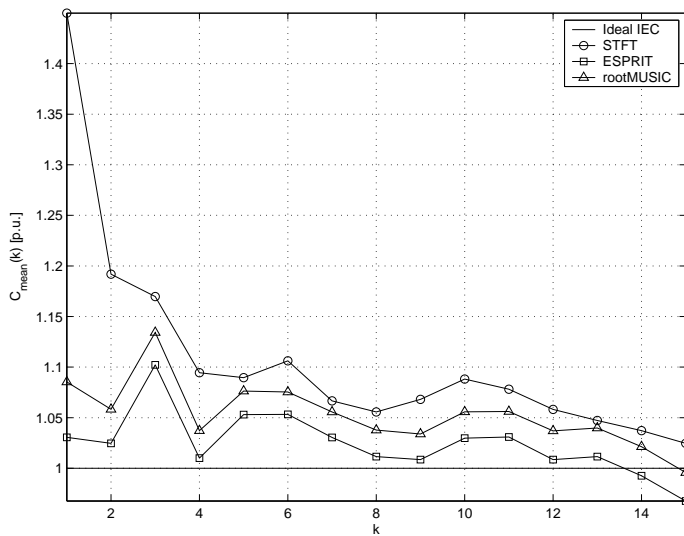


Figure 10.35. Progressive average of the eleventh interharmonic subgroup of the voltage

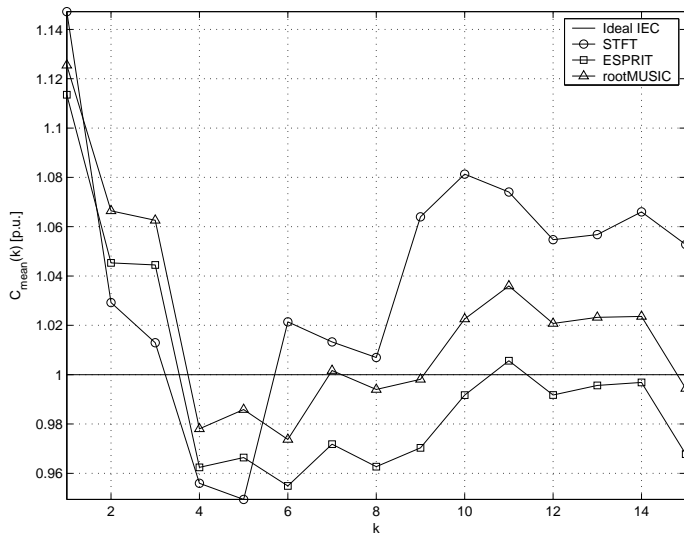


Figure 10.36. Progressive average of the twelfth interharmonic subgroup of the voltage

Table 10.1. Mean square error (MSE) of the progressive average of the current harmonic subgroups estimation. Value of Ideal IEC [A]

| Method | 1 st | 3 rd | 5 th | 7 th | 11 th | 13 th |
|---------------|-----------------|-----------------|-----------------|-----------------|------------------|------------------|
| STFT | 3.38 | 1.23 | 0.23 | 0.85 | 16.00 | 2.23 |
| ESPRIT | 5.96 | 1.33 | 0.22 | 0.05 | 2.83 | 2.08 |
| MUSIC | 5.80 | 1.37 | 0.22 | 0.07 | 1.26 | 2.24 |
| Ideal IEC [A] | 1757.90 | 17.00 | 13.85 | 23.64 | 95.50 | 46.76 |

Table 10.2. Mean square error (MSE) of the progressive average of the current interharmonics subgroups estimation. Value of Ideal IEC [A]

| Method | 1 st | 2 nd | 11 th | 12 th |
|---------------|-----------------|-----------------|------------------|------------------|
| STFT | 34.88 | 52.47 | 24.93 | 4.60 |
| ESPRIT | 9.22 | 3.02 | 2.67 | 8.14 |
| MUSIC | 8.40 | 6.19 | 4.57 | 5.35 |
| Ideal IEC [A] | 61.13 | 43.56 | 29.26 | 29.58 |

Table 10.3. Mean square error (MSE) of the progressive average of the voltage harmonics subgroups estimation. Value of Ideal IEC [V]

| Method | 1 st | 3 rd | 5 th | 7 th | 11 th | 13 th |
|---------------|-----------------|-----------------|-----------------|-----------------|------------------|------------------|
| STFT | 221.29 | 106.37 | 6.30 | 2.27 | 92.53 | 28.74 |
| ESPRIT | 202.17 | 201.79 | 2.37 | 6.33 | 14.18 | 27.36 |
| MUSIC | 1085.90 | 210.50 | 3.08 | 5.14 | 12.14 | 28.91 |
| Ideal IEC [V] | 11718.00 | 124.80 | 26.17 | 19.63 | 242.57 | 158.60 |

Tables 10.1–10.4 show values of the mean square error (MSE) of the estimation of interharmonic subgroups and allow comparison with the value of Ideal IEC. Values of MSE show excellent performance of parametric methods when computing interharmonic subgroups and slightly decreased accuracy in the case of harmonic subgroups, especially of voltage waveforms.

For all results presented previously, it can be seen (Table 10.5) that the ESPRIT method offers reduction of the average relative MSE of estimation of harmonic subgroups by 54% and MUSIC method by 50%, compared to FFT-based method.

Table 10.4. Mean square error (MSE) of the progressive average of the voltage interharmonics subgroups estimation. Value of Ideal IEC [V]

| Method | 1 st | 2 nd | 11 th | 12 th | 13 th |
|---------------|-----------------|-----------------|------------------|------------------|------------------|
| STFT | 367.48 | 205.84 | 116.20 | 26.29 | 55.41 |
| ESPRIT | 107.87 | 23.24 | 7.76 | 11.81 | 15.90 |
| MUSIC | 118.49 | 9.42 | 20.08 | 13.21 | 17.78 |
| Ideal IEC [V] | 70.20 | 75.20 | 72.69 | 82.87 | 75.70 |

Table 10.5. Relative mean square error (MSE) of the progressive average of harmonic and interharmonic subgroups estimation

| Method | Error of current | | Error of voltage | | Total error |
|--------|------------------|------------|------------------|------------|-------------|
| | harmonics | interharm. | harmonics | interharm. | |
| STFT | 0.057 | 1.271 | 1.419 | 4.480 | 1.731 |
| ESPRIT | 0.029 | 0.180 | 2.193 | 0.531 | 0.796 |
| MUSIC | 0.027 | 0.231 | 2.364 | 0.563 | 0.861 |

10.5. Classification of events

10.5.1. Introduction

The problem of classifying signals obtained from the industrial power frequency converters, using a new method (presented in Chapter 9) is considered in this section. The object of signal classification can be control or optimization of the modern frequency power converters, which generate a wide spectrum of harmonic components. Especially, the task of fault detection is difficult. A subset of faults, which are usually not detected by the protections (in underload conditions), is particularly hard to classify. In large converter systems, which generate not only characteristic harmonics typical of the ideal converter operation, but also a considerable amount of non-characteristic harmonics and interharmonics, the task of fault detection is particularly difficult [28], [58]. The characteristics of the signal can be better analyzed and understood if the correct representation is chosen. In case of heavily distorted signals, whose contents change with time, it can be expected that the time and frequency characteristics are the most important. The parametric time-frequency transformation can provide advantages when analyzing non-stationary signals due to its better temporal resolution, excellent performance in the presence of noise, and no phase dependence as with classical Fourier-based spectra. In

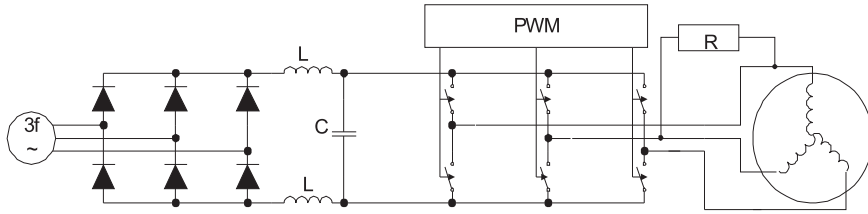


Figure 10.37. Simplified scheme of the simulated converter configuration. R – resistance of the short-circuit

the case of time-frequency representation of a signal it is possible to study simultaneously the time and frequency characteristics of the signal with best possible resolution non-parametric time-frequency transformations than. The signal classification is the assignment of the time-series to a specific class with given characteristics.

10.5.2. Numerical simulations

The signals under investigation are short-circuit currents obtained from a 3 kVA PWM converter simulated with the Power System Blockset of MATLAB[®] (Figures 10.37 and 10.38). Simulation system contains inverter and asynchronous machine models, as well as fault simulation circuit and space-phasor online computation modules.

Parameters of the simulated converter drive include:

- six-pulse (three-arm bridge) PWM inverter with ideal switches, carrier frequency 1000 Hz,
- three-phase supply with 25 kV/600 V 50 kVA transformer,
- lowpass filter with $L = 0.2$ mH, $C = 5$ μ F to 10 μ F,
- squirrel-cage type asynchronous machine $U_n = 220$ V, $P_n = 2.2$ kW, 50 Hz.

For classification purposes, all investigated three-phase waveforms were transformed to the complex space-phasor (see Equation (6.1)). Then its absolute value (example in Figure 10.39 for short-circuit resistance $R = 1$ Ω) is transformed to its time-frequency representation using parametric ESPRIT method with the help of temporal sliding window as shown in Figure 10.40.

Taken the representation of the waveform in time-frequency plane, as the next step, the areas in this plane can be chosen, either manually (based on observation) or automatically (based on some optimization algorithm, which, e.g., minimizes the classification error). Optimization approach is not developed in this work.

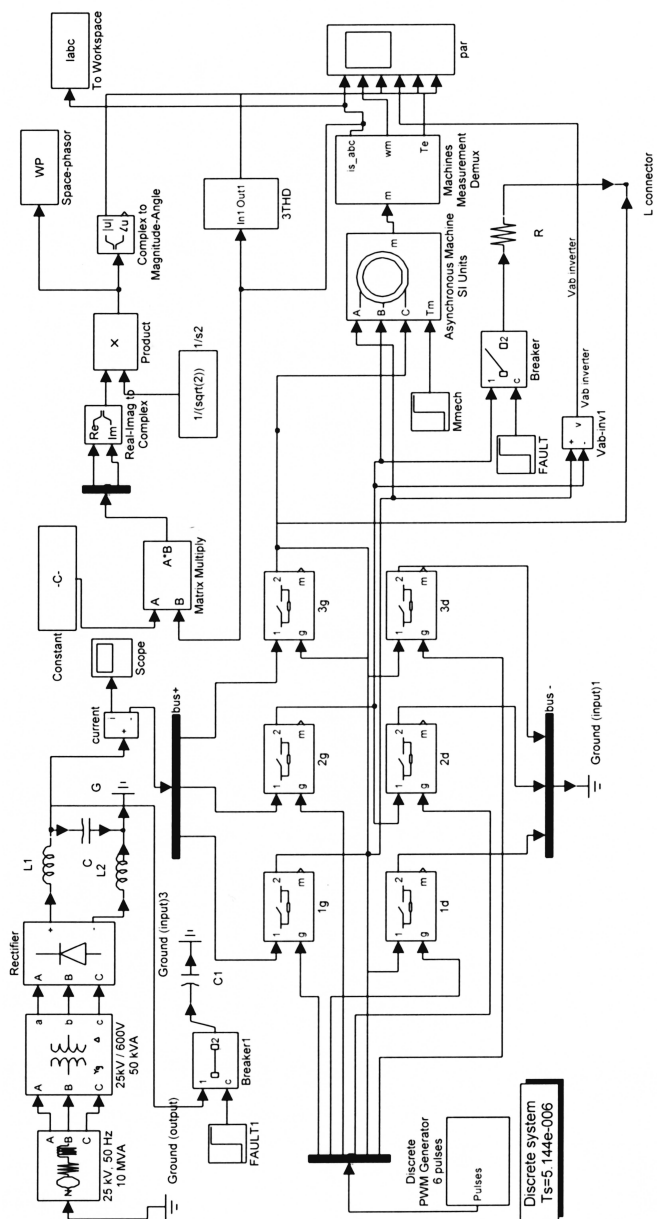


Figure 10.38. Model of the inverter drive in MATLAB[®] SimPowerSystem

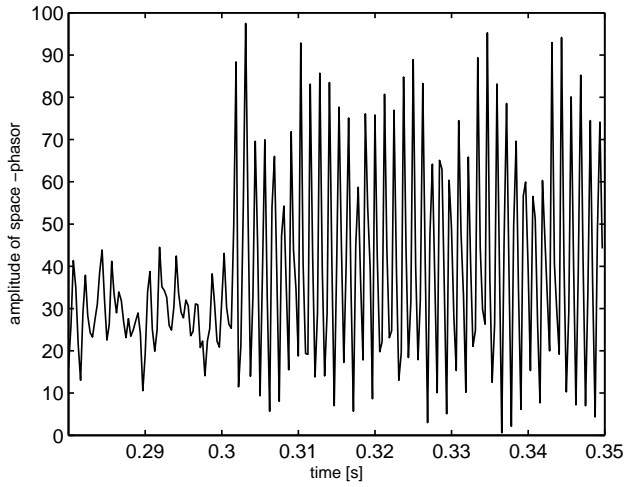


Figure 10.39. Absolute value of the space phasor of the inverter output currents. Short-circuit resistance $R = 1 \Omega$

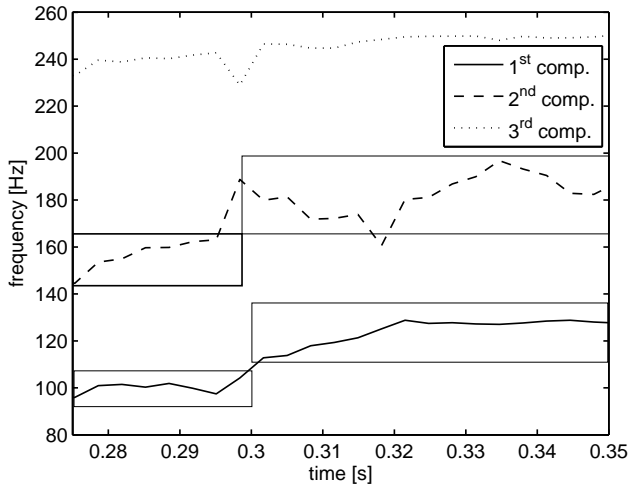


Figure 10.40. Time-frequency representation (ESPRIT-based) of the modulus of the space-phasor

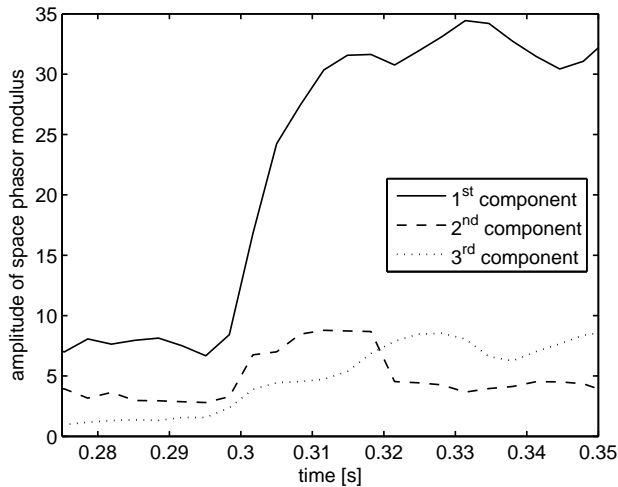


Figure 10.41. Corresponding amplitudes of components as in Figure 10.40

In Figure 10.40, the time-frequency representation (ESPRIT-based) of the modulus of the space-phasor of inverter output currents is presented. Three components are shown here and the fundamental component is removed. Corresponding amplitudes of components are shown in Figure 10.41. Selected areas for subsequent reconstruction are outlined as rectangular areas in time-frequency plane and summarized below:

- time interval: 0.27–0.3 s; frequency band: 92–108 Hz,
- time interval: 0.27–0.3 s; frequency band: 143–165 Hz,
- time interval: 0.3–0.35 s; frequency band: 112–138 Hz,
- time interval: 0.3–0.35 s; frequency band: 165–200 Hz.

There follows a classification procedure. As already shown in Figure 9.1, the parameters of the signal and pattern are extracted from their time-frequency representations, by taking only those parts of the signal which are contained within the selected "regions of interest" (examples shown in Figures 10.42). Extracted parameters (components' frequencies, amplitudes, duration in time, etc.) allow "reconstitution" (incomplete reconstruction) of preprocessed signals and patterns. The procedure is then followed by computation of classical, time-domain correlation sequence. The result of classification

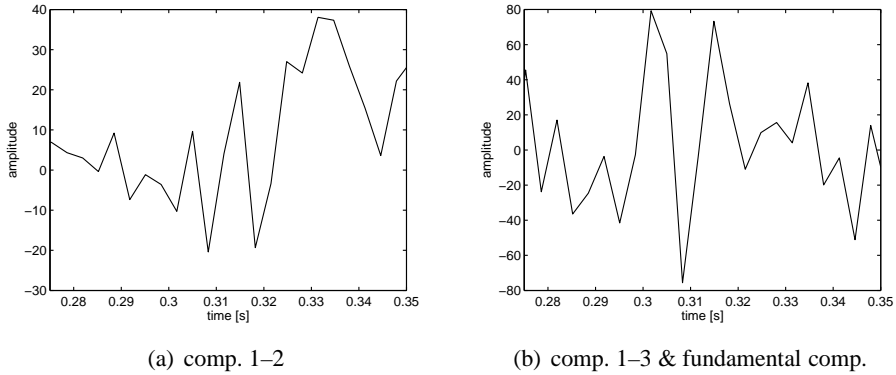


Figure 10.42. Reconstructed signal from components as shown in Figure 10.40

depends on the highest value of the correlation coefficient which shows, to some extent, the degree of similarity between signal under classification and previously selected pattern.

Result of application of the classification scheme described are presented in Table 10.6. Over 500 waveforms were simulated using different drive parameters (parameters of LC filter (from $5\mu\text{F}$ to $10\mu\text{F}$), value of short-circuit resistance (from $1\ \Omega$ to $100\ \Omega$), value of the shaft mechanical torque applied to the asynchronous machine (from 50 to 100 Nm – see Figure 10.38) in order to validate this classification approach.

From the analysis of Table 10.6 it should be noted that the use of high-resolution ESPRIT method and selection of areas of obtained time-frequency representation allows highest sensitivity of detection of a pattern (here: short-circuit waveform) hidden in the current waveform at the converter output (precisely the signal is composed of all three currents in the form of space-phasor). Classical time-domain correlation is almost useless for this classification task.

Table 10.6. Average of the highest correlation coefficients over 500 trials using ESPRIT, STFT and time-domain correlation

| Method | Classification ESPRIT-based | Classification STFT-based | Time-domain Correlation |
|-------------------------|--------------------------------|------------------------------|----------------------------|
| Signal contains pattern | 0.63 | 0.57 | 0.35 |
| No pattern | 0.15 | 0.22 | 0.33 |

In this section, a new method of classification of electric signals has been presented, based on the time-frequency representation and automatic signal classification with the help of a standard correlation technique. The investigations proved the validity of the proposed approach, however this method can lead to further improvements which can additionally increase its performance. Further work can include the design of the classification system with many classes, optimized and/or automatic choice of "areas of interest" in the time-frequency plane, application of other classification algorithms, etc.

Conclusions

The main goal of this work was to present a new approach to analysis in spectral domain of power systems using parametric spectrum estimation methods. After detailed theoretical treatment of many aspects of the approach proposed, including preprocessing using bandpass filters or filter banks (Chapter 5), estimation of the model order (Chapter 7), and analysis of non-stationary waveforms (Chapter 4) (including classification of events, Chapter 9), the second part is presented, devoted mainly to practical aspects and numerical analysis (Chapter 10).

In practical applications, one of the most important questions concerns the optimal choice of analysis methods when taking into account known parameters of the signal and limitations of the chosen analysis technique. These problems were addressed in section 10.2. Testing signals were chosen that correspond to most often encountered waveforms in power systems. Most important results show that an optimal size of the correlation matrix can be chosen. Further increase of the size of the correlation matrix or the use of forward–backward technique does not improve the accuracy – such a conclusion contradicts the established widespread opinions. In general, parametric methods show similar values of accuracy (with slight advantage of ESPRIT method) which greatly outperform the accuracy of FFT-based non-parametric method. Moreover, parametric methods show almost complete immunity to masking effect (see Figure 10.5) to variable initial phase of harmonic components and to many other deficiencies of FFT-based techniques, as shown in [32]). Interestingly, when comparing strongly simplified theoretical expressions related to performance of ESPRIT and MUSIC (see equations (3.51) and (3.56)), the main result is confirmed in numerical simulations (ESPRIT is more accurate than MUSIC), although the difference of performance is not as high as sixfold.

Results of estimation of the model order concern the problem specific to parametric methods. It is necessary to obtain the exact number of components contained within the analyzed signal. Wrong estimation of the number of components leads to errors, although ESPRIT seems to be less affected [35]. The analysis performed by the author shows the possibility of application of known statistical information criteria (Section

10.3). It should be noted that the on-line estimation of the number of components works well for few components only, but this shortcoming can be overcome by narrow-band local analysis of the signal. This approach limits the number of components to be determined, improves the SNR and increases the spacing between close spectral lines (improves resolution), as shown in Chapter 5). However, in many applications there is no need for estimation of the number of components because this information is known in advance.

Chapter 8 and section 10.4 are devoted to the assessment of the power quality. Most power quality indices use FFT-based techniques. It was shown that application of parametric methods allows approximately 50% reduction of the estimation error (page 92). This result was obtained despite the fact that for comparison a procedure was chosen where the minimum error is expected for FFT-based technique (i.e., analysis window length equal to one period of the fundamental harmonic). Even higher gains in accuracy were achieved when analyzing waveforms with high inter/sub-harmonic contents [58, 60].

The proposed classification approach, presented in Chapter 9, uses the space-phasor for representation of three-phase signal, its parametric time-frequency representation and subsequent selection of most significant areas in the time-frequency plane.

The author proved that for the analysis of narrow-band (line-spectra) it is sufficient to analyze narrow band- and time-limited areas of their time-frequency representations plane (see Chapter 4). Such approach not only provides sufficient information for subsequent analysis (see Section 4.2). It also improves its performance by enhancing the signal-to-noise ratio, improving the resolution (see Chapter 5) and improving the classification rate of correlation-based classification approach (see Theorem 13). The use of high-resolution methods significantly improves the accuracy of many parameter estimation techniques. Both approaches combined allow further improvements (in Chapter 10 numerous examples are shown).

There exist in the recent literature a large group of methods aiming at reduction of the computational burden associated with the estimation of the correlation matrix. These methods include subspace tracking, projection approximation, partial update of the correlation matrix and many others, not considered in this work. From preliminary investigations the author concluded that the expected gain in computation time is not a justification for significant increase of the error of parameter estimation, especially for non-stationary signals. With the constant increase of computational power of modern processors the calculation time becomes less troublesome than the accuracy of results achieved. Moreover, the results presented in Figure 10.2 show that optimal accuracy is practically achieved when using quite small correlation matrices which can be computed

in little time (see Figures 10.2 and 10.3). The complete TLS-ESPRIT procedure including correlation matrix computation takes 0.01–0.1 s only on an average PC running Matlab®³.

In the light of precedent considerations the main thesis (see page 9) of this work appears to be proven.

Outlook

The approaches to signal analysis in power systems, presented in this work, will be extended in the future in many ways.

Sliding window approach, used for non-stationary signal analysis, can be modified by using variable length windows, where the window length can be determined on the basis of optimization of a chosen output parameter. Such an approach is quite widely applied (e.g., in [63]), although the advantages seem not to be very important for the applications considered in this work.

Classification procedure can be improved by applying the optimization procedure to the choice of "areas of interest", by applying other classification algorithms [40], other time-frequency representations. It is foreseeable that such improvements could bring about some enhancement in sensitivity and specificity of the classification procedure.

One important problem is the reliable estimation of waveform parameters when the signals under investigation have a strong stochastic nature (for example, electric arc furnace). It is often desirable to get representative results also for such signals which present impulse disturbances. In such cases robust statistical methods can be efficiently applied and allow elimination of stochastic (non-repetitive) part of the signal [36].

³ PC with 2.8 GHz processor clock , 1 GB of RAM, Matlab® ver. 7.0.1.

Bibliography

- [1] Altmann J., *Surfing the Wavelets*, Monash University, <http://www.wavelet.org/tutorial/>, 1996, online.
- [2] Beckmann C.F., Smith S.M., *Probabilistic Independent Component Analysis for Functional Magnetic Resonance Imaging*, FMRIB Technical Report TR02CB1, Department of Clinical Neurology, University of Oxford, Oxford, UK, 2003.
- [3] Bozdogan H., *Model selection and Akaike's information criterion (AIC): The general theory and its analytical extensions*, *Psychometrika*, Vol. 51, 1987, pp. 345–370.
- [4] Bracale A., Carpinelli G., Lauria D., Leonowicz Z., Łobos T., Rezmer J., *On some spectrum estimation methods for analysis of non-stationary signals in power systems. Part 1. Theoretical aspects*, 11th International Conference on Harmonics and Quality of Power, ICHQP, Lake Placid, New York, Sept. 12–15, 2004, CD-ROM.
- [5] Bracale A., Carpinelli G., Lauria D., Leonowicz Z., Łobos T., Rezmer J., *On some spectrum estimation methods for analysis of non-stationary signals in power systems. Part 2. Numerical applications*, 11th International Conference on Harmonics and Quality of Power, ICHQP, Lake Placid, New York, Sept. 12–15, 2004, CD-ROM.
- [6] Bracale A., Carpinelli G., Lauria D., Leonowicz Z., Łobos T., Rezmer J., *Spectrum estimation of non-stationary signals in traction systems*, Proceedings of the International Conference on Power Systems, (ICPS 2004), Kathmandu, Nepal, Nov. 3–5, 2004, Vol. 1, pp. 821–826.
- [7] Bracale A., Carpinelli G., Leonowicz Z., Łobos T., Rezmer J., *Evaluation of Compensation Devices of DC Arc Furnaces using Advanced Spectrum Estimation Methods*, Power System Computation Conference, Liège, Belgium (PSCC 2005), CD-ROM.
- [8] Bracale A., Carpinelli G., Leonowicz Z., Łobos T., Rezmer J., *Waveform Distortions due to AC/DC Converters Feeding DC Arc Furnaces*, 8th International Conference "Electrical Power Quality and Utilisation" (EPQU'2005), Kraków, 2005.
- [9] Bracale A., Carpinelli G., Leonowicz Z., Łobos T., Rezmer J., *Measurement of IEC groups and subgroups using advanced spectrum estimation methods*, Proceedings of the 23rd IEEE Instrumentation and Measurement Technology Conference (IMTC/06), Sorrento, Italy, 24-27 April 2006, pp. 1015–1020.
- [10] Cichocki A., Shishkin S., Musha T., Leonowicz Z., Asada T., Kurachi T., *EEG filtering based on blind source separation (BSS) for early detection of Alzheimer's disease*, *Clin. Neurophysiology*, Vol. 116, No. 3, 2005, pp. 729–737.

- [11] Claasen T.A.C.M., Mecklenbrauker W.F.G., *The Wigner distribution – A tool for time-frequency signal analysis – Part II: Discrete-time signals*, Philips J. Res., Vol. 35, Oct. 1980, pp. 276–300.
- [12] Canadian-American User Group, *EMTP-ATP Rule Book*, 1987–1992.
- [13] Cohen L., *Time-Frequency Analysis*, Englewood Cliffs, NJ, Prentice–Hall, 1995.
- [14] Dickie J.R., Nandi A.K., *A comparative study of AR order selection methods*, Signal Processing, Vol. 40, 1996, pp. 239–255.
- [15] Flandrin P., *Time-Frequency/Time-Scale Analysis*, San Diego, Academic Press, 1998.
- [16] Flores R., *Signal Processing Tools for Power Quality Event Classification*, Technical Report No. 477L, Department of Signals and Systems, Department of Electric Power Engineering, Chalmers University of Technology, Göteborg, Sweden, 2003.
- [17] Golub G.H., Van Loan C.F., *Matrix Computations*, London, The Johns Hopkins University Press, Third edition, 1996.
- [18] Gröchenig K., *Foundations of Time-Frequency Analysis*, Boston, Birkhäuser, 2001.
- [19] Hari K.V.S., Ramakrishnan B.V., *Performance analysis of modified spatial smoothing technique for direction estimation*, Signal Processing, No. 79, 1999, pp. 73–85.
- [20] Iaramillo S.H., Heydt G.T., Neill Carrello E.O., *Power Quality Indices for Aperiodic Voltages and Currents*, IEEE Trans. on Power Delivery, Vol. 15, April 2000, pp. 784–790.
- [21] IEC, *General Guide on Harmonics and Interharmonics Measurements, for Power Supply Systems and Equipment Connected Thereto*, IEC Std. 61000-4-7.
- [22] IEC, *Power Quality Measurement Methods, Testing and Measurement Techniques*, IEC Std. 61000-4-30.
- [23] Janik P., Leonowicz Z., Schegner P., *Analyse nicht stationärer Signale in Energiesystemen*, Elektrische, No. 9/12, 2002, pp. 321–328.
- [24] Kandil M.S., Farghal S.A., Elmitwally A., *Refined Power Quality Indices*, IEE Proc. Gener., Trans. Distr., Vol. 148, Nov. 2001, pp. 590–596.
- [25] Kangas A., Stoica P., Söderström T., *Finite sample and modelling error effect on ESPRIT and MUSIC direction estimators*, IEE Proceedings on Radar, Sonar and Navigation, Vol. 141, No. 5, 1994, pp. 249–255.
- [26] Kangas A., Stoica P., Söderström T., *Large-Sample Analysis of MUSIC and Min-Norm Direction Estimators in the Presence of Model Errors*, IEEE Trans. on Circuits, Systems, and Signal Processing, Vol. 15, 1996, pp. 377–393.
- [27] Kil D.H., Shin F.B., *Pattern Recognition and Prediction with Applications to Signal Characterization*, Woodbury, N.Y., AIP Press, 1996.
- [28] Kay S.M., *Modern Spectral Estimation*, Englewood Cliffs, NJ, Prentice–Hall, 1988.
- [29] Koglin H.-J., Leonowicz Z., Łobos T., *Identification of out-of-step operation of synchronous machines using high resolution spectrum estimation methods*, Modern Electric Power Systems (MEPS '02), Wrocław, Sept. 11–13, 2002, pp. 378–383.
- [30] Kovacs K.P., *Symmetrische Komponenten in Wechselstrommaschinen*, Birkhäuser Verlag, 1962.
- [31] Kusuma J., *Parametric Frequency Estimation: ESPRIT and MUSIC*, Rice University, <http://cnx.rice.edu/content/m10588/>, 2002.

- [32] Leonowicz Z., *Analysis of non-stationary signals in power systems*, International Journal for Computation and Mathematics in Electronic Engineering COMPEL (Great Britain), Vol. 23, No. 2, 2004, pp. 381–391.
- [33] Leonowicz Z., *Performance of parametric spectrum estimation methods*, XXIX Międzynarodowa Konferencja z Podstaw Elektrotechniki i Teorii Obwodów (IC–SPETO 2006), Gliwice-Ustroń, 24-27.05.2006, Vol. 2, pp. 227–230.
- [34] Leonowicz Z., Karvanen J., Tanaka T., Rezmer J., *Model order selection criteria: comparative study and applications*, Computational problems of electrical engineering. Proceedings of the $V I^{th}$ International Workshop, Zakopane, Sept. 1–4, 2004, pp. 193–196.
- [35] Leonowicz Z., Karvanen J., Tanaka T., Rezmer J., *Model order selection criteria: comparative study and applications*, Prz. Elektrotech., R. 81, No. 2, 2005, pp. 47–50.
- [36] Leonowicz Z., Karvanen J., Shishkin S., *Trimmed estimators for robust averaging of event-related potentials*, J. Neurosci. Methods, Vol. 142, No. 1, 2005, pp. 17–26.
- [37] Leonowicz Z., Łobos T., *Advanced spectral analysis of out-of-step operation of synchronous machines*, IFAC Symposium on Power Plants and Power Systems Control 2003, Seoul, Korea, Sept. 15–19, 2003, CD-ROM.
- [38] Leonowicz Z., Łobos T., *Analysis of Traction System Time-Varying Signals using ESPRIT Subspace Spectrum Estimation Method*, 32nd Annual Conference of the IEEE Industrial Electronics Society, IECON 2006, accepted.
- [39] Leonowicz Z., Łobos T., *Application of time-frequency distribution and neural networks for fault classification in power electronics*, IEEE International Symposium on Computational Intelligence for Measurement Systems and Applications (CIMSA '03), Lugano, Switzerland, July 29–31, 2003, pp. 67–71.
- [40] Leonowicz Z., Łobos T., *Automatic fault classification in power electronics using time-frequency distribution and neural networks*, 12th Intelligent Systems Applications to Power Systems Conference (ISAP 2003), Lemnos, Greece, 31 August–3 September, 2003, CD-ROM.
- [41] Leonowicz Z., Łobos T., *Modern spectral analysis of non-stationary signals in power electronics*, 5th Workshop on Electronics, Control, Modelling, Measurement and Signals, Université Paul Sabatier, Toulouse, May 30–31, June 1, 2001, pp. 115–119.
- [42] Leonowicz Z., Łobos T., *Power Quality Evaluation using Advanced Spectrum Estimation Methods*, 2006 International Conference on Power System Technology "Opportunities and Challenges under Rapid Power Growth", accepted.
- [43] Leonowicz Z., Łobos T., *Time-frequency analysis of non-stationary three phase signals*, 15th Triennial World Congress of the International Federation of Automatic Control, Barcelona (IFAC 2002), 21–26 July 2002, CD-ROM.
- [44] Leonowicz Z., Łobos T., Rezmer J., *Advanced spectrum estimation methods for signal analysis in power electronics*, IEEE Trans. Industr. Electron., Vol. 50, No. 3, 2003, pp. 514–519.
- [45] Leonowicz Z., Łobos T., Rezmer J., *Spectrum estimation of non-stationary signals in power systems*, Proceedings of the 5th International Conference on Power Systems Transients (IPST 2003), New Orleans, Louisiana, USA, Sept 28–Oct 2, 2003, CD-ROM.

- [46] Leonowicz Z., Łobos T., Rezmer J., *Spectrum estimation of non-stationary electrical signals*, XXVI Międzynarodowa Konferencja z Podstaw Elektrotechniki i Teorii Obwodów (IC-SPETO 2003), Gliwice-Niedzica, May 28–31, 2003, Vol. 2, pp. 411–414.
- [47] Leonowicz Z., Łobos T., Rezmer J., *Spectrum estimation methods for signal analysis in the supply system of DC arc furnace*, Proceedings of the XIII International Symposium on Theoretical Electrical Engineering (ISTET '05), Lviv, July 4–7, 2005, pp. 161–164.
- [48] Leonowicz Z., Łobos T., Ruczewski P., Szymańda J., *Analysis of distorted signals using HOS*, International Journal for Computation and Mathematics in Electronic Engineering COMPEL (Great Britain), Vol. 17, Issue 5/6, 1998, pp. 602–611.
- [49] Leonowicz Z., Łobos T., Schegner P., *Modern spectral analysis of non-stationary signals in electrical power systems*, 14th Power System Computation Conference (PSCC 2002), Sevilla, Spain, June 24–28, 2002, CD-ROM.
- [50] Leonowicz Z., Łobos T., Schegner P., *Time-frequency distribution for automatic fault classification in power electronics*, Proceedings of the 13th International Conference on Power System Protection (PSP 2002), Bled, Slovenia, Sept. 25–27, 2002, pp. 93–97.
- [51] Leonowicz Z., Łobos T., Sikorski T., *Time-frequency analysis of three phase signals using Wigner distribution*, IVth International Workshop: Computational Problems of Electrical Engineering, Zakopane, Sept. 2–5, 2002, pp. 81–84.
- [52] Leonowicz Z., Łobos T., Waclawek Z., Schegner P., *Time-frequency distribution for fault classification in electrical engineering*, XXV Międzynarodowa Konferencja z Podstaw Elektrotechniki i Teorii Obwodów (IC-SPETO 2002), Gliwice-Ustroń May, 22–25, 2002, Vol. 2, pp. 521–524.
- [53] Leonowicz Z., Łobos T., Woźniak K., *Zastosowanie transformaty S do analizy sygnałów niestacjonarnych w elektrotechnice*, XXVIII Międzynarodowa Konferencja z Podstaw Elektrotechniki i Teorii Obwodów (IC-SPETO 2005), Gliwice-Ustroń, May 11–14, 2005, Vol. 2, pp. 379–382.
- [54] Łobos T., *Fast estimation of symmetrical components in real time*, IEE Proceedings-C, Vol. 139, No. 1, 1992, pp. 27–30.
- [55] Łobos T., Leonowicz Z., *Badania stanów awaryjnych układów przekształtnikowych z zastosowaniem statystyk wyższych rzędów*, Jakość i Użytkowanie Energii Elektrycznej, Vol. V, Iss. 1, 1999, pp. 37–42.
- [56] Łobos T., Leonowicz Z., *Hochauflösende Signalverarbeitungsmethoden in der elektrischen Energietechnik*, Elektrie, 2002, No. 9/12, pp. 315–320.
- [57] Łobos T., Leonowicz Z., Rezmer J., *Advanced spectrum estimation methods for signal analysis in power electronics*, The 2001 IEEE International Symposium on Diagnostics for Electrical Machines, Power Electronics and Drives (SDEMPED 2001), Grado, Italy, Sept. 1–3, 2001, pp. 333–337.
- [58] Łobos T., Leonowicz Z., Rezmer J., *Harmonics and interharmonics estimation using advanced signal processing methods*, IEEE Ninth International Conference on Harmonics and Quality of Power, Orlando, Florida, Oct. 1–4, 2000, Vol. 1, pp. 335–340.
- [59] Łobos T., Leonowicz Z., Rezmer J., Koglin H.-J., *Advanced signal processing methods*

- of harmonics and interharmonics estimation*, IEE Seventh International Conference on Developments in Power System Protection, Amsterdam, 9–12 April, 2001, pp. 315–318.
- [60] Łobos T., Leonowicz Z., Rezmer J., Koglin H.-J., *Advanced spectrum estimation methods for signal analysis in electrical engineering*, XI International Symposium on Theoretical Electrical Engineering (ISTET '01), Johannes Kepler University Linz, Linz, Austria, August 19–22, 2001, CD-ROM.
- [61] Łobos T., Leonowicz Z., Rezmer J., Schegner P., *High resolution spectrum estimation methods for signal analysis in power systems.*, IEEE Trans. Instrum. Meas., 2006, Vol. 55, No 1, pp. 219–225.
- [62] Łobos T., Sikorski T., Leonowicz Z., *Time-frequency analysis of complex space-phasor in power electronics*, Proceedings of the 21st IEEE Instrumentation and Measurement Technology Conference (IMTC/04), Como, Italy, 18–20 May, 2004, Vol. 3, pp. 2115–2119.
- [63] Mallat S., Papanicolaou G., Zhang Z., *Adaptive covariance estimation of locally stationary processes*, Annals of Statistics, Vol. 26, 1998, pp.1–47.
- [64] Martin W., Flandrin P., *Wigner–Ville Spectral Analysis of Nonstationary Processes*, IEEE Trans. on Acoustics, Speech and Signal Processing, Vol. Assp. 33, No. 4, Dec. 1985, pp. 1461–1470.
- [65] Mikołajuk K., *Podstawy analizy obwodów energoelektronicznych*, Warszawa, Wydawnictwo Naukowe PWN, 1998.
- [66] Minka T., *Automatic Choice of Dimensionality for PCA*, Advances in Neural Information Processing Systems (NIPS), MIT Press, Vol. 13, 2000.
- [67] Naidu P.S., *Modern Spectrum Analysis of Time Series*, Boca Raton, Florida, CRC Press, 1996.
- [68] Pisarenko V.F., *The retrieval of harmonics from a covariance function*, Geophysics J. Roy. Astron. Soc., Vol. 33, 1973, pp. 347–366.
- [69] Quian S., Chen D., *Joint Time-Frequency Analysis; Methods and Applications*, Upper Saddle River, NJ, Prentice–Hall PTR, 1996, pp. 45–199.
- [70] Rao B.D., Hari K.V.S., *Performance Analysis of ESPRIT and TAM in determining the direction of arrival of plane waves in noise*, IEEE Trans. on Acoustics, Speech and Signal Processing, Vol. 37, No. 12, 1989, pp. 1990–1995.
- [71] Rao B.D., Hari K.V.S., *Performance Analysis of Root-Music*, IEEE Trans. on Acoustics, Speech and Signal Processing, Vol. 37, No. 12, 1989, pp. 1939–1949.
- [72] Rice J.R., *Mathematical Statistics and Data Analysis*, Belmont, Duxbury Press, 1995.
- [73] Rissanen J., Speed T., Yu B., *Density estimation by stochastic complexity*, IEEE Trans. on Information Theory, 1992, pp. 315–323.
- [74] Roy R., Kailath T., *ESPRIT – Estimation of Signal Parameters via Rotational Invariance Techniques*, IEEE Transactions on Acoustics, Speech, and Signal Processing, Vol. ASSP–37, 1989, pp. 984–995.
- [75] Ruhm D., *Visualisierung einer stromrichtergespeisten Asynchronmaschine*, PhD dissertation, Rozprawa doktorska, Politechnika Wrocławska, Wydział Elektryczny, Wrocław, promotor Tadeusz Łobos, 2001.

- [76] Schmidt R.O., *Multiple emitter location and signal parameter estimation*, Proc. RADC Spectrum Estimation Workshop, Griffiss AFB, NY, 1979, pp. 243–258.
- [77] Schwarz G., *Estimating the dimension of a model*, Annals of Statistics, Vol. 6, 1978, pp. 461–464.
- [78] Sedjić E., Jiang J., *Comparative study of three time-frequency representations with applications to a novel correlation method*, Proc. of IEEE International Conf. on Acoustics, Speech, and Signal Processing (ICASSP), Montreal, May 17–21, 2004, Vol. 2, pp. 633–636.
- [79] Serrano-Iribarnegaray L., *The modern space-phasor theory, Part I, 1st coherent formulation and its advantages for transient analysis of converter-fed AC machines*, ETEP, Vol. 3, No. 2, March/April 1993, pp. 171–180.
- [80] Shan P., Beex A.A., *High-resolution instantaneous frequency estimation based on time-varying AR modeling*, Proceedings of the IEEE–SP Int. Symposium on Time-Frequency and Time-Scale Analysis, Pittsburgh, USA, Oct. 6–9, 1998, pp. 109–112.
- [81] Stoica P., Moses R., *Introduction to Spectral Analysis*, Upper Saddle River, New Jersey, Prentice–Hall PTR, 1997.
- [82] Stoica P., Nehorai A., *Music, maximum-likelihood and the Cramer–Rao bound*, IEEE Trans. on Signal Processing, No. 37, 1989, pp. 720–741.
- [83] Stoica P., Nehorai A., *Performance comparison of subspace rotation and Music-like methods*, IEEE Trans. Acoust. Speech, Signal Processing, No. 39, 1991, pp. 446–453.
- [84] Swami A., *Cumulant-Based Approach to the Harmonic Retrieval and Related Problems*, IEEE Transactions on Signal Processing, Vol. 39, Iss. 5, 1995, pp. 1099–1108.
- [85] Therrien C.W., *Discrete Random Signals and Statistical Signal Processing*, Englewood Cliffs, New Jersey, Prentice Hall PTR, 1992.
- [86] Tkacenko A., Vaidyanathan P.P., *The role of filter banks in sinusoidal frequency estimation*, Journal of the Franklin Institute, Vol. 338, No. 5, 2001, pp. 517–547.
- [87] Vaidyanathan P.P., *Multirate Systems and Filter Banks*, Englewood Cliffs, NJ, Prentice–Hall, Inc., 1993.
- [88] Vaidyanathan P.P., *Orthonormal and biorthonormal filter banks as convolvers, and convolutional coding gain*, IEEE Trans. Signal Processing, Vol. 41, No. 6, 1993, pp. 2110–2130.
- [89] Velez E.F., Absher R.G., *Spectral Estimation Based on the Wigner–Ville Representation*, Signal Processing, vol. 20, No. 4, 1990, pp. 325–347.
- [90] Wax M., Kailath T., *Detection of Signals by Information Theoretic Criteria*, IEEE Trans. on Acoustics, Speech, and Signal Processing, Vol. ASSP–33, No. 2, 1985, pp. 387–392.

Parametryczne metody analizy czasowo-częstotliwościowej sygnałów elektrycznych

Praca niniejsza jest kontynuacją i rozwinięciem cyklu publikacji autora (Literatura strony 103–108 pozycje literaturowe [4]–[10], [29], [32]–[53], [55]–[62]), mającą na celu ich usystematyzowanie i uzupełnienie. Autor proponuje nową metodologię analizy widmowej sygnałów elektrycznych (w tym trójfazowych) i wiele metod pochodnych przy pomocy metod podprzestrzeni (metod o wysokiej rozdzielczości, parametrycznych metod estymacji widma, takich jak MUSIC i ESPRIT), a także poddaje analizie właściwości różnych metod analizy widmowej, zastosowanych w praktyce.

W pracy przedstawiono kilka nowych koncepcji, które wzajemnie się uzupełniają, tworzą ramy nowego podejścia do analizy widmowej sygnałów elektrycznych. Koncepcje te obejmują zagadnienie wykorzystania większej dokładności metod parametrycznych w porównaniu do klasycznych metod wykorzystujących transformatę Fouriera, koncepcję analizy i identyfikacji na podstawie wybranych obszarów reprezentacji czasowo-częstotliwościowej sygnału, wykorzystania wektora przestrzennego do transformacji sygnałów trójfazowych, wykorzystania filtrów pasmowych (banki filtrów) do poprawy dokładności wyznaczania parametrów.

Praca obejmuje szczegółową analizę teoretyczną prezentowanych zagadnień, która jest jednak ściśle podporządkowana praktycznym aspektom zastosowania metod parametrycznych do analizy sygnałów elektrycznych. Przedstawiono w pracy także wyniki badań symulacyjnych obejmujących porównanie dokładności metod parametrycznych, wyznaczania rzędu modelu, wskaźników jakości energii i klasyfikacji zakłóceń.

List of Figures

| | | |
|-------|--|----|
| 1.1. | Jean-Baptiste Joseph Fourier | 13 |
| 4.1. | Energy concentration of two harmonic components in the time-frequency plane. | 42 |
| 5.1. | Filter bank approach for spectrum estimation | 44 |
| 5.2. | M -channel uniform analysis filter bank | 46 |
| 5.3. | Ideal analysis filter. | 47 |
| 5.4. | Spectrum of two sinusoidal components and filter | 48 |
| 6.1. | Simple cases of asymmetry and distortion of three-phase waveforms | 54 |
| 8.1. | Evolution of power quality monitoring equipment [16] | 60 |
| 8.2. | Examples of harmonic (\uparrow) and interharmonic (\downarrow) subgroups according to IEC Standard drafts 61000-4-7 and 61000-4-30 [4] | 62 |
| 9.1. | Scheme of correlation-based classification relying on TF transformation. | 65 |
| 10.1. | MSE of frequency and power estimation (ESPRIT, MUSIC) depending on SNR. Averaged 1000 independent runs | 70 |
| 10.2. | MSE of frequency and power estimation (ESPRIT, MUSIC) depending on the size of correlation matrix. Averaged 1000 independent runs | 71 |
| 10.3. | MSE of frequency and power estimation (ESPRIT, MUSIC) and average calculation time depending on the data window length. Averaged 10000 independent runs | 72 |
| 10.4. | MSE of frequency and power estimation (ESPRIT, MUSIC) depending on the method of calculation of the correlation matrix (straight versus forward–backward approach). Averaged 1000 independent runs | 72 |
| 10.5. | MSE of frequency estimation (ESPRIT, MUSIC, power spectrum) depending on the relative amplitude of higher harmonics amplitudes. Averaged 10000 independent runs | 73 |

| | |
|---|----|
| 10.6. MSE of amplitude estimation (ESPRIT, MUSIC, power spectrum) depending on the relative amplitude of higher harmonics amplitudes. Averaged 10000 independent runs | 73 |
| 10.7. Accuracy of the dimension estimation by AIC, MDL and MIBS depending on the signal length | 74 |
| 10.8. Accuracy of the dimension estimation by AIC, MDL and MIBS depending on the relative amplitude of two sinusoidal components | 75 |
| 10.9. Accuracy of the dimension estimation by AIC, MDL and MIBS depending on the difference of frequencies of two sinusoids with equal amplitude | 75 |
| 10.10. Accuracy of the dimension estimation by AIC, MDL and MIBS depending on the number of signal components (a) and on SNR (b) | 76 |
| 10.11. Scheme of the simulated transmission line system | 77 |
| 10.12. Waveform of the A-phase current during switching of the capacitor banks in the transmission line | 78 |
| 10.13. Short-Time Fourier Transform of the A-phase current during switching of the capacitor banks in the transmission line | 78 |
| 10.14. Time-varying frequency of two components of the current | 79 |
| 10.15. Time-varying amplitude of two components of the current | 79 |
| 10.16. Simulated DC arc furnace plant | 80 |
| 10.17. Voltage waveform of the arc furnace supply – medium voltage AC busbar | 81 |
| 10.18. Current waveform of the arc furnace supply – medium voltage T2 input | 82 |
| 10.19. Total Harmonic Distortion of the current evaluated with parametric spectral methods | 83 |
| 10.20. Progressive average of the first harmonic subgroup of the current | 83 |
| 10.21. Progressive average of the third harmonic subgroup of the current | 84 |
| 10.22. Progressive average of the fifth harmonic subgroup of the current | 84 |
| 10.23. Progressive average of the third harmonic subgroup of the current | 85 |
| 10.24. Progressive average of the fifth harmonic subgroup of the current | 85 |
| 10.25. Progressive average of the eleventh harmonic subgroup of the current | 86 |
| 10.26. Progressive average of the thirteenth harmonic subgroup of the current | 86 |
| 10.27. Progressive average of the first interharmonic subgroup of the current | 87 |
| 10.28. Progressive average of the second interharmonic subgroup of the current | 87 |
| 10.29. Progressive average of the first harmonic subgroup of the voltage | 88 |
| 10.30. Progressive average of the fifth harmonic subgroup of the voltage | 88 |
| 10.31. Progressive average of the seventh harmonic subgroup of the voltage | 89 |
| 10.32. Progressive average of the eleventh harmonic subgroup of the voltage | 89 |
| 10.33. Progressive average of the first interharmonic subgroup of the voltage | 90 |
| 10.34. Progressive average of the second interharmonic subgroup of the voltage | 90 |
| 10.35. Progressive average of the eleventh interharmonic subgroup of the voltage | 91 |
| 10.36. Progressive average of the twelfth interharmonic subgroup of the voltage | 91 |
| 10.37. Simplified scheme of the simulated converter configuration. R – resistance of the short-circuit | 94 |
| 10.38. Model of the inverter drive in MATLAB [®] SimPowerSystem | 95 |

| | |
|---|----|
| 10.39. Absolute value of the space phasor of the inverter output currents. Short-circuit resistance $R = 1 \Omega$ | 96 |
| 10.40. Time-frequency representation (ESPRIT-based) of the modulus of the space-phasor | 96 |
| 10.41. Corresponding amplitudes of components as in Figure 10.40 | 97 |
| 10.42. Reconstructed signal from components as shown in Figure 10.40 | 98 |

List of Tables

| | |
|---|----|
| 3.1. Comparison of basic performance characteristics of parametric spectral methods. . . | 34 |
| 10.1. Mean square error (MSE) of the progressive average of the current harmonic subgroups estimation. Value of Ideal IEC [A] | 92 |
| 10.2. Mean square error (MSE) of the progressive average of the current interharmonics subgroups estimation. Value of Ideal IEC [A] | 92 |
| 10.3. Mean square error (MSE) of the progressive average of the voltage harmonics subgroups estimation. Value of Ideal IEC [V] | 92 |
| 10.4. Mean square error (MSE) of the progressive average of the voltage interharmonics subgroups estimation. Value of Ideal IEC [V] | 93 |
| 10.5. Relative mean square error (MSE) of the progressive average of harmonic and interharmonic subgroups estimation | 93 |
| 10.6. Average of the highest correlation coefficients over 500 trials using ESPRIT, STFT and time-domain correlation | 98 |

Index

- autocorrelation, 24
 - sequence, 22
- autocovariance
 - function, 35
- Caratheodory's theorem, 25
- classification, 86
- component
 - frequency, 21
 - power, 26
 - stationary, 36
 - time-varying, 36
- computational cost, 31
- convolution
 - time-varying, 37
- correlation
 - coefficient, 89
 - matrix, 22
- covariance, 36
 - matrix, 38
 - operator, 35, 36
- cross-terms, 20
- DFT, 57, 76
- eigendecomposition, 29
- eigenvalue, 24, 27
- eigenvector, 24, 27, 29, 37
- ergodicity, 35
- error
 - eigenvalue estimation, 34
 - ESPRIT, 31
 - estimation, 31, 33
 - MSE, 32
 - root-MUSIC, 31
- ESPRIT
 - TLS, 30
- fault detection, 86
- FFT, 13
- filter
 - annihilating, 25, 26
- Fourier
 - analysis, 17
 - duality, 18
 - Joseph, 12
 - transform, 13, 19, 37
- frequency
 - harmonic, 55
 - interharmonic, 55
- frequency converter, 86
- function
 - autocovariance, 35
- Gabor
 - Dennis, 14
- grouping, 57
- harmonic
 - grouping, 55
 - groups, 74
- Heisenberg–Pauli–Weyl
 - inequality, 18
- interharmonic
 - grouping, 55
 - groups, 74
- invariance
 - rotational, 28, 29
 - shift, 28
- matrix
 - autocorrelation, 21, 22, 24, 25, 29
 - autocovariance, 23
 - correlation, 21, 22, 27
 - sample, 73

- covariance
 - estimate, 32
 - reversal, 23
 - sample covariance, 23
 - selector, 29
 - Toeplitz, 22
 - unitary, 30
- method
 - ESPRIT, 28
 - forward-backward, 23
 - maximum entropy, 21
 - MUSIC, 26, 28
 - Pisarenko, 25
 - root-MUSIC, 28
- model
 - autoregressive, 21
 - multi-component signal, 24
 - one-component signal, 24
- MSE, 34
- noise
 - eigenfilter, 27
 - eigenvalue, 25
 - eigenvector, 25, 27
- Parseval theorem, 37
- power quality
 - monitoring, 54
- process
 - Gaussian, 35
 - locally stationary, 35–37
 - non-stationary, 35
 - stochastic, 21, 22
 - zero-mean, 36
- pseudospectrum, 26–28
- quasi-stationarity, 35
- self-term, 20
- sensitivity
 - root-MUSIC, 33
- signal
 - eigenvector, 30
 - harmonic, 15
 - transient, 15
 - space-phasor, 87
 - spectrogram, 19, 20
 - spectrum
 - parametric, 15
 - power, 15
 - time-varying, 37
 - stationarity
 - local, 38
 - STFT, 18–20
 - STHD, 57
 - stochastic
 - process, 21
 - vector, 21
 - subspace, 29
 - noise, 31
 - signal, 25, 30, 31
 - subspaces, 25
 - SVD, 30
 - THD, 57, 74, 76
 - theorem
 - Caratheodory's, 25
 - Parseval, 37
 - time-frequency
 - representation, 18
 - support, 38
 - uncertainty principle, 17, 20
 - vector
 - singular, 30
 - Ville
 - Jean, 13, 14
 - waveform
 - distortion, 55
 - wavelets, 14
 - Wigner
 - Hermann, 14
 - Wigner-Ville
 - transform, 14
 - window
 - function, 37
 - Gaussian, 20
 - sliding, 16, 73, 87

Contents

| | |
|---|----|
| Notation | 4 |
| Abbreviations | 6 |
| Preface | 7 |
| Research objective | 9 |
| Contributions | 11 |
| Chapter 1. Introduction | 12 |
| 1.1. Time-domain analysis | 12 |
| 1.2. Frequency-domain analysis | 12 |
| 1.3. Time-Frequency signal analysis | 14 |
| 1.4. Analysis of non-stationary signals | 15 |
| 1.4.1. Classes of non-stationary signals | 15 |
| 1.4.2. Parametric spectral estimation | 16 |
| Chapter 2. Fourier Analysis | 18 |
| 2.1. Limitations | 18 |
| 2.2. Time-Frequency Approach | 19 |
| Chapter 3. Parametric frequency estimation | 23 |
| 3.1. Eigenanalysis-based methods | 23 |
| 3.1.1. Introduction | 23 |
| 3.1.2. Preliminaries | 23 |
| 3.1.3. Autocorrelation matrix | 24 |
| 3.1.4. Autocovariance matrix | 25 |
| 3.2. Subspace methods – Introduction | 26 |
| 3.2.1. Single frequency component in noise | 26 |

| | | |
|--------------------|---|-----------|
| 3.2.2. | Multiple frequency components in noise | 27 |
| 3.2.3. | Pisarenko harmonic decomposition | 27 |
| 3.2.4. | Pisarenko pseudospectrum | 29 |
| 3.3. | MUSIC | 29 |
| 3.3.1. | MUSIC pseudospectrum | 30 |
| 3.3.2. | MUSIC and Root-MUSIC | 30 |
| 3.4. | ESPRIT | 31 |
| 3.4.1. | Total least squares ESPRIT | 33 |
| 3.5. | Properties of frequency estimation methods | 34 |
| 3.6. | Performance analysis of MUSIC | 35 |
| 3.7. | Performance analysis of ESPRIT | 37 |
| Chapter 4. | Time-Varying Spectrum | 39 |
| 4.1. | Quasi-stationarity | 39 |
| 4.2. | Locally stationary processes | 39 |
| Chapter 5. | Filter banks for line spectra | 44 |
| 5.1. | Introduction | 44 |
| 5.2. | Usefulness of filter banks | 45 |
| 5.2.1. | Subband filtering | 45 |
| 5.2.2. | Increase of the resolution of line spectra | 46 |
| 5.2.3. | Backward mapping of the subband frequencies into fullband | 47 |
| 5.2.4. | Increase of the SNR | 48 |
| 5.2.5. | Limits | 49 |
| Chapter 6. | Complex space-phasor | 50 |
| 6.1. | Definitions | 50 |
| 6.2. | The space-phasor and three-phase systems | 51 |
| 6.3. | Visualization of the three-phase system | 53 |
| Chapter 7. | Estimation of the order of the model | 55 |
| 7.1. | Information theoretic criteria | 55 |
| 7.1.1. | Approach based on "observation" | 56 |
| 7.1.2. | Approach based on information theoretic criteria | 56 |
| 7.1.3. | Bayesian model selection – MInka’s Bayesian model order Selection Criterion (MIBS) | 58 |
| Chapter 8. | Power quality assessment | 59 |
| 8.1. | Introduction | 59 |
| 8.2. | Power Quality Indices | 60 |
| Chapter 9. | Automatic Classification of Events | 64 |
| 9.1. | Preliminaries | 64 |
| 9.2. | Correlation of signal and pattern | 65 |
| Chapter 10. | Experiments and simulations | 69 |

| | |
|---|------------|
| 10.1. Signal-to-Noise Ratio (SNR) | 69 |
| 10.2. Basic performance comparison of MUSIC and ESPRIT | 69 |
| 10.3. Estimation of the number of components | 74 |
| 10.4. Power quality indices | 80 |
| 10.4.1. Experimental setup and preprocessing | 80 |
| 10.4.2. Results and discussion | 82 |
| 10.5. Classification of events | 93 |
| 10.5.1. Introduction | 93 |
| 10.5.2. Numerical simulations | 94 |
| Conclusions | 100 |
| Bibliography | 103 |
| Parametryczne metody analizy czasowo-częstotliwościowej sygnałów elektrycznych | 109 |
| List of Figures | 110 |
| List of Tables | 113 |

PRACE NAUKOWE INSTYTUTU PODSTAW ELEKTROTECHNIKI
I ELEKTROTECHNOLOGII
(wydane w latach 1992–2006)

- Nr 27, *Studia i Materiały* nr 9, A. Skopec, *Modele i metody redukcji w teorii pola. Wybrane zagadnienia*, Wrocław 1992
- Nr 28, Konferencje nr 7, *Izolacja wysokonapięciowa w elektroenergetyce IWE '94*. IV ogólnopolska konferencja naukowo-techniczna, Wrocław 1994
- Nr 29, *Studia i Materiały* nr 10, W.A. Pluta, *Oddziaływanie linii przesyłowych wysokiego napięcia prądu stałego na środowisko*, Wrocław 1994
- Nr 30, Monografie nr 11, J. Wańkowicz, *Przeskok zabrudzeniowy. Wybrane zagadnienia eksploatacyjne i materiałowo-konstrukcyjne izolatorów elektroenergetycznych*, Wrocław 1996
- Nr 31, Konferencje nr 8, *Postępy w elektrotechnologii*, Wrocław 1996
- Nr 32, Konferencje nr 9, *Napowietrzna izolacja wysokonapięciowa w elektroenergetyce. NIWE '97*. V ogólnopolska konferencja naukowo-techniczna, Wrocław 1997
- Nr 33, Monografie nr 12, J. Pospieszna, *Wybrane zagadnienia interakcji polimer-syciwo w układach izolacyjnych kondensatorów energetycznych wysokiego napięcia*, Wrocław 1998
- Nr 34, Konferencje nr 10, *Postępy w elektrotechnologii*, Wrocław 1998
- Nr 35, Monografie nr 13, E. Motyl, *Ładunek przestrzenny w dielektrykach stałych. Analiza metod pomiarowych i badania*, Wrocław 2000
- Nr 36, Konferencje nr 11, *Napowietrzna izolacja wysokonapięciowa w elektroenergetyce. NIWE '2000*. Wrocław 2000
- Nr 37, Konferencje nr 12, *Postępy w elektrotechnologii*. IV Konferencja naukowa. Wrocław 2000
- Nr 38, Konferencje nr 13, *Postępy w elektrotechnologii*. V Konferencja naukowa. Wrocław 2003
- Nr 39, Konferencje nr 14, *Workshop. Environmental friendly materials and technologies in electrotechnics*, Wrocław 2003
- Nr 40, Konferencje nr 15, *Second international conference on advances in processing, testing and application of dielectric materials. APTADM 2004*, Wrocław 2004
- Nr 41, Monografie nr 14, R. Kacprzyk, *Wybrane zagadnienia badań ładunku i jego zaniku w dielektrykach stałych*, Wrocław 2004
- Nr 42, Konferencje nr 16, *Workshop. Modelling and elaboration of renewable energy sources and energy storage systems*, Wrocław 2005
- Nr 43, Konferencje nr 17, *Forum of Experts. Centre of Excellence for Materials for Low-energy Consuming Technologies in Electrotechnics MALET*, Wrocław 2006



BIBLIOTEKA GŁÓWNA

326571L/1

Wydawnictwa Politechniki Wrocławskiej
są do nabycia w księgarni
„Tech”
plac Grunwaldzki 13, 50-377 Wrocław
budynek D-1 PWr.
Prowadzimy sprzedaż wysyłkową

ISSN 0324-945x